Effects of 25-hydroxyvitamin D_3 on cell growth and cell death *via* regulation of the vitamin D metabolising system in a cervical adenocarcinoma cell line

by

Esther V.M. Zhou

A dissertation submitted in fulfilment of the requirements for the degree

Master of Science

in

Chemical Pathology

in the

Faculty of Health Sciences

at the

University of Pretoria

Supervisor: Dr. R. Punchoo

Co-supervisor: Prof. T.S. Pillay

March 2023

© University of Pretoria

Candidate:

Miss E.V.M. Zhou

15016308

Department of Chemical Pathology

Faculty of Health Sciences

University of Pretoria

Supervisor:

Dr R. Punchoo

Chemical Pathologist, and Senior Lecturer

Department of Chemical Pathology

Faculty of Health Sciences

University of Pretoria

Head of Department and Co-supervisor:

Prof T. Pillay

Chief Specialist, and Head of Department

Chemical Pathology

Faculty of Health Sciences

University of Pretoria

© University of Pretoria

Declaration of originality

Department of Chemical Pathology

Faculty of Health Sciences

University of Pretoria

I, Esther V. M. Zhou (Student number: 15016308) declare that:

I understand what plagiarism is and am aware of the university's policy in this regard.

I declare that this project is my own original work. Where other People's work has been used, this has been properly acknowledged and referenced in accordance with departmental requirements.

I have not used work previously produced by another student or any other person to submit as my own.

I have not allowed, and will not allow anyone to copy my work with the intension of presenting it as their own.

Signature: ……Ezhou……

Date: 31/03/2023

© University of Pretoria

Table of Contents

© University of Pretoria

© University of Pretoria

© University of Pretoria

© University of Pretoria

© University of Pretoria

Acknowledgements

Firstly, I would like to acknowledge God, for this was not completed in my own strength but through His divine grace and favour.

To my supervisor, Dr Punchoo, thank you for the many years of support and mentorship. Your advice and guidance have helped me grow as a researcher and have pushed me to aim higher as an emerging scientist.

To my co-supervisor, Prof Pillay, thank you for your time and input into this project. It was highly appreciated.

To my friends, thank you for your support throughout this degree. Thank you for allowing me to vent my frustrations, holding me when I was having a difficult day and celebrating the milestones (both big and small) with me. Also, thank you for the words of prayer and encouragement; I appreciate them more than words can express.

To my family, thank you for always supporting my dreams. Your constant love, encouragement and prayers have pushed me to strive to greater heights. I love and appreciate you.

Funding: I would like to acknowledge the funding provided by Research Committee of the Faculty of Health Sciences at the University of Pretoria (ResCom), the South African Medical Research Counsil (SAMRC) and the National Laboratory Health Services (NHLS) that made this project possible.

© University of Pretoria

Ethics

UNIVERSITEIT VAN PRETORIA
UNIVERSITY OF PRETORIA
YUNIBESITHI YA PRETORIA

Faculty of Health Sciences

Institution: The Research Ethics Committee, Faculty Health Sciences, University of Pretoria complies with ICH-GCP guidelines and has US Federal wide Assurance.

- FWA 00002567, Approved dd 22 May 2002 and Expires 03/20/2022.
- IORG #: IORG0001762 OMB No. 0990-0279 Approved for use through February 28, 2022 and Expires: 03/04/2023.

Faculty of Health Sciences **Research Ethics Committee**

15 July 2021

Approval Certificate
New Application

Dear Miss EVM Zhou

Ethics Reference No.: 343/2021
Title: Effects of 25-hydroxyvitamin D3 on cell growth and cell death via regulation of the vitamin D metabolising system in a cervical adenocarcinoma cell line

The **New Application** as supported by documents received between 2021-06-24 and 2021-07-14 for your research, was approved by the Faculty of Health Sciences Research Ethics Committee on 2021-07-14 as resolved by its quorate meeting.

Please note the following about your ethics approval:

- Ethics Approval is valid for 1 year and needs to be renewed annually by 2022-07-15.
- Please remember to use your protocol number (343/2021) on any documents or correspondence with the Research Ethics Committee regarding your research.
- Please note that the Research Ethics Committee may ask further questions, seek additional information, require further modification, monitor the conduct of your research, or suspend or withdraw ethics approval.

Ethics approval is subject to the following:

- The ethics approval is conditional on the research being conducted as stipulated by the details of all documents submitted to the Committee. In the event that a further need arises to change who the investigators are, the methods or any other aspect, such changes must be submitted as an Amendment for approval by the Committee.

We wish you the best with your research.

Yours sincerely

On behalf of the FHS REC, Dr R Sommers
MBChB, MMed (Int), MPharmMed, PhD
Deputy Chairperson *of the Faculty of Health Sciences Research Ethics Committee, University of Pretoria*

The Faculty of Health Sciences Research Ethics Committee complies with the SA National Act 61 of 2003 as it pertains to health research and the United States Code of Federal Regulations Title 45 and 46. This committee abides by the ethical norms and principles for research, established by the Declaration of Helsinki, the South African Medical Research Council Guidelines as well as the Guidelines for Ethical Research: Principles Structures and Processes, Second Edition 2015 (Department of Health)

Research Ethics Committee
Room 4-60, Level 4, Tswelopele Building
University of Pretoria, Private Bag x323
Gezina 0031, South Africa
Tel +27 (0)12 356 3084
Email deepeka.behari@up.ac.za
www.up.ac.za

Fakulteit Gesondheidswetenskappe
Lefapha la Disaense tša Maphelo

© University of Pretoria

UNIVERSITEIT VAN PRETORIA
UNIVERSITY OF PRETORIA
YUNIBESITHI YA PRETORIA

Faculty of Health Sciences

Institution: The Research Ethics Committee, Faculty Health Sciences, University of Pretoria complies with ICH-GCP guidelines and has US Federal wide Assurance.

- FWA 00002567. Approved dd 18 March 2022 and Expires 18 March 2027.
- IORG #: IORG0001762 OMB No. 0990-0278 Approved for use through August 31, 2023

Faculty of Health Sciences **Research Ethics Committee**

15 June 2022

Approval Certificate
Annual Renewal

Dear Miss EVM Zhou,

Ethics Reference No.: 343/2021 – Line 1
Title: Effects of 25-hydroxyvitamin D3 on cell growth and cell death via regulation of the vitamin D metabolising system in a cervical adenocarcinoma cell line

The **Annual Renewal** as supported by documents received between 2022-05-18 and 2022-06-15 for your research, was approved by the Faculty of Health Sciences Research Ethics Committee on 2022-06-15 as resolved by its quorate meeting.

Please note the following about your ethics approval:

- Renewal of ethics approval is valid for 1 year, subsequent annual renewal will become due on 2023-06-15.
- Please remember to use your protocol number (343/2021) on any documents or correspondence with the Research Ethics Committee regarding your research.
- Please note that the Research Ethics Committee may ask further questions, seek additional information, require further modification, monitor the conduct of your research, or suspend or withdraw ethics approval.

Ethics approval is subject to the following:

- The ethics approval is conditional on the research being conducted as stipulated by the details of all documents submitted to the Committee. In the event that a further need arises to change who the investigators are, the methods or any other aspect, such changes must be submitted as an Amendment for approval by the Committee.

We wish you the best with your research.

Yours sincerely

On behalf of the FHS REC, Dr R Sommers
MBChB, MMed (Int), MPharmMed, PhD
Deputy Chairperson *of the Faculty of Health Sciences Research Ethics Committee, University of Pretoria*

The Faculty of Health Sciences Research Ethics Committee complies with the SA National Act 61 of 2003 as it pertains to health research and the United States Code of Federal Regulations Title 45 and 46. This committee abides by the ethical norms and principles for research, established by the Declaration of Helsinki, the South African Medical Research Council Guidelines as well as the Guidelines for Ethical Research: Principles Structures and Processes, Second Edition 2015 (Department of Health)

Research Ethics Committee
Room 4-60, Level 4, Tswelopele Building
University of Pretoria, Private Bag x323
Gezina 0031, South Africa
Tel +27 (0)12 356 3084
Email: deepeka.behari@up.ac.za
www.up.ac.za

Fakulteit Gesondheidswetenskappe
Lefapha la Disaense tša Maphelo

© University of Pretoria

UNIVERSITEIT VAN PRETORIA
UNIVERSITY OF PRETORIA
YUNIBESITHI YA PRETORIA

Faculty of Health Sciences

Institution: The Research Ethics Committee, Faculty Health Sciences, University of Pretoria complies with ICH-GCP guidelines and has US Federal wide Assurance.

- FWA 00002567, Approved dd 18 March 2022 and Expires 18 March 2027.
- IORG #: IORG0001762 OMB No. 0990-0278 Approved for use through August 31, 2023.

Faculty of Health Sciences **Research Ethics Committee**

18 May 2023

Approval Certificate
Annual Renewal

Dear Miss EVM Zhou,

Ethics Reference No.: 343/2021 – Line 2
Title: Effects of 25-hydroxyvitamin D3 on cell growth and cell death via regulation of the vitamin D metabolising system in a cervical adenocarcinoma cell line

The **Annual Renewal** as supported by documents received between 2023-04-18 and 2023-05-17 for your research, was approved by the Faculty of Health Sciences Research Ethics Committee on 2023-05-17 as resolved by its quorate meeting.

Please note the following about your ethics approval:

- Renewal of ethics approval is valid for 1 year, subsequent annual renewal will become due on 2024-05-18.
- Please remember to use your protocol number (343/2021) on any documents or correspondence with the Research Ethics Committee regarding your research.
- Please note that the Research Ethics Committee may ask further questions, seek additional information, require further modification, monitor the conduct of your research, or suspend or withdraw ethics approval.

Ethics approval is subject to the following:

- The ethics approval is conditional on the research being conducted as stipulated by the details of all documents submitted to the Committee. In the event that a further need arises to change who the investigators are, the methods or any other aspect, such changes must be submitted as an Amendment for approval by the Committee.

We wish you the best with your research.

Yours sincerely

On behalf of the FHS REC, Dr R Sommers
MBChB, MMed (Int), MPharmMed, PhD
Deputy Chairperson *of the Faculty of Health Sciences Research Ethics Committee, University of Pretoria*

The Faculty of Health Sciences Research Ethics Committee complies with the SA National Act 61 of 2003 as it pertains to health research and the United States Code of Federal Regulations Title 45 and 46. This committee abides by the ethical norms and principles for research, established by the Declaration of Helsinki, the South African Medical Research Council Guidelines as well as the Guidelines for Ethical Research: Principles Structures and Processes, Second Edition 2015 (Department of Health)

Research Ethics Committee
Room 4-60, Level 4, Tswelopele Building
University of Pretoria, Private Bag x323
Gezina 0031, South Africa
Tel +27 (0)12 356 3084
Email: deepeka.behari@up.ac.za
www.up.ac.za

Fakulteit Gesondheidswetenskappe
Lefapha la Disaense tša Maphelo

© University of Pretoria

Study Output

Conference presentation and published abstract in conference proceedings (Appendix H)

Conference: Microscopy Society of Southern Africa (MSSA), Johannesburg, South Africa

Title: 25-Hydroxyvitamin D3 induces biochemical and morphological apoptosis in the HeLa cell line.

Authors: Zhou E.V.M., Bhoora S., Pillay T.S. and Punchoo R.

Date: 5-8 December 2022

Conference proceedings: ISSN 0250-0418 and ISBN 978-0-6398435-0-6

© University of Pretoria

Abstract

Cervical cancer is the leading cause of cancer-related mortalities in South African women. Vitamin D and its metabolites exert anti-cancer actions in various cancers; however, few studies have explored the effects of vitamin D in cervical cancer.

The vitamin D metabolising system (VDMS) is responsible for the activation and breakdown of the vitamin. Vitamin D is activated by two hydroxylation steps facilitated by 25-hydroxylase (CYP27A1/CYP2R1) and 25-hydroxyvitamin D-1α-hydroxylase (CYP27B1). The resulting active hormone, 1α,25-dihydroxyvitamin D_3 ($1,25(OH)_2D_3$), binds vitamin D receptor (VDR) in target cells to exert its effects. Both $1,25(OH)_2D_3$ and its precursor $25(OH)D_3$ are catabolised by 24-hydroxylase (CYP24A1). This study aimed to use the cervical cancer cell line, HeLa treated with $25(OH)D_3$, to investigate the cell health parameters (cell count, viability, and cell cycle), cell death (apoptosis, autophagy and necrosis) by brightfield and transmission electron microscopy, and flow cytometry, and regulation of expression of genes and proteins in the VDMS by qPCR and Western blot.

Results indicated that treatment with 5000 nM $25(OH)D_3$ significantly decreased cell count and viability and increased the sub-G1 population without inducing cell cycle arrest. Treatment-induced intrinsic apoptosis through disruption of mitochondrial membrane potential, externalisation of phosphatidylserines and activation of executioner caspases -3 and -7. Classic morphological features of apoptosis were also observed with brightfield and transmission electron microscopy. In addition, high-dose treatment with vitamin D increased CYP27B1, CYP24A1 and VDR gene and protein expression. Interestingly, multinucleated cells were observed in all cultures, but the cells were significantly larger following high dose $25(OH)D_3$ treatment.

Collectively, the findings indicate that the VDMS acts in an autocrine manner to mediate the effects of supraphysiological doses of $25(OH)D_3$ on the growth and death of HeLa cells. Based on the data, it can be inferred that $25(OH)D_3$ holds promise as a therapeutic agent for cervical cancer treatment, and further clinical studies are warranted to explore this potential.

Keywords: Cervical cancer; 25-hydroxyvitaminD3; apoptosis; 1α-hydroxylase (CYP27B1); 24-hydroxylase (CYP24A1); vitamin D receptor (VDR); multinucleated cells (MNC); polyploid giant cancer cells (PGCC)

© University of Pretoria

List of Abbreviations

1αOHase	1α-hydroxylase
1,25(OH)$_2$D$_3$	1α,25-dihydroxyvitamin D$_3$
24OHase	24-hydroxylase
25(OH)D$_3$	25-hydroxyvitamin D$_3$
7-AAD	7-Aminoactinomycin D
ANOVA	Analysis of variance
Atg	Autophagy-related protein
Bax	Bcl-2 Associated X-protein
BCA	Bicinchoninic acid
Bcl-2	B-cell lymphoma 2
BSA	Bovine Serum Albumin
Ca^{2+}	Calcium ions
CDK	Cyclin-dependent kinase
cDNA	Complementary deoxyribonucleic acid
CO_2	Carbon dioxide
CYP	Cytochrome P-450 mixed-function oxidases
CYP24A1	24-hydroxylase
CYP2R1/CYP27A1	25-Hydroxylase
CYP27B1	25-Hydroxyvitamin D-1α-hydroxylase
DEVD	Amino acid sequence Asp-Glu-Val-Asp
DMEM	Dulbecco's Modified Eagle Medium
DNA	Deoxyribonucleic acid
ER	Endoplasmic reticulum

© University of Pretoria

ERSP57	Endoplasmic reticulum stress protein 57
FGF-23	Fibroblast growth factor 23
GI_{50}	50% growth inhibition
GMP	Cyclic guanosine monophosphate
H&E	Haematoxylin and Eosin
HBSS	Hank's Balanced Salt Solution
HPV	Human Papilloma Virus
IOM	Institute of Medicine
IGFBP-3	Insulin growth factor binding protein 3
INT	2-p-iodophenyl-3-p-nitrophenyl-5-phenyl tetrazolium
LC3	Microtubule-associated protein 1A/1B-light chain 3
LC3-I	Microtubule-associated protein 1A/1B-light chain 3-1
LC3-II	Microtubule-associated protein 1A/1B-light chain 3-2
LDH	Lactate dehydrogenase
LDS	Lithium dodecyl sulphate
M	Molar
MAP	Mitogen-activated protein kinase
MARRS	Membrane-associated rapid-response steroid-binding protein
mL	millilitre
MNC	Multinucleated cell
M-PER	Mammalian Protein Extraction Reagent
MPT	Mitochondrial permeability transition
mRNA	Messenger ribonucleic acid
NADH/NAD+	Nicotinamide adenine dinucleotide

© University of Pretoria

NCCD	Nomenclature Committee of Cell Death
ng/mL	Nanograms per millilitre
nM	Nanomolar
OD	Optical density
p21	Cyclin-dependent kinase inhibitor protein 21
p27	Cyclin-dependent kinase inhibitor protein 27
p53	Tumour protein p53
PBS	Phosphate-buffered saline
PCD	Programmed cell death
PGCC	Polyploid giant cancer cell
PI	Propidium iodide
PMS	N-methylphenazonium methyl sulphate
PTH	Parathyroid hormone
RB	Retinoblastoma protein
PVDF	Polyvinylidene fluoride
REDOX	reduction-oxidation
RNA	Ribonucleic acid
RT-qPCR	Reverse transcription quantitative polymerase chain reaction
RXR	Retinoic X receptor
SDS	Sodium dodecyl sulphate
SEM	Standard error of mean
TEM	Transmission electron microscopy
TMRE	Tetramethylrhodamine ethyl ester
µg	micrograms

© University of Pretoria

µL	microlitres
UVB	Ultraviolet radiation B
VDBP	Vitamin D binding protein
VDR	Vitamin D receptor
VDRE	Vitamin D receptor response element
WHO	World Health Organisation
WR	Working reagent
x g	Times gravity

© University of Pretoria

List of Figures

© University of Pretoria

© University of Pretoria

List of Tables

© University of Pretoria

Chapter 1

Literature review

1.1 Introduction

Cervical cancer is the leading cause of cancer-related mortalities in South African women[1]. It affects approximately 1 in 40 women and is the second most diagnosed malignancy among women in the country. Vitamin D and its metabolites exert anti-cancer actions in breast, colon, prostate, skin, and lung cancers. Cervical tissues express the vitamin D metabolising system (VDMS), but only a few studies have explored the relationship between the VDMS, its metabolites and cervical cancer.

1.2 Vitamin D: History, Metabolism, and Intracellular Signalling

1.2.1 Discovery of Vitamin D

Vitamins are trace nutrients obtained from the diet are essential for specific physiological processes[2]. Professor Elmer McCollum's research provided evidence that cod liver oil contained a curative or preventative agent for rickets, though the exact nature of this agent was not yet identified[3]. Sir Edward Mellanby's experiments with dogs in 1920 aimed to uncover the precise component of cod liver oil responsible for treating or preventing rickets[4]. These studies ultimately led to the discovery and classification of vitamin D[2-3]. Huldshinsky and Chick *et al*. conducted independent studies that demonstrated how exposing children to sunlight or ultraviolet light could prevent or cure rickets[2]. Their findings prompted many animal studies, which proved that sunlight plays a critical role in activating vitamin D and maintaining calcium balance[2-3].

Subsequent experiments proved the existence of two variations of vitamin D. Vitamin D_2 (ergocalciferol), sourced from plants, is derived from the provitamin ergosterol (Figure 1.1a). Vitamin D_3 (cholecalciferol) is obtained from animals (Figure 1.1b)[4-5]. In addition, vitamin D_3 can be synthesised in the skin upon exposure to solar ultraviolet B (UVB) radiation. Ultraviolet radiation cleaves 7-dehydrocholesterol in the skin to pre-vitamin D_3. Pre-vitamin D_3 thermally isomerises to vitamin D_3 (cholecalciferol)[6]. Both vitamin D_2 and D_3 can be sourced from the diet; however, very few foods naturally contain or are fortified with vitamin D[5].

© University of Pretoria

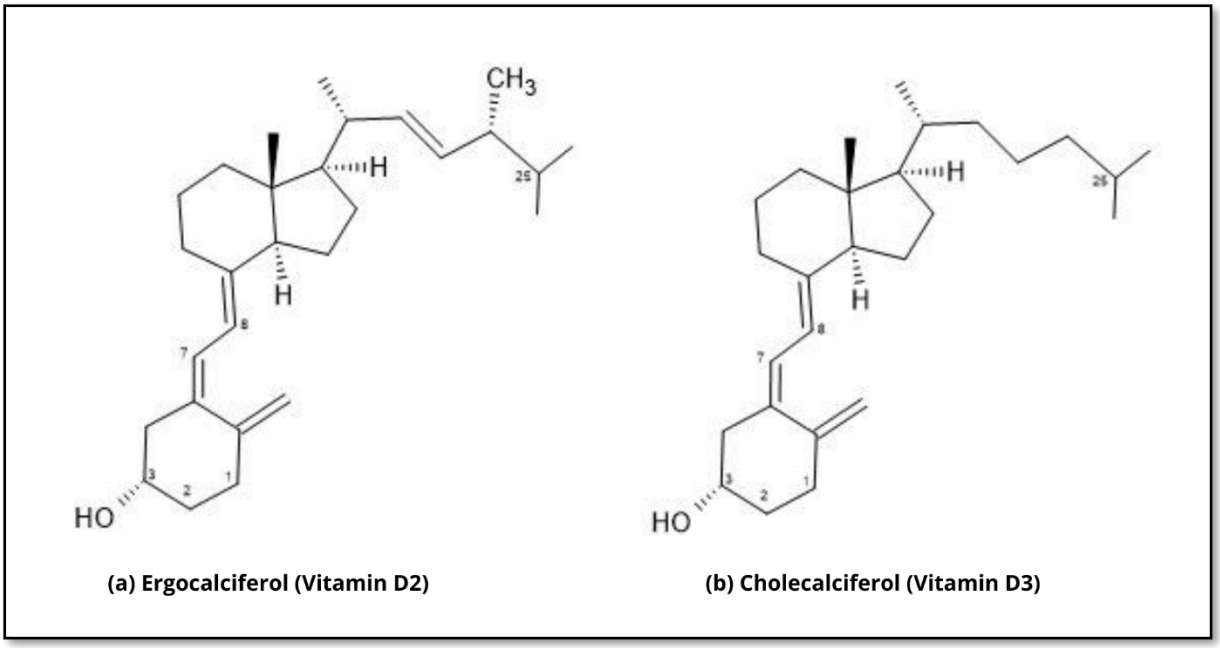

Figure 1.1 Chemical structures of forms of Vitamin D. Structures of vitamin D_2 and D_3 drawn using ACD/ChemSketch (Freeware) 2021.1.0. These two compounds undergo two sequential hydroxylation steps to produce the active metabolite, 1,25-dihydroxyvitamin D (calcitriol).

1.2.2 Vitamin D metabolism

Cytochrome P-450 mixed function oxidases (CYPs) activate vitamin D_2 and D_3 obtained from the diet and skin through two hydroxylation steps. The initial hydroxylation, which takes place on carbon-25 (C25), is carried out by 25-hydroxylase (CYP2R1/CYP27A1) in the liver. The resulting metabolite, 25-hydroxyvitamin D_3 (25(OH)D_3/calcidiol), circulates in blood bound to the vitamin D binding protein (VDBP) or albumin. In the kidneys, 25-hydroxyvitamin D-1α-hydroxylase (CYP27B1, 1αOHase) mediates the second hydroxylation step by adding a hydroxyl group to the alpha position of carbon 1 on 25(OH)D_3[7]. This process produces 1α,25-dihydroxyvitamin D_3 (1,25$(OH)_2D_3$/calcitriol), which is the potent form of vitamin D_3 (Figure 1.2)[4]. Both 25(OH)D_3 and 1,25$(OH)_2D_3$ are catabolised by 24-hydroxylase (CYP24A1, 24OHase), resulting in an inactive water-soluble compound called calcitroic acid that is excreted in bile[5,7].

© University of Pretoria

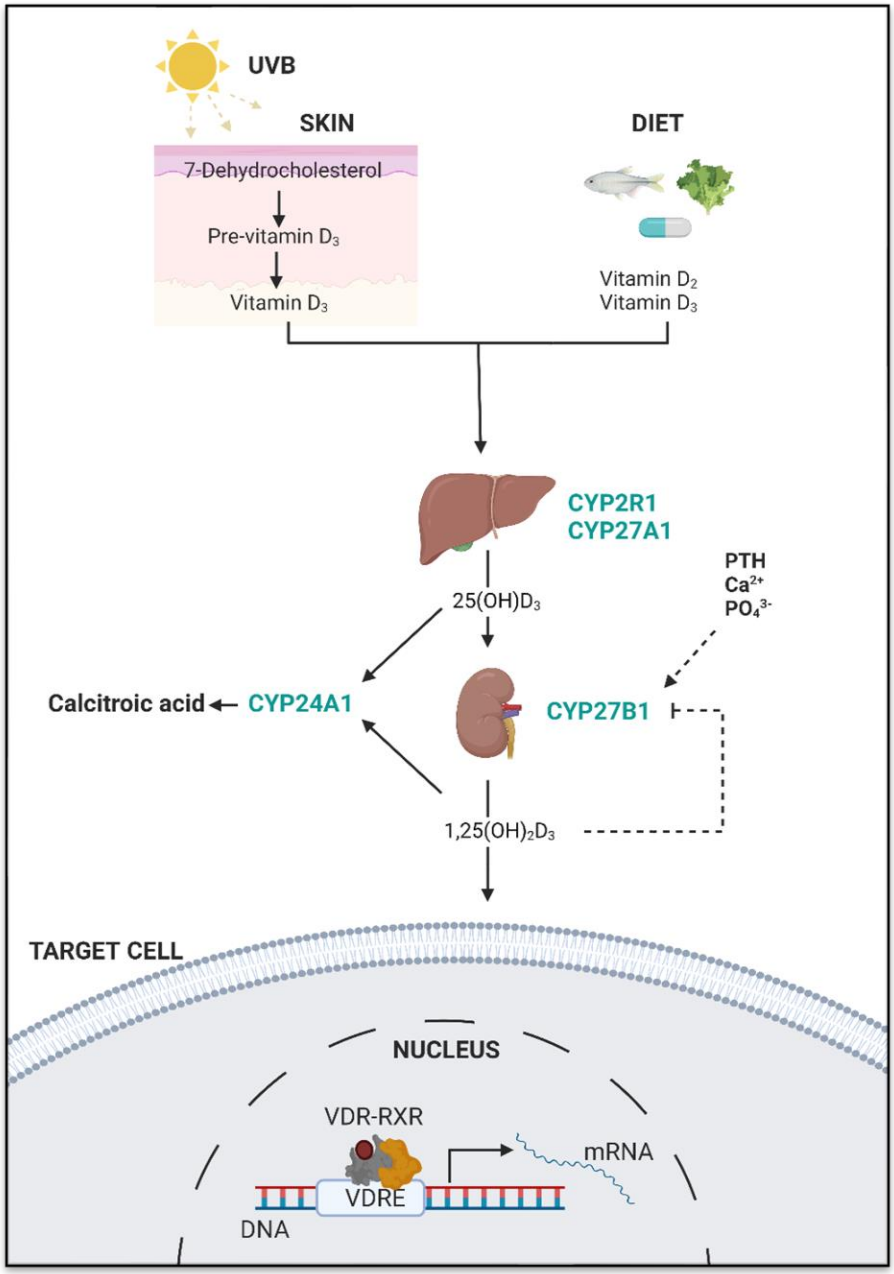

Figure 1.2 **Vitamin D metabolism and cell signalling.** Vitamin D_3 is synthesised upon exposure to ultraviolet B radiation (UVB) or is taken up in the diet. It is transported to the liver, where it undergoes hydroxylation via CYP2R1 or CYP27A1. The product, $25(OH)D_3$, is transported to the kidneys, where it is hydroxylated to produce $1,25(OH)_2D_3$ via CYP27B1. This $1,25(OH)_2D_3$ can inhibit CYP27B1 expression through a negative feedback mechanism. CYP27B1 expression can be increased by parathyroid hormone (PTH) and calcium (Ca^{2+}), and phosphate ions (PO_4^{3-}). The $1,25(OH)_2D_3$ binds the vitamin D receptor (VDR), which then dimerises with the retinoid x receptor and initiates transcription in the target cell. Both $25(OH)D_3$ and $1,25(OH)_2D_3$ are broken down by CYP24A1 to produce calcitroic acid. Created with BioRender.com

The cytochrome P450 oxidases involved in vitamin D metabolism are located in either the endoplasmic reticulum (ER) (CYP2R1) or in the mitochondria (CYP27A1, CYP27B1 and

© University of Pretoria

CYP24A1) of a cell[8]. The activity of these enzymes is not solely limited to the liver and kidney but has been observed in several other tissues such as the lungs, adrenal glands, intestines, colon, breast, and prostate[6]. Therefore, $1,25(OH)_2D_3$ can exert its effects in either an endocrine or intracrine, autocrine, or paracrine mode of action[7].

1.2.3 Genomic effects of $1,25(OH)_2D_3$

The most biologically active metabolite of vitamin D, $1,25(OH)_2D_3$, is hormonally active. The binding of $1,25(OH)_2D_3$ to the vitamin D receptor (VDR) in target cells is utilised in signal transduction pathways[4,9]. The VDR is a member of the steroid-thyroid-retinoid receptor superfamily of ligand-activated transcription factors (nuclear receptors) and can interact with other transcription factors[7]. The retinoid X receptor (RXR) is the best-studied transcription factor to bind to VDR. The liganded VDR heterodimerises with RXR and then binds to regulatory vitamin D response elements (VDRE) in promoter regions of target genes[10-11]. As a result, coregulators are recruited, and transcription is initiated.

The VDR is present in several tissues, and $1,25(OH)_2D_3$ regulates 3-5% of genes. Therefore, vitamin D can stimulate upregulation or downregulation of gene expression in multiple physiological systems and tissues[7,12]. One such gene is CYP24A1 which deactivates $1,25(OH)_2D_3$. This autoregulation renders excess $1,25(OH)_2D_3$ inactive[13-14].

1.2.4 Non-genomic effects of vitamin D_3

The activity of $1,25(OH)_2D_3$ has been observed in non-genomic pathways. The non-genomic actions of vitamin D influence various signalling pathways by acting through receptors such as the membrane-associated rapid-response steroid-binding protein ($1,25D_3$-MARRS) receptor[15], a membrane-associated receptor. The downstream regulated pathways operate through phosphoinositide, calcium ions (Ca^{2+}), cyclic guanosine monophosphate (GMP), and mitogen-activated protein (MAP) kinase[9]. The MARRS receptor is identical to the endoplasmic reticulum stress protein 57 (ERSP57)[15], which, when associated with vitamin D, has a protective effect against skin cancer and sunlight-induced deoxyribonucleic acid (DNA) damage[7]. However, the non-genomic actions in most cells are not clear.

Although all the actions and mechanisms of vitamin D metabolites are not completely understood, some mechanisms have been clarified by studying various diseases such as cancer.

© University of Pretoria

1.2.5 Vitamin D deficiency

Vitamin D is best known for stimulating calcium and phosphorus absorption, vital for healthy bone mineralisation. Vitamin D deficiency is associated with osteomalacia, osteoporosis, osteopenia, heart disease, diabetes, hypertension, asthma, and cancer[5]. Serum 25(OH)D_3 clinically establishes vitamin D status. The Institute of Medicine (IOM) and the Endocrine society define the cut-off for deficiency at 20 and 30 ng/mL (50 and 75 nmol/L), respectively[7]. Studies have shown that serum levels above 40 ng/mL (100 nmol/L) correlate with reduced risk of several cancers[14]. Dietary supplementation at amounts ranging from 2000-4000 international units daily are required to maintain serum 25(OH)D levels above 100 nmol/L[14].

1.3 Vitamin D and cancer

The World Health Organisation (WHO) classifies cancer as a leading cause of death worldwide[16]. The term cancer broadly describes the uncontrolled growth and division of abnormal cells. More specifically, cancer originates from genomic mutations triggered by environmental exposure, oncoviruses, and replication errors, leading to alterations in the epigenetics, heterotypic interactions, and the number and arrangement of chromosomes in a cell[17]. These changes, known as the hallmarks of cancer, undergo evolutionary and clonal selection during malignancy.

There are believed to be about eight defined hallmarks of cancer[17]. These are evading growth suppressors, sustaining proliferative signalling, inducing angiogenesis, resisting cell death, avoiding immune destruction, enabling replicative immortality, deregulating cellular metabolism, and triggering invasion and metastasis[18], as shown in Figure 1.3. Vitamin D, combined with enzymes and other proteins, has been demonstrated to negatively affect cell proliferation, angiogenesis, and metastasis[7,9] in prostate, breast, and colon cancers.

© University of Pretoria

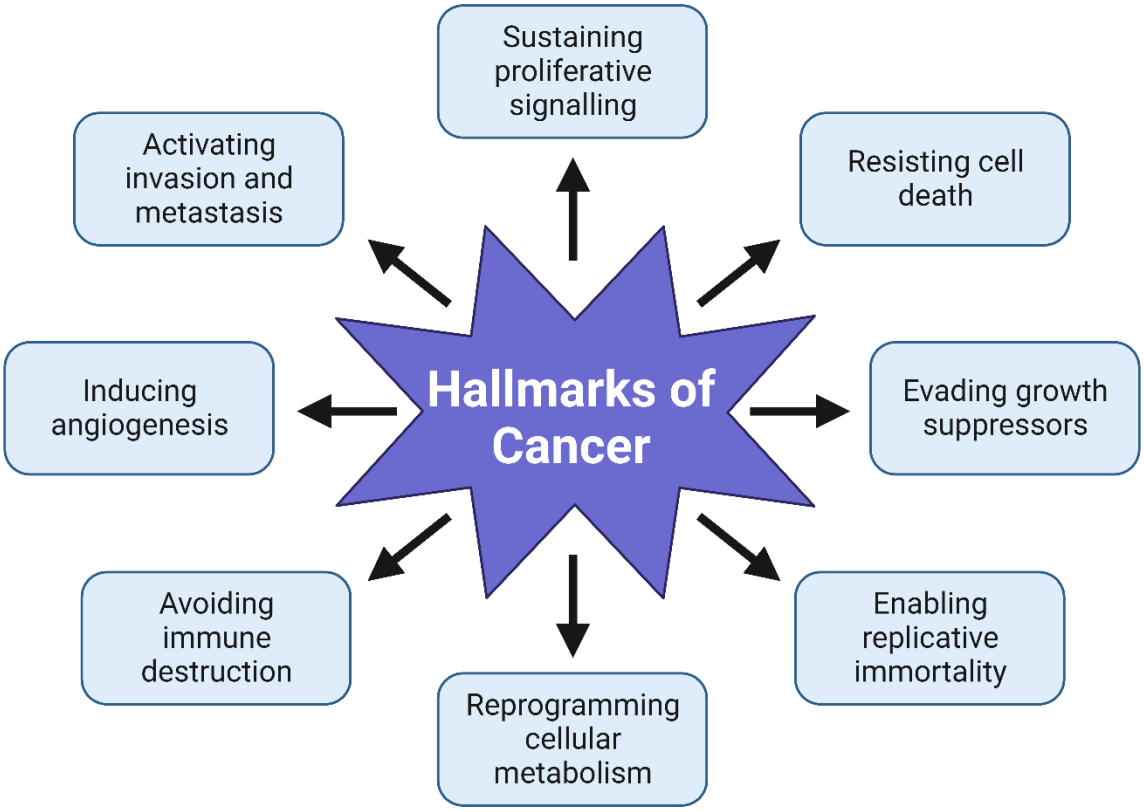

Figure 1.3 **Hallmarks of cancer.** The eight hallmarks of cancer were proposed by Hanahan and Weinburg in 2000. These hallmarks are believed to be how cells are selected during malignancy. The hallmarks are: sustaining proliferative signalling, resisting cell death, evading growth suppressors, enabling replicative immortality, reprogramming cellular metabolism, avoiding immune destruction, inducing angiogenesis, and activating invasion and metastasis.[18]

1.3.1 Anti-proliferation

Cell proliferation is the process by which cells grow and replicate. Normal cells divide continuously until they reach a differentiated state, after which proliferation is arrested. Carcinogenesis results from the deregulation of proliferation[19]. Growth factors and receptors are usually altered in carcinogenesis, resulting in abnormal proliferation. This can be counteracted when the cell cycle is tightly regulated[17]. Deregulation of the cell cycle enhances the development of malignancy and the overall survival of the abnormal cells.

Vitamin D metabolites inhibit cell proliferation in both normal and malignant cells through multiple cell-specific mechanisms[20-21]. They regulate growth factors, the cell cycle, and signalling pathways, demonstrating anti-proliferative properties. Vitamin D treatment increases the expression of insulin-like growth factor-binding protein 3 (IGFBP-3) and cyclin-dependent kinase (CDK) inhibitors such as cyclin-dependent kinase inhibitor protein -21 and -27 (p21 and

© University of Pretoria

p27, respectively), thereby inhibiting cell proliferation. Calcitriol also inhibits telomerase activity and the Wnt/β-catenin signalling pathway, essential for adult tissue homeostasis[21-22].

1.3.2 Cell cycle arrest

The cell cycle is an ordered process necessary for normal cell growth and the maintenance of tissue homeostasis[17,23]. The cycle is divided into five phases: quiescence or resting phase (G_0), Gap 1 (G_1), DNA synthesis (S), Gap 2 (G_2), and mitosis (M)[24]. During the S phase, DNA is replicated to produce two copies of genetic material[25]. The genetic material is evenly distributed between two daughter cells during M phase. The two gap phases (G_1 and G_2) are required for cell growth (Figure 1.4).

The progression of the cycle is tightly regulated by cyclins, cyclin-dependent protein kinases (CDKs), and tumour suppressors[26]. For a cell to divide, DNA replication must occur to produce daughter cells that are identical[24]. Progression through the G_1/S checkpoint is regulated by Cyclin D-CDK4 and cyclin E-CDK2. These cyclin complexes phosphorylate the retinoblastoma (RB) protein leading to the release of E2F transcription factors, enhancing the expression of genes required for DNA replication[25,27]. Cyclin A-CDK2 phosphorylates cdc6 and E2F1, and drives cells out of the S phase into the G_2 phase of the cell cycle once DNA replication has occurred, Progression through the G_2/M phase is mediated by cyclin B-CDK1 which triggers mitosis[28].

If significant DNA damage is detected in the G_1 phase, tumour protein p53 stimulates the transcription of cyclin-dependent kinase inhibitor 1 (p21), inhibiting all cyclin-dependent kinase complexes. This leads to cell cycle arrest until the damage is resolved[26]. Tumour suppressors such as p53 prevent uninhibited cell proliferation, characteristic of cancer[26]. Cancer cells differ because the signalling pathway has one or more alterations giving them a proliferative and growth advantage[17].

© University of Pretoria

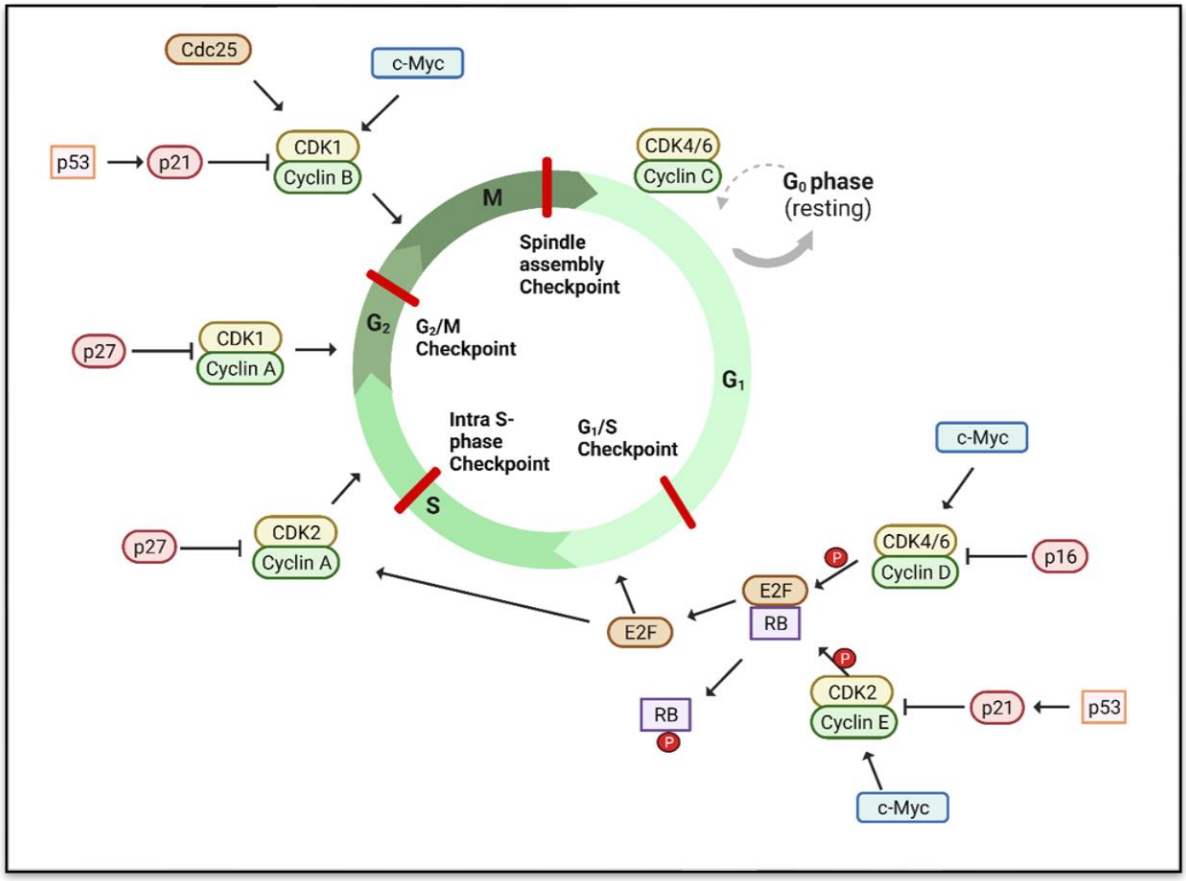

Figure 1.4 **The cell cycle.** The cell cycle consists of four phases: (1) the G_1/G_0 phase, (2) the S phase, (3) the G2 phase and (4) the M phase. Cyclins and cyclin-dependent kinases regulate progression through the cycle. Cyclin-CDKs are inhibited by the p16, p21 and p27 proteins. Created with BioRender.com

Vitamin D derivatives have been reported to arrest the cell cycle at the G_0/G_1 phase[29] through the upregulation of p21[30]. This occurs via the transcription factor actions of liganded of VDR at the p21 promoter region[30]. As previously mentioned, the transcription of p21 is also regulated by p53. Studies have demonstrated that p53 can bind to VDR to regulate the transactivation of p21 messenger ribonucleic acid (mRNA). Activated vitamin D has also been reported to cause cell cycle arrest at the G_2/M phase in ovarian cancer cells via upregulation of the growth arrest and DNA-Damage-Inducible alpha (GADD45α) protein; however, further studies are needed to explore the mechanism.

1.3.3 Cell death

Cell death is part of a regenerative process by which a cell ceases to perform its function. Under normal circumstances, old cells naturally degrade in an organised manner, defined as programmed cell death (PCD)[31]. This creates an equilibrium between cell death and the

© University of Pretoria

survival of normal cells. PCD determines the fate of the cell when the balance is disrupted[32]. The Nomenclature Committee of Cell Death (NCCD) categorizes programmed cell death into apoptosis, autophagy, and necrosis based on morphological differences[31,33-34].

1.3.3.1 Apoptosis

Cells primarily eliminate themselves through apoptosis, classified as type 1 PCD. Biochemical and morphological changes are used to differentiate apoptosis from autophagy and necrosis[31-32,35]. Biochemical changes include alterations in mitochondrial membrane potential[36], the externalization of phosphatidylserines on the cell membrane[37], activation of terminal caspases[38-39], and DNA fragmentation[32,40]. Morphological changes include cell shrinkage, chromatin condensation, and plasma membrane blebbing[41]. The resulting apoptotic bodies are phagocytosed, degraded, and removed without inciting an inflammatory response[35,41]. Moreover, apoptosis enables organisms to regulate their cell numbers and tissue size and confers the ability to protect against foreign invasion[40].

Apoptosis can occur via the intrinsic pathway or the extrinsic pathway. In the intrinsic pathway, stimuli cause the mitochondrial permeability transition (MPT) pore to open. This disrupts the mitochondrial membrane potential and leads to the release of pro-apoptotic proteins into the cell. These proteins activate caspases which in turn fragment DNA. The extrinsic pathway involves binding a ligand to death receptors in the target cell membrane, thereby activating caspase activity and inducing apoptotic cell death[34,40,42].

Cancer cells are characterised distinctly by their abnormal control of apoptotic pathways[43]. Studies have shown that $1\alpha,25(OH)_2D_3$ suppresses pro-survival proteins B-cell lymphoma 2 (Bcl-2) and telomerase reverse transcriptase while simultaneously activating pro-apoptotic protein Bcl-2 associated X-protein (BAX), thereby inducing apoptosis[7,12].

1.3.3.2 Autophagy

Autophagy-dependent cell death is classified as type 11 PCD[31], and in normal cellular homeostasis, it is essential in recycling cellular content[31,44]. As its name suggests, autophagy is a self-digestion process aiding in the degradation of damaged organelles[44-45]. The process of autophagy can, therefore, relieve acute cellular stress or lead to cell death[32,46]. Liu et al. (2010) stipulated that autophagy regulates multiple physiological processes, such as cell starvation, differentiation, survival and death[45].

© University of Pretoria

During autophagy, stressor molecules trigger the expression of signal molecules on the surface of damaged organelles. This promotes the formation of a double-membrane vesicle around the organelle known as the autophagosome[42]. The autophagosome will fuse with a lysosome containing hydrolytic enzymes that degrade the engulfed organelles. The autophagy-related (Atg) genes regulates the multi-step process. The most common molecular detection of autophagy is the antibody-based detection of the Microtubule-associated protein 1A/1B-light chain 3 (LC3) gene. This gene is expressed in most cells and is the LC3 protein is cleaved to LC3-I and LC3-II. The latter is localised in the autophagosome membrane and can be detected through immunoblotting to identify autophagy[46-47].

Vitamin D induces autophagy in HL-60 human myeloid leukaemia cells and MCF-7 breast cancer cells by upregulating proteins that inhibit mTOR[11,48]. However, because autophagy can lead to cell death or cell survival, studies must be conducted at varying stages of tumour progression or under varying *in vitro* conditions to conclude how vitamin D treatment can be used in tumour treatments.

1.3.3.3 Necrosis

Necrosis, categorised as type III PCD[31], is defined as the accidental death of cells resulting in disruption of the plasma membrane causing spillage of intracellular proteins, consequently activating host immune response[47]. In contrast to apoptosis, necrosis is a random, uncontrolled and passive process[31].

Necrosis can be detected in cells by assessing the lactate dehydrogenase (LDH) activity[49]. The LDH enzyme is involved in the interconversion of pyruvate and lactate, simultaneously with the oxidation and reduction of nicotinamide adenine dinucleotide (NADH/NAD+)[49]. When necrosis occurs, LDH leaks into the cytosol. Necrosis is an adaptive form of PCD as it can eliminate cell survival and induce an immune response in target cells[43].

1.3.4 Vitamin D metabolising enzymes and receptor in cancer

1.3.4.1 VDR

The vitamin D receptor mediates many effects of $1,25(OH)_2D_3$. The VDR has a short N-terminal domain, followed by a DNA-binding domain with two zinc fingers and an RXR-binding domain. Within these domains lie the ligand and coactivator binding domains[12].

© University of Pretoria

Research findings have shown that the impact of cancer on VDR differs vastly across tissues. It has been hypothesised that VDR expression in cancerous tissues is lower than in healthy tissues. However, treatment with vitamin D metabolites has been shown to increase the expression of VDR in colon, breast and lung cancer cell lines[22].

1.3.4.2 CYP27B1

Vitamin D metabolising system features both classification of cytochrome P450 enzymes (CYPs), microsomal and mitochondrial. These CYP subtypes do not function independently and are part of the electron transport chain[50]. The CYP27B1 is classified as a mitochondrial vitamin D related CYP and is situated on the inner mitochondrial membrane.

Several factors regulate the expression of both renal and extrarenal CYP27B1. Increased parathyroid hormone (PTH), pro-inflammatory cytokines and low calcium upregulate CYP27B1 expression. In contrast, fibroblast growth factor 23 (FGF-23), hyperphosphataemia, and $1,25(OH)_2D_3$ downregulate CYP27B1 gene expression via VDR-mediated action[50].

Although $1,25(OH)_2D_3$ is chiefly synthesised in the kidney, biochemical investigations have shown its expression in extrarenal and cancer tissues. Numerous in vitro studies have shown that the activity of CYP27B1 is lost with increased cancer severity[22]. Hsu et al. demonstrated that $25(OH)D_3$ treatment decreased CYP27B1 activity and growth inhibition in normal and benign prostatic primary cultures[51]. It is suggested that the level CYP27B1 determines the anti-cancer protection action of $25(OH)D_3$[22].

1.2.4.3 CYP24A1

The CYP24A1 enzyme is an inner mitochondrial membrane CYP[50] responsible for neutralising vitamin D activity[52]. The expression and function of CYP24A1 are regulated in a classic negative-feedback loop[50].

It has been hypothesised that CYP24A1 expression is upregulated in cancer compared to normal tissue. Upregulation of CYP24A1 expression has been shown in colorectal, breast, ovarian and lung carcinomas[53-54] suggesting that a feature of advanced cancer is increased catabolism of intracellular $1,25(OH)_2D_3$. Elevated CYP24A1 degrades high $1,25(OH)_2D_3$ intracellular concentrations and thus induces cancer actions[22].

© University of Pretoria

1.4 Cervical cancer

1.4.1 Epidemiology and pathophysiology

Cervical cancer is the fourth most common cancer among females worldwide, with roughly 90% of cases occurring in low- and middle-income countries[55-57]. Approximately 600 000 new cases and over 300 000 deaths from this cancer are reported annually[56]. Cervical cancer is highly treatable when detected in the early stages[58]. However, prevention and management are significantly affected by socio-economic conditions, health care infrastructure and competing illnesses[55]. According to a report by the World Health Organisation, only 62% of countries globally have cervical cancer screening programmes, with under half of them reaching the target populations, further increasing the burden of the disease[57].

Cervical cancer originates in the narrow, muscular opening of the uterus, known as the cervix. The cervix is divided into the ectocervix (stratified squamous epithelial cells) and the endocervix (columnar epithelial cells)[55]. The two regions meet at the "transformation zone," which is believed to be the site of premalignant transformation. The common histological subtypes of cervical cancer that arise are squamous cell carcinoma and adenocarcinomas, accounting for approximately 70% and 25% of all cervical cancers, respectively[56].

The main etiological agent in developing cervical cancer cases is high-risk Human Papillomavirus (HPV)[56,59]. Human papillomaviruses are small double-stranded DNA viruses that can integrate into the host genome due to persistent infection[55]. Invasive cervical cancers are attributed to HPV-16 and HPV-18, which contain transcriptional units E6 and E7 essential for viral replication[59].

In South Africa, cervical cancer is the most frequent cancer among women between 15 and 44 years of age[60]. A cervical cancer diagnosis at an earlier age is due to the burden of HIV infections, which decreases immunity and favours HPV acquisiton[56]. Women infected with HIV have an increased risk of cervical cancer compared to HIV-negative women.

1.4.2 Cervical cancer and vitamin D

Unambiguous evidence has been presented on the anti-cancer effects of vitamin D_3 in various cancers; however, few studies have indicated the direct method by which vitamin D affects cervical cancer. Some patient studies have validated an inverse correlation between UVB irradiation and the incidence rate of cervical cancer and mortality from cervical cancer[10,61].

© University of Pretoria

As previously mentioned, the vitamin D receptor and members of the vitamin D metabolising system play a role in the anti-cancer actions of vitamin D and its metabolites. Investigations by Kloss and colleagues revealed that the human cervical cancer cell line, HeLa, expresses CYP27A1, CYP27B1 and CYP24A1[62] and that treatment with $1,25(OH)_2D_3$ significantly increased gene expression of CYP24A1. Kloss *et al*. also treated HeLa cells with cholecalciferol and $25(OH)D_3$, and their results indicated that both cell lines expressed VDR, which is essential for the expression of the other vitamin D metabolising enzymes. Results also showed that CPY24A1 expression increased 13-fold and 176-fold after 72-hour incubation with 100nM of $1,25(OH)_2D_3$ in HeLa and OVCAR-3 cells, respectively.

Studies *in vitro* studies by our research group have demonstrated a decrease in cell count and cell viability, induction of apoptosis and upregulation of vitamin D metabolising enzymes in SiHa cells after treatment with cholecalciferol[63]. In another study, our research group demonstrated similar results in the CaSki cervical cancer cell line[30].

To date, there is strong evidence for using vitamin D to prevent colon, rectal and breast cancer[14]. It has also been postulated that vitamin D may effectively prevent cancers associated with the bladder, brain, endometrial lining, oesophagus, gallbladder, kidney, lungs, ovaries, pancreas, prostate, and stomach[14]. However, the lack of clinical trials, randomized trial evidence and inconsistent observational research remain challenging to understand vitamin D's potential as an anti-cancer therapeutic, thus limiting its development and use in cancer treatment[12]. One of the underlying research issues is the concern of increasing serum $25(OH)D_3$ to a dangerously high level due to treatment[12]. Hence, further studies are needed to elucidate the effects of vitamin D in the treatment and prevention of cancer. Furthermore, there is insufficient evidence to elucidate the effects of vitamin D on cervical cancer.

1.5 Aim and objectives

1.5.1 Aim

This study aimed to use the cervical cancer cell line, HeLa, treated with $25(OH)D_3$ to investigate the cell growth, cell death and regulation of expression of genes and proteins in the vitamin D metabolising system.

© University of Pretoria

1.5.2 Objectives

The objectives were:

- To determine the concentration of 25(OH)D_3 that causes 50% growth inhibition (GI50) using the crystal violet assay
- To assess cell growth in 25(OH)D_3 treated cells by enumerating cells with crystal violet assay, alamarBlue® assay and the Muse® Cell Cycle assay
- To evaluate biochemical apoptosis using the Muse® Mitopotential assay, the Muse® Annexin V and Dead Cell assay, and the Muse® Caspase-3/7 assay
- To evaluate biochemical markers of autophagic and necrotic cell death using the Muse® autophagy LC3-antibody-based kit and lactate dehydrogenase assay, respectively
- To assess gross morphological and ultrastructural changes using brightfield microscopy and transmission electron microscopy (TEM)
- To evaluate the expression of CYP27B1, CYP24A1, and VDR, vitamin D metabolising mRNA and proteins using the Quantitative reverse transcription Polymerase Chain Reaction (RT-qPCR) and Western blots

© University of Pretoria

Chapter 2

Materials and Methods

2.1 Cell culture

2.1.1 Materials

The human cervical cancer cell line, HeLa, was purchased from the American Type Culture Collection (ATCC® CCL-2™). Dulbecco's Modified Eagle Medium (DMEM) was purchased from Invitrogen (Carlsbad, CA, USA). Glutamine, Pen-strep and 25-hydroxycholecalciferol (Catalogue number: H4014) were purchased from Sigma-Aldrich (St. Louis, MO, USA) and foetal calf serum from Inqaba Biotechnical Industries (Pretoria, South Africa). Sodium chloride, potassium chloride, potassium dihydrogen phosphate, and sodium dihydrogen phosphate were purchased from Alfa Aesar (Haverhill, MA, USA). Disposable cell-culture flasks were purchased from Lasec (Capetown, South Africa).

2.1.2 Thawing cells

HeLa cells were thawed at room temperature and centrifuged for 5 minutes at 200 x g. Cells were resuspended in pre-warmed DMEM and transferred to a 25 mL culture flask containing 4 mL growth medium. The culture flask was incubated in a ASTEC Water Jacket Type incubator (Model: WCI-165, Japan) at 37°C and 5% carbon dioxide (CO_2) until cells reached 90% confluency, at which point seeding was conducted.

2.1.3 Cell seeding and treating

The cells were exposed to 1 mL of trypsin (0.25%) following their washing with 1X phosphate-buffered saline (PBS; pH 7.4; explained in Appendix A) three times. After incubation at 37°C for 2 minutes, detached cells were collected in 2 mL of fresh medium and counted using Trypan Blue and a haemocytometer. Cells were seeded at different concentrations for various assays and incubated overnight before treatment with 25(OH)D_3 at physiological (260 nM) and supraphysiological (5000 nM) concentrations for 72 hours. Solvent (0.5% ethanol, *v/v*) and medium controls were included in all experiments.

© University of Pretoria

2.2 Growth inhibition concentration determination

Growth inhibition of 50% (GI_{50}) refers to the concentration of the drug in the medium, which inhibits cell growth by 50% under standard cell incubation conditions[64]. To determine the GI_{50} concentration of 25(OH)D_3, HeLa cells were seeded at 25 000 cells/mL in a 96-well plate and treated with a serial dilution series of seven concentrations of 25(OH)D_3, with a maximum concentration of 5000 nM. Solvent and medium controls were included. After 72 hours of incubation at 37°C and 5% CO_2, the crystal violet assay (described in section 2.3) was used to determine the GI_{50} concentration, with absorbances read at 570 nm using the ELx800 Universal Microplate Reader (Bio-Tek Instruments Inc., Winooski, VT, USA).

2.3 Crystal violet

2.3.1 Principle of assay

Crystal violet is a triarylmethane dye that binds to and stains ribose-containing molecules. As cells undergo death, they detach from culture plates, which makes crystal violet a useful tool for determining the number of viable cells. The degree of staining is directly proportional to the number of viable cells present[65-66].

2.3.2 Materials and overview of assay

Crystal violet indicator (Catalogue number: C0775), Glutaraldehyde (Catalogue number: G5882) and Triton X-100 (Catalogue number: X100) were purchased from Sigma-Aldrich (St. Louis, MO, USA).

A six-step process was followed in crystal violet experiments to analyse protein extracts from HeLa cell cultures (Figure 2.1).

© University of Pretoria

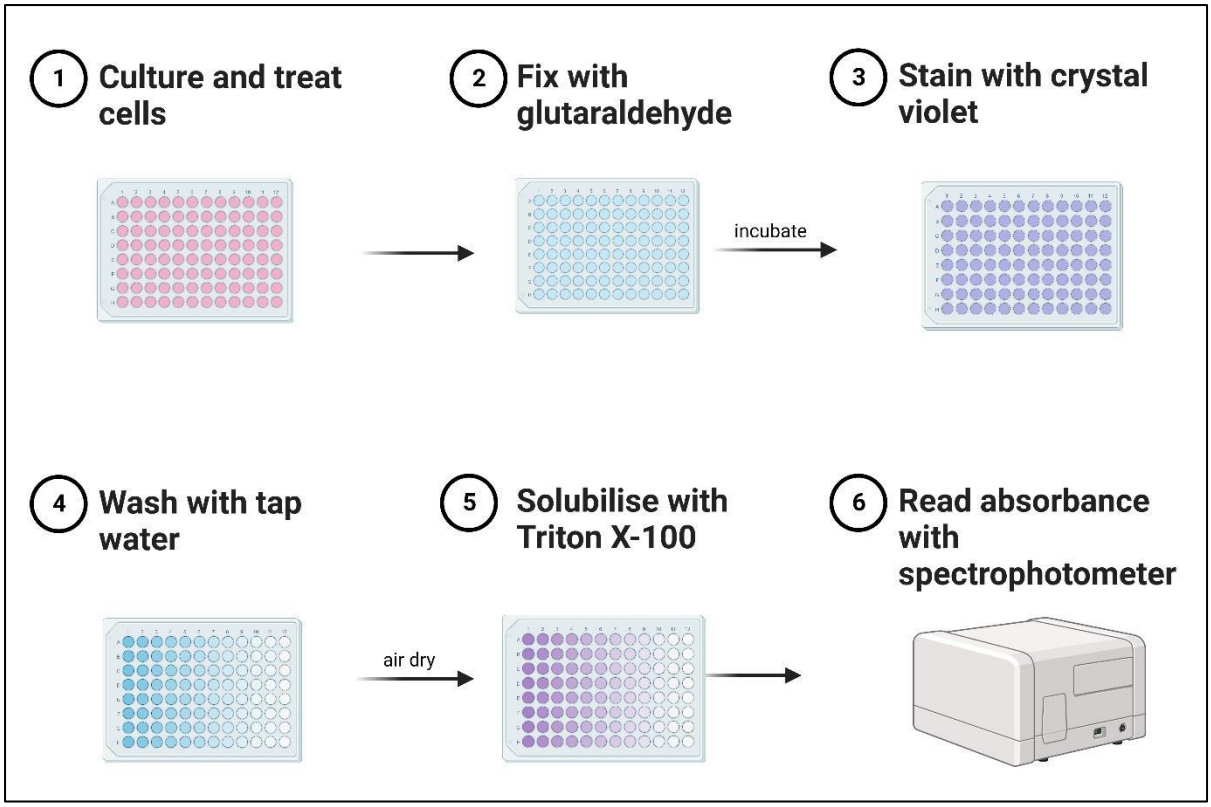

Figure 2.1 **Overview of workflow for crystal violet experiments** (Source: personal collection created with Biorender.com)

2.3.3 Methodology

The assay was conducted following instructions by Feoktiskova *et al.* [65]. Cells were seeded at 25 000 cells/mL in a 96-well plate and treated with 25(OH)D_3 following overnight incubation. After 72 hours of incubation, cells were fixed with 100 µL of 1% glutaraldehyde (Sigma-Aldrich) for 15 minutes at room temperature and stained with 100 µL of 0.1% crystal violet (Sigma-Aldrich) for 30 minutes. Stained cells were washed under running water and air-dried overnight. The stain was solubilised with 200 µL of 0.5% triton X-100 (Sigma-Aldrich). The optical density was measured at 570 nm by the ELx800 Universal Microplate Reader (Bio-Tek Instruments Inc., Winooski, VT, USA).

© University of Pretoria

2.4 AlamarBlue® assay

2.4.1 Principle of the assay

The alamarBlue® reagent uses the reduction-oxidation (REDOX) indicator resazurin, a non-toxic and cell-permeable phenoxazine-3-one dye that acts as an electron acceptor in the electron transport chain[66]. When reduced to resorufin, fluorescence increases and the colour of the cell culture medium changes from blue to red. The fluorescence/absorbance change is measured over 4 hours to determine the metabolic activity of the cells[67].

2.4.2 Materials and overview of assay

The alamarBlue® dye (catalogue number: DAL1025) was purchased from ThermoFisher (Waltham, MA, USA).

A three-step process was followed in alamarBlue® experiments to analyse protein extracts from HeLa cell cultures (Figure 2.2).

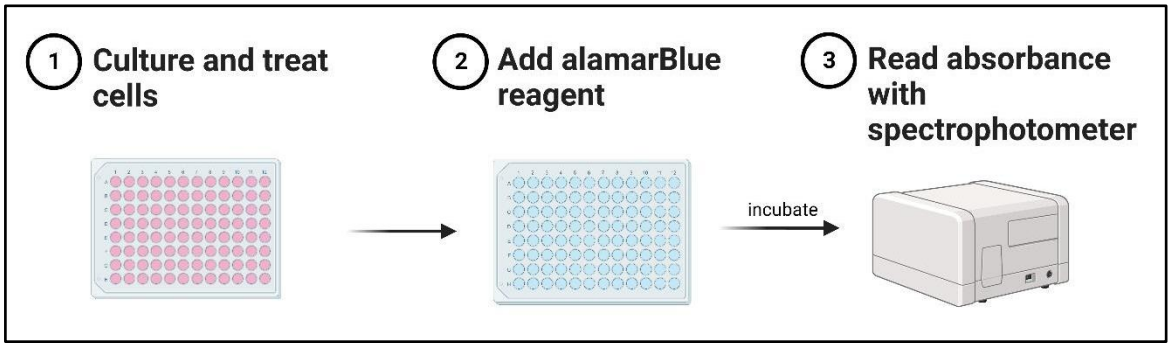

Figure 2.2 **Overview of workflow for alamarBlue® experiments** (Source: personal collection created with Biorender.com)

2.4.3 Methodology

Following the Invitrogen protocol[67], HeLa cells were seeded at a concentration of 25 000 cells/mL in a 96-well plate and treated with 25(OH)D_3 following overnight incubation. After a 72-hour incubation with treatment, the culture medium was replaced with 100 µL of fresh medium and 10 µL alamarBlue®. The 96-well plate was covered with foil and incubated for 4 hours at 37°C and 5% CO_2. Absorbance was measured at 570 nm and 600 nm using the ELx800 Universal Microplate Reader (Bio-Tek Instruments Inc., Winooski, VT, USA). Percentage cytotoxicity was calculated using the following equation:

© University of Pretoria

$$\%\ cytotoxicity\ = \left(\frac{Average\ 600\ nm\ absorbance - 570\ nm\ absorbance}{Avaerage\ (average\ 600\ nm\ absorbance - 570\ nm\ absorbance\ of\ solvent)}\right) \times 100$$

2.5 Cell cycle assay

2.5.1 Principle of the assay

The cell cycle is the fundamental mechanism through which cells grow and divide. To distinguish cells at different stages of the cell cycle, a flow cytometric assay utilising a unique combination of propidium iodide (PI) and RNAse A is employed. Propidium iodide binds to DNA and indicates DNA content. The assay distinguishes cells based on their DNA content, with fluorescence intensity from PI increasing as DNA replication takes place[68].

2.5.2 Materials and overview of assay

Muse™ Cell Cycle Kit (Catalogue Number: MCH100106) was purchased from Merck (Modderfontein, South Africa). Micro pipettor tips and 1.5 mL microcentrifuge tubes were purchased from Lasec (Cape Town, South Africa). Ethanol (96%) was purchased from Sigma-Aldrich (St. Louis, MO, USA).

A six-step process was followed in cell cycle experiments to analyse protein extracts from HeLa cell cultures (Figure 2.3).

© University of Pretoria

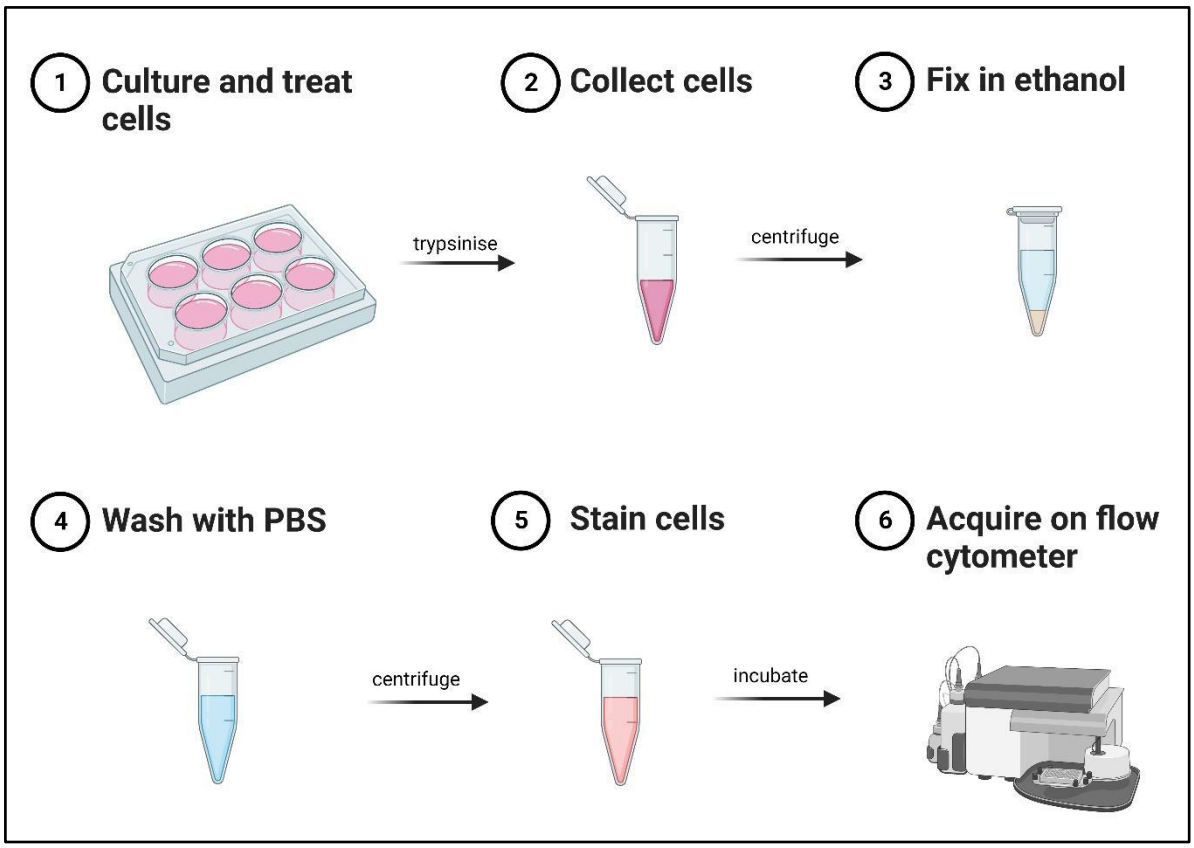

Figure 2.3 **Overview of workflow for cell cycle experiments** (Source: personal collection created with Biorender.com)

2.5.3 Methodology

Following the manufacturer's instructions[68], experimental and control cells were seeded at a concentration of 1 x 10^6 cells/mL. After a 72-hour incubation period with the treatment, cultures were transferred to 50 mL conical tubes and centrifuged at 300 x g for 5 minutes. The supernatants were discarded, and the pellets were re-suspended in 1X PBS (pH 7.4) and gently vortexed. The cells were centrifuged again at 300 x g for 5 minutes, and the supernatant was removed, leaving approximately 50 µL of 1X PBS (pH 7.4) per 1 x 10^6 cells. The cells were re-suspended in the remaining PBS by gentle vortexing and fixed by adding the cell suspension to 1 mL of ice-cold 70% ethanol drop-wise while vortexing at medium speed. The samples were then frozen at -20°C for 3 hours.

To stain the experimental and control cell cultures, 200 µL of the ethanol-fixed cells were pipetted into microcentrifuge tubes, and the cells were centrifuged at 300 x g for 5 minutes. The supernatant was discarded, and the pellets were washed by re-suspending in 1X PBS (pH 7.4) and centrifuging again. The supernatant was discarded, and the cells were re-suspended in 200 µL of Muse™ Cell Cycle Reagent. The samples were incubated at room temperature for

© University of Pretoria

30 minutes and protected from light. The samples were then analysed using the Guava® Muse™ Cell Analyser (Luminex; Austin, TX, USA). The Muse™ software v1.8.0.3 (Windows, Luminex Corporation, Austin, TX, USA) plotted DNA content index vs cell count. The cell populations in the cell cycle's G0/G1, S and G2/M phases were analysed.

2.6 Mitopotential assay

2.6.1 Principle of the assay

This assay aims to identify apoptosis by evaluating modifications in mitochondrial membrane potential. The MitoPotential dye (tetramethylrhodamine ethyl ester, TMRE) discriminates depolarised and non-depolarised mitochondria, whereas the 7-aminoactinomycin D (7-AAD) dye distinguishes live and dead cells[40,69]. The dot plots show the distribution of four cell populations: live, live and depolarised, dead and depolarised, and dead cells.

2.6.2 Materials and overview of assay

A Muse™ MitoPotential Kit (Catalogue Number: MCH100110) containing Muse™ MitoPotential Dye (Part No.4700-1580), Muse™ MitoPotential 7-AAD (Part No. 4700-1585) and 1X Assay Buffer (Part No. 4700-1330) was purchased from Merck (Modderfontein, South Africa). Micropipette tips and microcentrifuge tubes were purchased from Lasec (Cape Town, South Africa).

A six-step process was followed in mitopotential experiments to analyse protein extracts from HeLa cell cultures (Figure 2.4).

© University of Pretoria

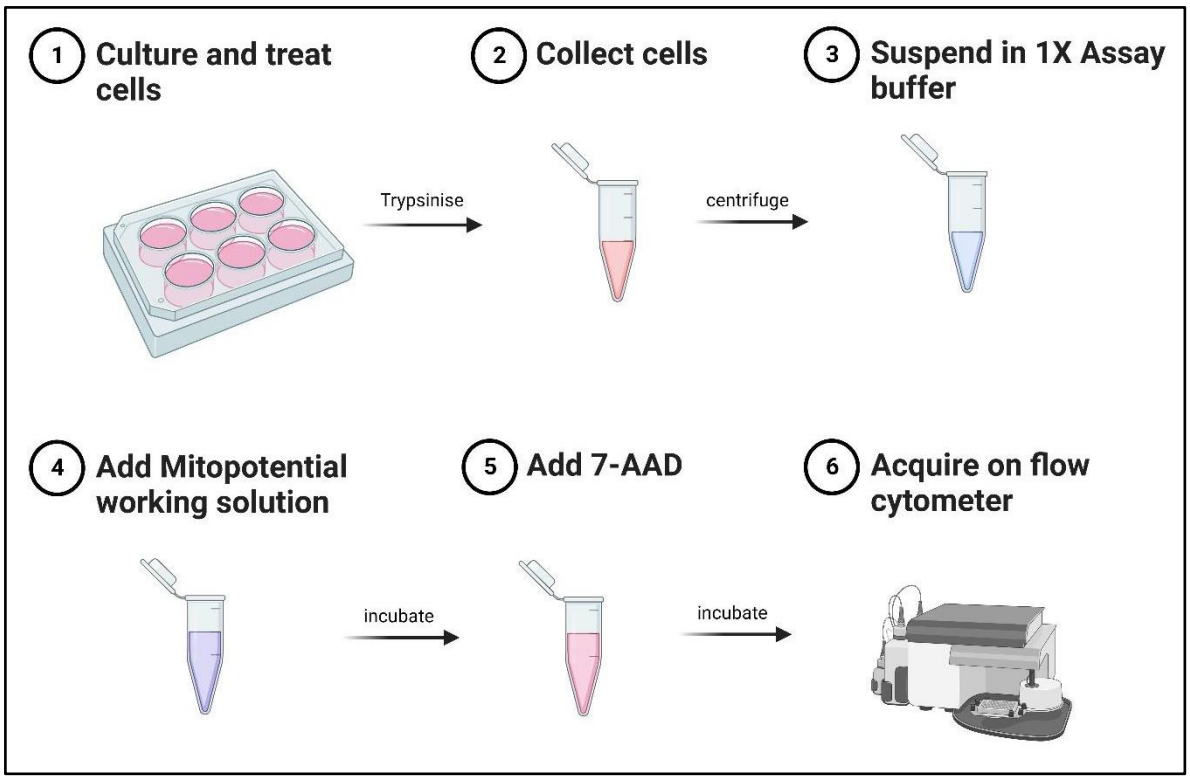

Figure 2.4 **Overview of workflow for mitopotential experiments** (Source: personal collection created with Biorender.com)

2.6.3 Methodology

As instructed by the Muse™ MitoPotential Kit User Guide[69], cells were seeded at a concentration of 1×10^6 cells/mL. Actinomycin D was used as a positive control. The experimental and control cells were trypsinised, collected in DMEM, centrifuged and re-suspended at 1×10^5 cells/mL in 1X Assay Buffer. A working solution was prepared by diluting the Muse™ MitoPotential Dye 1:1000 in 1X Assay buffer. Each sample required 95 µL of the working solution and 100 µL of cell suspension. The cells were incubated for 20 minutes in a 37°C incubator with 5% CO_2. Then 5 µL of Muse™ MitoPotential 7-aminoactinomycin D (7-AAD) reagent was added to each sample and incubated for 5 minutes at room temperature. Cells were analysed using the Guava® Muse™ Cell Analyser. Negative and positive control samples were used for gating to exclude cellular debris. Dot plots of mitopotential vs viability were plotted by the Muse™ v1.8.0.3. software (Windows, Luminex Corporation, Austin, TX, USA).

© University of Pretoria

2.7 Annexin V assay

2.7.1 Principle of assay

The primary goal of this assay is to identify the phase of apoptosis, specifically the early and late stages, by utilising Annexin V. This protein binds to externalised phosphatidylserines in the cell membrane. Additionally, including 7-AAD dye enables the differentiation of live cells from dead cells[70]. The dot plots generated show the distribution of four cell populations, which are live, early apoptotic, late apoptotic and dead, and dead cells.

2.7.2 Materials and overview of assay

Muse™ Annexin V & Dead Cell Reagent (Part No. 4700-1485) was purchased from Merck (Modderfontein, South Africa). Micropipette tips and microcentrifuge tubes were purchased from Lasec (Cape Town, South Africa).

A four-step process was followed in annexin V experiments to analyse protein extracts from HeLa cell cultures (Figure 2.5).

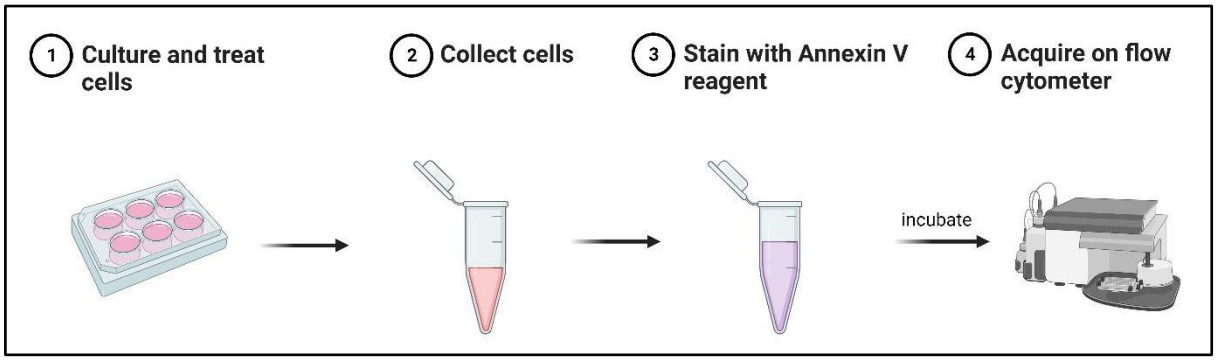

Figure 2.5 **Overview of workflow for annexin V experiments** (Source: personal collection created with Biorender.com)

2.7.3 Methodology

As instructed by the Muse™ Annexin V & Dead Cell Reagent Kit User' Guide[70], cells were seeded at a concentration of 1×10^6 cells/mL. Actinomycin D was used as a positive control. The experimental and control cells were treated with trypsin for 2 minutes to allow for detachment. The trypsin was discarded, and the cells were collected with DMEM. Each sample required 100 µL of the cell suspension and 150 µL of the Muse™ Annexin V & Dead Cell Reagent (warmed to room temperature) mixed by gentle vortexing. The samples were then

© University of Pretoria

incubated at room temperature for 20 minutes, protected from light. Cells were analysed using the Guava® Muse™ Cell Analyser (Luminex; Austin, TX, USA). Negative and positive control samples were used for gating for method quality control, excluding cell debris and standardising plots. The Muse™ software v1.8.0.3(Windows, Luminex Corporation, Austin, TX, USA) plotted dot plots of annexin vs viability.

2.8 Caspase-3/7 assay

2.8.1 Principle of assay

This assay aimed to identify apoptosis by evaluating the activity of terminal caspases -3 and -7, which are detected using the DEVD peptide (amino acid sequence Asp-Glu-Val-Asp). Caspases-3 and -7 are executioner caspases activated in response to various apoptosis inducers. Once activated, the caspases cleave the initially colourless peptide, which results in the release of a fluorescent product[71]. The assay distinguishes between apoptotic and normal cells and live and dead cells[72].

2.8.2 Materials and overview of assay

The Muse™ Caspase-3/7 Kit containing Muse™ Caspase-3/7 Reagent (Part No. 4700-1505,), Muse™ Caspase 7-AAD (Part No. 4700-1510), 1X Assay Buffer BA (Part No. 4700-1360) and 1X PBS (Part No. 4700-1515) was purchased from Merck (Modderfontein, South Africa). Micropipette tips and microcentrifuge tubes were purchased from Lasec (Cape Town, South Africa).

A six-step process was followed in caspase-3 and -7 experiments to analyse protein extracts from HeLa cell cultures (Figure 2.6).

© University of Pretoria

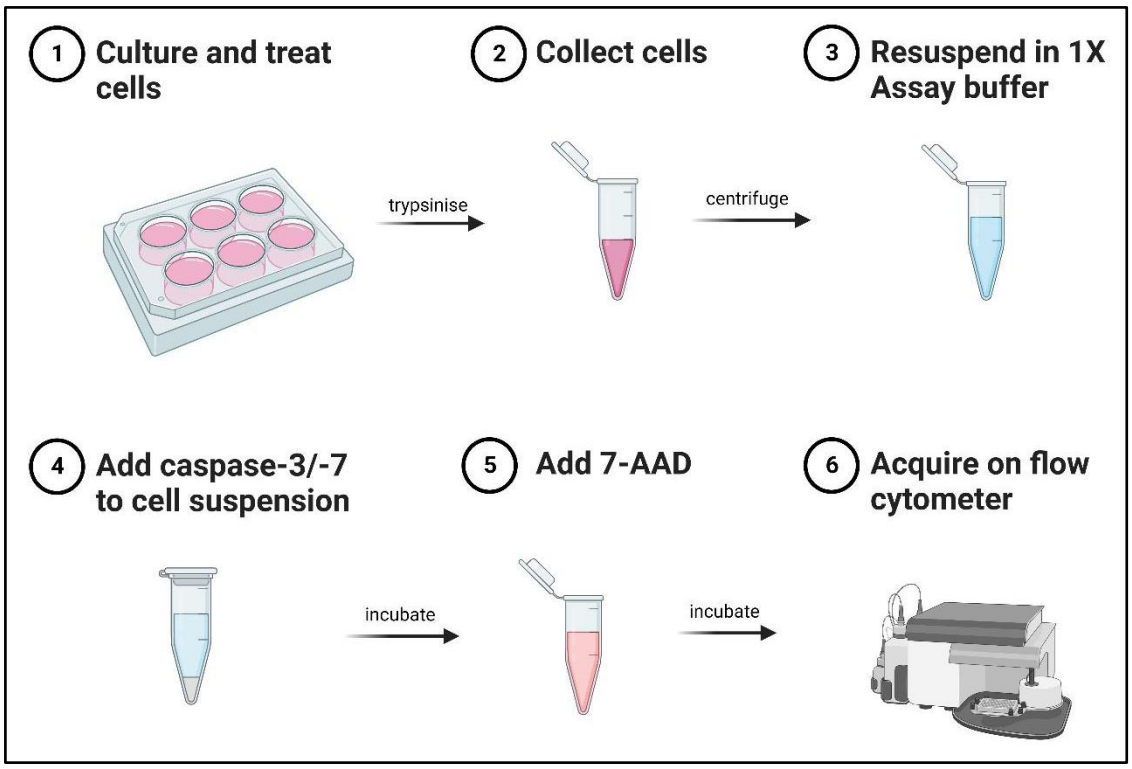

Figure 2.6 **Overview of workflow for caspase-3/-7 experiments** (Source: personal collection created with Biorender.com)

2.8.3 Methodology

As instructed by the manufacturer[72], cells were seeded at a concentration of 1×10^6 cells/mL. Actinomycin D was used as a positive control. The Muse™ Caspase-3/7 Reagent, 1X Assay Buffer BA, 1X PBS (pH 7.4), and Muse™ Caspase 7-AAD were acclimatised to room temperature. A Muse™ Caspase-3/7 Reagent working solution was prepared with 3.1 µL Muse™ Caspase-3/7 Reagent and 21.9 µL 1X PBS. A Muse™ Caspase 7-AAD working solution was prepared with 10 µL Muse™ Caspase 7-AAD and 740 µL 1X Assay Buffer BA. The experimental and control cells were detached from the culture vessel using trypsin and suspended in 1X Assay Buffer BA. Each sample required a mixture of 50 µL of the cell suspension and 5 µL of Muse™ Caspase-3/7 Reagent working solution in microcentrifuge tubes. The caps of the tubes were loosened, and the tubes were incubated for 30 minutes at 37°C and 5% CO_2 in a humidified incubator. After incubation, 150 µL of Muse™ Caspase 7-AAD working solution was added to each tube and mixed with a vortex at medium speed for 5 seconds before incubating at room temperature for 5 minutes, protected from light. Cells were analysed using the Guava® Muse™ Cell Analyser. Negative and positive control samples were used for gating to exclude cellular debris and standardise plots. The Muse™ software

© University of Pretoria

v1.8.0.3 (Windows, Luminex Corporation, Austin, TX, USA) plotted dot plots of caspase-3/-7 vs. viability.

2.9 Autophagy LC3-II assay

2.9.1 Principle of assay

The purpose of this assay is to identify autophagic cells. The assay contains an anti-LC3 mouse monoclonal antibody conjugated to Fluor™ 555, which discriminates between cytosolic LC3-I and autophagosome-associated LC3-II by protecting LC3-II sequestered into the autophagosome during autophagy[73].

2.9.2 Materials and overview of assay

The Muse™ Autophagy LC3-antibody kit containing 20X Anti-LC3 Alexa Fluor™ 555, clone 4E12 (Part No. CS208164), Autophagy Detection Reagent Pack (Part No. CF200093), Autophagy reagent A (Part No. CS208212), Autophagy reagent B (Part No. CS208215), and 5X Assay Buffer (Part No. CS202124) was purchased from Merck (Modderfontein, South Africa). Microcentrifuge tubes were purchased from Lasec (Cape Town, South Africa).

A six-step process was followed in autophagy LC3-II experiments to analyse protein extracts from HeLa cell cultures (Figure 2.7).

© University of Pretoria

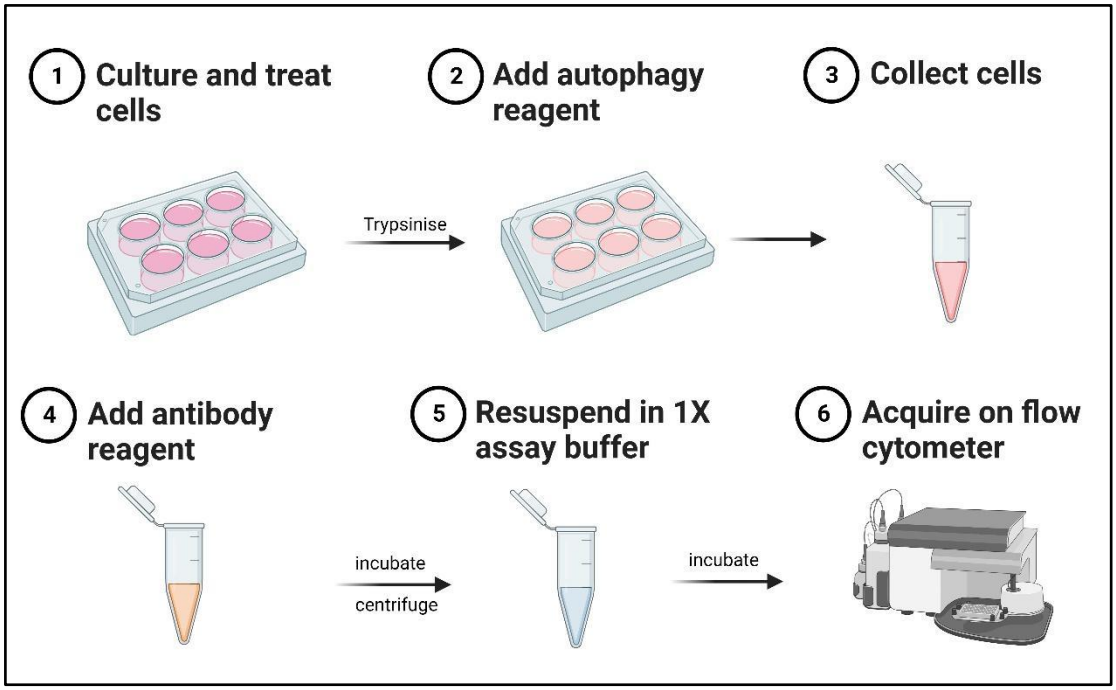

Figure 2.7 **Overview of workflow for autophagy LC3-II experiments** (Source: personal collection created with Biorender.com)

2.9.3 Methodology

Following the manufacturer's instructions[73], cells were seeded at a concentration of 1×10^6 cells/mL. Rapamycin was used as a positive control. Experimental and control cells were washed once with 1X Hank's Balanced Salt Solution (HBSS). The medium was then replaced with a solution of 200 µL of EBSS and 0.2 µL Autophagy Reagent A (1:1000 dilution) and was incubated at 37°C for 2-6 hours to induce autophagy under starvation conditions. After the 2-6 hours of incubation treatment, the wells were aspirated to remove culture supernatants and washed with 1X HBSS. To detach cells from the surface of the plate, 100 µL of Accutase was added for 5 minutes at 37°C. The cells were transferred to Eppendorf tubes, and 100 µL 1X HBSS was added to each sample tube. The sample tubes were spun down at 300 x g for 5 minutes at 4°C, and the supernatant was discarded. 5 µL of Anti-LC3 Alexa Fluor™ 555 and 95 µL of 1X Autophagy Reagent B were added to each sample tube. The sample tubes were incubated on ice for 30 minutes and protected from light. The sample tubes were spun down again at 300 x g for 5 minutes at 4°C. The supernatant was discarded, and the cells were washed with 1X Assay Buffer. The samples were re-suspended in 200 µL 1X Assay Buffer, analysed immediately by Muse™ and evaluated with the Muse™ v1.8.0.3. software (Windows, Luminex Corporation, Austin, TX, USA) to ensure that event counts per µL do not exceed 800.

© University of Pretoria

The software developed plots of LC3 intensity vs cell count that indicate the distribution of autophagy induction.

2.10 Lactate dehydrogenase assay

2.10.1 Principle of assay

The lactate dehydrogenase assay was used to determine the presence of necrotic cells. One key feature of necrotic cells is the permeabilization of the plasma membrane, releasing intracellular contents into the extracellular milieu. Lactate dehydrogenase (LDH) is a cytoplasmic enzyme that catalyses the oxidation of lactate to pyruvate while simultaneously reducing nicotinamide adenine dinucleotide (NAD+) to NADH. When NADH is in the presence of the electron acceptor, 2-p-iodophenyl-3-p-nitrophenyl-5-phenyl tetrazolium chloride (INT), a tetrazolium salt, is converted to INT formazan, a colourful compound[66,74]. The colour change is detected with spectrophotometry.

2.10.2 Materials and overview of assay

Acetic acid, DL-Lactic Acid, 2-p-iodophenyl-3-p-nitrophenyl-5-phenyl tetrazolium chloride (INT), N-methylphenazonium methyl sulphate (PMS), nicotinamide adenine dinucleotide (NAD), Tris buffer, and Triton X-100 were purchased from Sigma-Aldrich (St. Louis, MO, USA). The 96-well culture plates and micropipette tips were purchased from Lasec (Capetown, South Africa).

A four-step process was followed in lactate dehydrogenase experiments to analyse protein extracts from HeLa cell cultures (Figure 2.8).

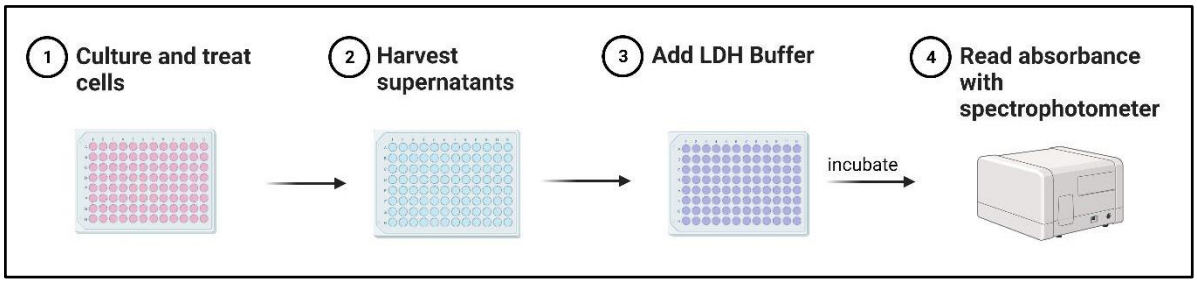

Figure 2.8 **Overview of workflow for Lactate dehydrogenase experiments** (Source: personal collection created with Biorender.com)

© University of Pretoria

2.10.3 Methodology

Following the protocol by Chan *et al.* [74], 5000 cells in 100 µL of culture medium were seeded per well in a sterile 96-well cell culture plate, also considering experimental controls; maximum LDH release, Medium alone and volume correction control. Cells were incubated for 12 hours before treatment and then cultured in a 37°C incubator with 5% CO_2. To the maximum LDH release and volume correction control wells, 10 µL of 10X lysis solution (Appendix B) was added, and the plate was incubated for 45 minutes in a 37°C incubator with 5% CO_2. The 96-well plate was centrifuged for 5 minutes at 200 x g. A multi-channel pipette was used to transfer 50 µL of the culture supernatant to a new 96-well plate, taking care not to transfer any cell materials. The 2X LDH assay buffer was reconstituted, and 50 µL was added to the supernatants. The samples were mixed by gently shaking the plate for 30 seconds. The plate was then incubated at room temperature for 30 minutes, protected from light, before mixing 50 µL of 1M acetic acid into each well. The optical density (OD) was measured at 490 nm using the ELx800 Universal Microplate Reader (Bio-Tek Instruments Inc., Winooski, VT, USA). The percentage cytotoxicity was calculated using the following equation:

$$\%\, cytotoxicity = 100 \times \frac{corrected\ OD\ from\ Test\ well - corrected\ OD\ from\ untreated\ well}{corrected\ maximum\ LDH\ release\ control - corrected\ OD\ from\ untreated\ well}$$

2.11 Haematoxylin and eosin stain

2.11.1 Principle of assay

Haematoxylin and eosin (H&E) staining assessed the gross morphological changes of 25(OH)D_3-treated HeLa cells. Haematoxylin dye is basic, and when conjugated with an aluminium salt, it stains the acidic structures of the cell, such as the nucleus, blue. Eosin dye is an acidic dye and is used as a counterstain. It stains the basic structures of the cell, such as the cytoplasm, pink[75].

2.11.2 Materials and overview of assay

Microscope slides and coverslips were purchased from Lasec (Capetown, South Africa). Bouin's fixative was purchased from Sigma-Aldrich (St. Louis, MO, USA). Mayer's

© University of Pretoria

haematoxylin solution, Eosin, Xylol and Entellan mounting fluid were purchased from Merck (Modderfontein, South Africa).

A six-step process was followed in haematoxylin and eosin staining experiments to analyse protein extracts from HeLa cell cultures (Figure 2.9).

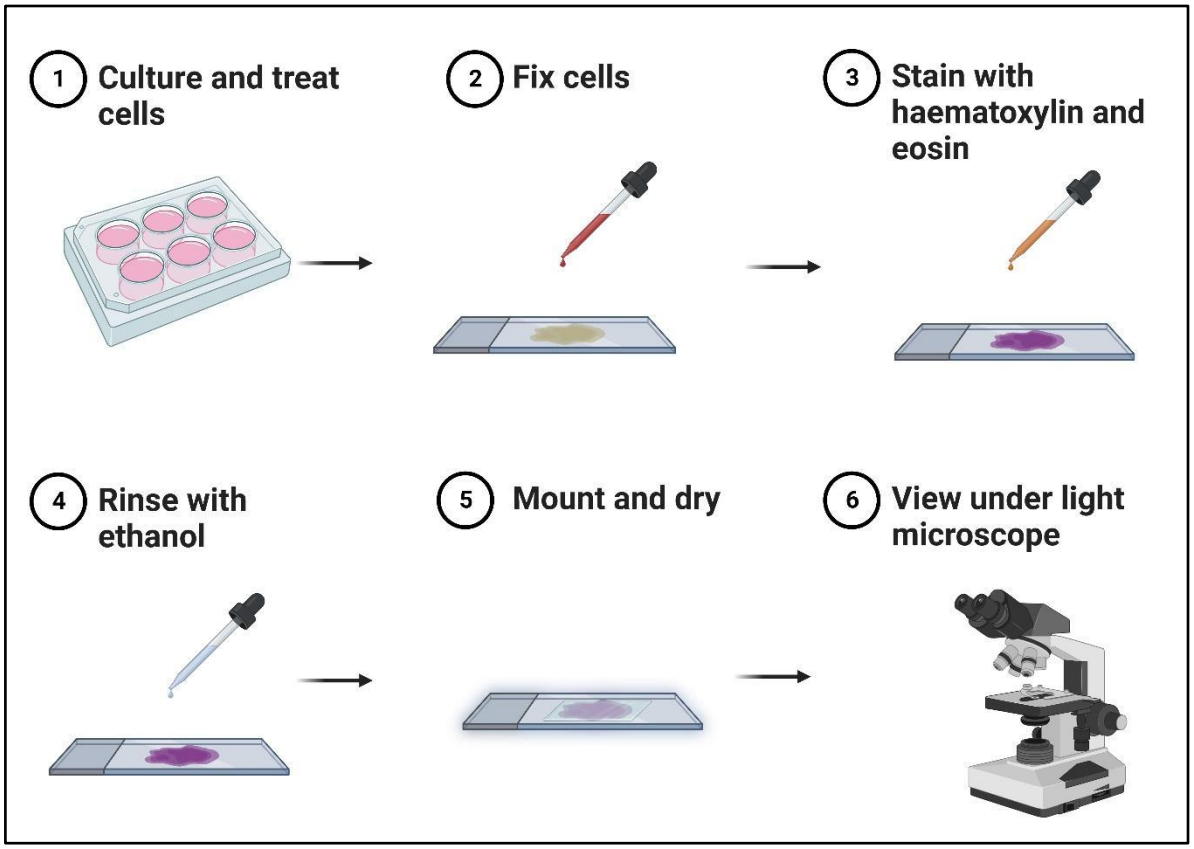

Figure 2.9 **Overview of workflow for haematoxylin and eosin experiments** (Source: personal collection created with Biorender.com)

2.11.3 Methodology

The protocol was adapted from Ausubel *et al.*[76] and Conn *et al.* [77]. Cells were seeded onto glass coverslips in a 6-well plate at a seeding density of approximately 5×10^4 cells per well in 3 mL of growth medium. The coverslips were gently rinsed with 1X PBS and then fixed with 500 µL Bouin's fixative for 30 minutes. The fixative was discarded and replaced with 500 µL 70% ethanol for 20 minutes. The coverslips were rinsed with tap water and left in Mayer's Hemalum for 20 minutes. The coverslips were rinsed using running tap water for 2 minutes, followed by 70% ethanol. The cells were stained with 500 µL 1% eosin for 7 minutes. The coverslips were rinsed with 70% ethanol, 95% ethanol, 100% ethanol and xylol, successively for 5 minutes each. This process was repeated once. The coverslips were mounted to microscope slides with

© University of Pretoria

resin and left to dry. The samples were viewed, and images were captured using an Olympus DP74 camera. Cells were counted, measured, and analysed for gross morphological changes using ImageJ 1.53e (Java 1.8.0_172; National Institutes of Health, USA).

2.12 Transmission electron microscopy

2.12.1 Principle of assay

The purpose of this experiment is to assess the ultrastructural features of 25(OH)D_3-treated HeLa cells to identify features of cell death. Transmission electron microscopy allows the visualisation of specimen electrons to pass through the specimen, revealing ultrastructural features[78].

2.12.2 Materials and overview of assay

Agar resin (product number: AGR1045), Araldite resin (product number: AGR1042), HAZ Benzyl Dimethylamine (product number: AGR1062), Dodecyl Succinic Anhydride EM grade redistilled (product number: AGR1053), UA-Zero® EM Stain (product number: AGR1000), HAZ Lead Citrate (product number: AGR1210-25) and Agar Grids 300 Mesh Copper 3.05mm (product number: AGG2300C) were purchased from Wirsam Scientific and Precision Equipment (Pty) Ltd. (Johannesburg, South Africa).

An eight-step process was followed in transmission electron microscopy experiments to analyse protein extracts from HeLa cell cultures (Figure 2.10).

© University of Pretoria

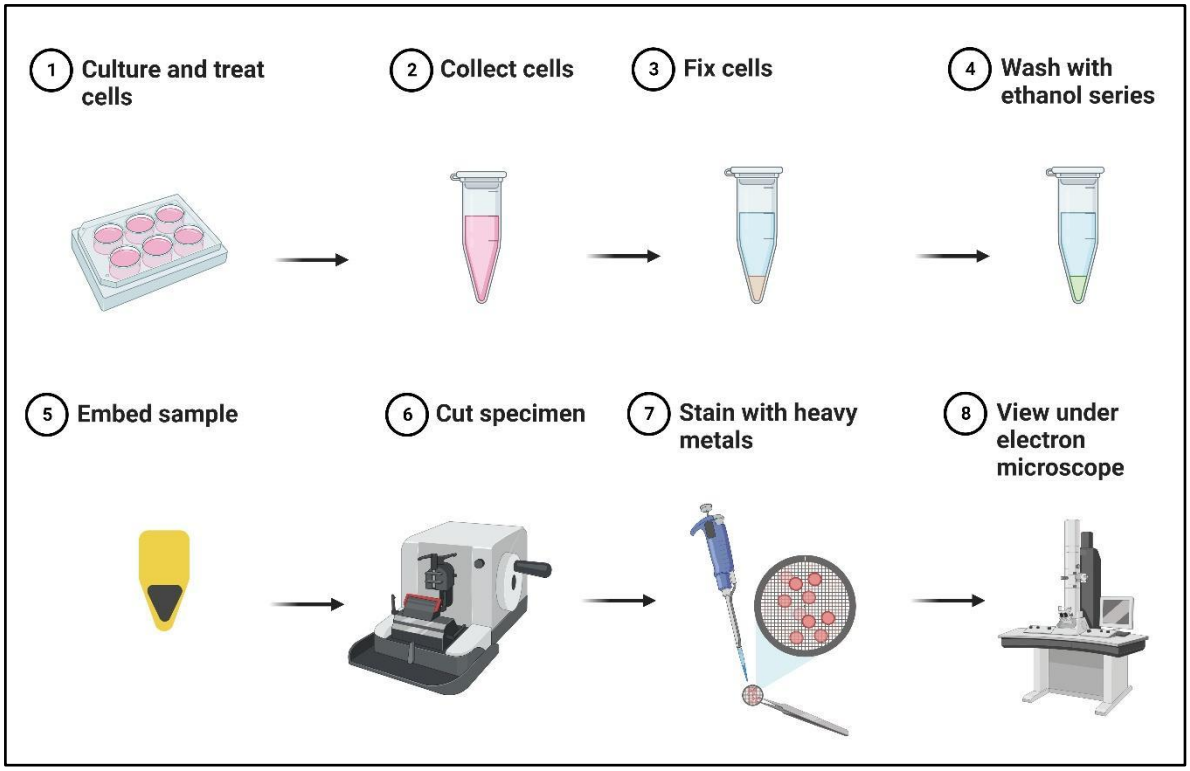

Figure 2.10 **Overview of workflow for transmission electron microscopy experiments** (Source: personal collection created with Biorender.com)

2.12.3 Methodology

The protocol for electron microscopy from the Anatomical Pathology department of the University of Pretoria was used, adapted from Weakley[79]. Treated cells were washed with 1X PBS and collected in Eppendorf tubes, suspended DMEM, after trypsinisation. The cells were centrifuged for 3 minutes at 300 x g, the supernatant was discarded, and cells were washed with 1 ml of 1X PBS (pH 7.4) and centrifuged.

The supernatant was discarded and replaced with 10 drops of Palade's fixative (Appendix C) for 1 hour of incubation at room temperature. The fixative was removed and replaced with 10 drops of 50% alcohol for 15 minutes. This step was repeated using 70% alcohol. After removing the 70% alcohol, 96% alcohol was added for 30 minutes, followed by two 30-minute incubations with 100% alcohol. Propylene oxide was added for 30 minutes, after which a 50/50 mixture of propylene oxide and embedding medium (Appendix C) was added for 90 minutes. The cells were centrifuged for 3 minutes and then transferred to gelatine capsules. 100% embedding media was added to the capsules, and they were placed in a 65°C oven overnight to allow the media to harden.

© University of Pretoria

Excess embedding media was cut from the edges of the capsule using a blade. Thin golden slices (50 nm) were cut with a Reichert-Jung Ultracut ultramicrotome. The slices were collected on Agar Grids 300 Mesh Copper discs (Wirsam Scientific) and stained with UA-Zero® EM Stain (Wirsam Scientific) for 1 hour, followed by lead citrate (Wirsam Scientific) for 3 minutes. The specimens were viewed using a camera from JEOL Ltd. (Tokyo, Japan) at the Veterinary campus of the University of Pretoria. The images were analysed qualitatively for ultrastructural changes.

2.13 Quantitative Reverse Transcription Polymerase Chain Reaction (RT-qPCR)

2.13.1 Principle of assay

The expression VDR, CYP27B1 and CYP24A1 genes were assessed using real-time reverse transcription polymerase chain reaction. The cells are lysed, and total RNA is extracted, synthesised to complementary deoxyribonucleic acid (cDNA) and amplified with PCR. Real-time reverse transcription polymerase chain reaction (RT-qPCR) uses fluorescent dyes to measure the amount of DNA produced during each cycle of the reaction[80].

2.13.2 Materials and overview of assay

The iScript™ cDNA Synthesis Kit (Catalogue number: 1708891), iTaq™ Universal SYBR Green (Catalogue number: 1725120) and TubeONE microcentrifuge tubes were purchased from Lasec (Capetown, South Africa). Sterile pipette tips, thin-walled cap tubes, and Lab mark PCR-grade water were purchased from Celtic Molecular Diagnostics (Capetown, South Africa). Qiazol lysis reagent and the Rotor gene were purchased from Whitehead Scientific (Lethabong, South Africa).

A four-step process was followed in PCR experiments to analyse protein extracts from HeLa cell cultures (Figure 2.11).

© University of Pretoria

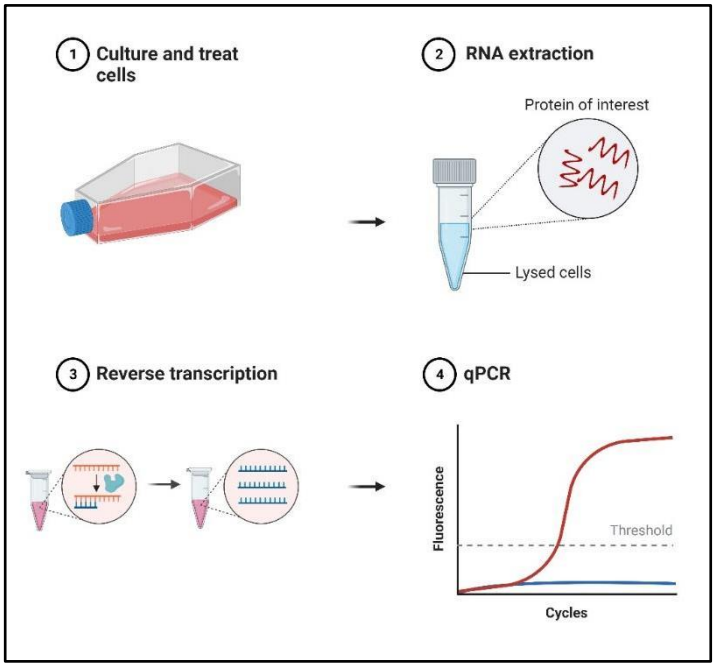

Figure 2.11 **Overview of workflow for PCR experiments** (Source: personal collection adapted from Biorender.com)

2.13.3 Methodology

Cells were cultured and treated on a 25cm^2 flask. Total RNA was extracted and quantified following a protocol by Chomczynski and Sacchi[81]. The experimental and control cell cultures were washed with cold PBS. About 500 µL of Qiazol lysis reagent was pipetted into each flask. The flasks were then incubated on ice for 5 minutes. Cells were then scraped off the flasks, and the residue was transferred to 1.5 mL tubes. The tubes were then frozen for 1 hour at -80 ºC. After thawing the samples, 100 µL of chloroform was added, and the samples were vigorously shaken for 1 second to mix. Samples were incubated at room temperature for 3 minutes and then centrifuged at 4 ºC for 15 minutes at 12 000 x g. Centrifuging separated samples into layers of RNA, DNA, and cellular debris. Then 250 µL of the RNA was transferred to a clean, sterile 1.5 mL tube and stored on ice. To each 1.5 mL tube, 250 µL of isopropanol was added, and the tubes were flicked to mix. The samples were incubated at -80 ºC for 1 hour. The samples were then centrifuged at 12000 x g for 20 minutes at 4 ºC, and the supernatant was discarded. The pellet was washed with 500 µL of cold 75 % ethanol and centrifuged at 7400 x g for 15 minutes at 4ºC. The ethanol was discarded, and the pellet was allowed to air dry for 5 minutes before re-suspending in 15 µL of nuclease-free water. The samples were incubated at room temperature for 3 minutes and then placed on ice. The RNA was quantified using an Optizen

© University of Pretoria

NanoQ™ (KLAB Keen Innovative Solutions, Daejeon, Republic of Korea). The total RNA was stored at -80ºC.

The total RNA extracted from experimental and control cultures was used to synthesise cDNA following the optimised iScript™ Reverse Transcription Supermix for RT-qPCR kit guidelines (Bio-Rad)[82]. All total RNA samples were normalised to a concentration of 400 ng/µL in a total volume of 10 µL. This 10 µL of RNA was mixed with 4 µL of 5x iScript™ RT Supermix and 6 µL nuclease-free water in a PCR tube to make a 20 µL reaction mixture. The PCR tubes were incubated in a Rotor-Gene Q thermal cycler (QIAGEN, Hilden, Germany). Thermal cycling followed the protocol: priming for 5 minutes at 25ºC, reverse transcription (RT) for 20 minutes at 26ºC, RT inactivation for 1 minute at 95ºC and a hold step at 4 ºC. The synthesised cDNA was then diluted with 40 µL of nuclease-free water. The cDNA was then aliquoted and stored at -80ºC.

The cDNA was amplified using the iTaq™ Universal SYBR® Green Supermix kit from BioRad[83]. The iTaq™ Universal SYBR® Green Supermix and cDNA were thawed to room temperature and centrifuged before storing on ice, protected from light. Reaction mixtures containing 5 µL of iTaq™ Universal SYBR® Green Supermix, forward and reverse primers (design in Appendix D) and nuclease-free water were prepared in qPCR tubes, on ice, for all qPCR reactions based on previously determined reaction conditions (Appendix D). The reaction mixtures were mixed by vortexing ensure homogeneity before adding the cDNA of experimental and control samples. A no template control, no reverse transcriptase control and 18S housekeeping gene control were also prepared on ice. The qPCR tubes were then sealed and vortexed for 30 seconds to mix and remove all bubbles in the samples. Amplification was conducted using the Rotor-Gene Q thermal cycler (QIAGEN, Hilden, Germany) programmed according to the following protocol: Polymerase activation and DNA denaturation at 95ºC for 30 seconds; Amplification: Denaturation at 95ºC for 5 seconds, Annealing, extension and reading for 30 seconds, for 40 cycles; Melt curve analysis: 65-95ºC in 0.5ºC increments at 5 seconds per step. Annealing temperatures for each primer set can be found in Appendix D. Amplification and melt curves were obtained and used to assess the specificity of the primers. The fold change in gene expression was determined using the delta-delta Ct method.

© University of Pretoria

2.14 Western blot

2.14.1 Principle of assay

Protein expressions of VDR, CYP27B1, and CYP24A1 were measured using Western blotting. Total protein was extracted from cells and separated by size using gel electrophoresis. The proteins are then transferred or blotted to a second matrix where they can be probed for proteins of interest using enzyme-labelled antibodies[84].

2.14.2 Materials and overview of assay

M-PER™ Mammalian Protein Extraction Reagent (Catalogue number: 78501), EDTA-free Halt™ Protease Inhibitor Cocktail (Catalogue number: 87785), Pierce™ Bicinchoninic acid (BCA) protein assay kit (Catalogue number: 23227), 4X NuPAGE™ Lithium dodecyl suphate (LDS) Buffer (Catalogue number: NP0008), NuPAGE™ 4-12% Bis-Tris protein gels (Catalogue number: NP0321PK2) and Clarity™ Western ECL Substrate (Catalogue number: 1705061) were purchased from ThermoFisher (Waltham, MA, USA). Methanol (Catalogue number: 34860) was purchased from Merck (Modderfontein, South Africa). Tween 20, 2-Mercaptoethanol (Catalogue number: M6250), and β-actin antibody were purchased from Sigma-Aldrich (St. Louis, MO, USA). Bovine serum albumin (BSA) was purchased from Inqaba Biotech (Pretoria, South Africa). Filter paper, Precision Plus Protein™ Dual Colour Standards (Catalogue number: 1610374), Western blot chemiluminescent substrate, 20X MOPS running buffer (Catalogue number: 161-0788), 10X Tris/Glycine buffer (Catalogue number: 1610734) and Immun-Blot® polyvinylidene fluoride (PVDF) membranes (Catalogue number: 1620177) were purchased from Lasec (Cape Town, South Africa). Anti-rabbit IgG, monoclonal (CYP27B1, Catalogue number: ab206655), Anti-rabbit IgG, polyclonal (CYP24A1, Catalogue number: ab175976) and Goat anti-rabbit IgG, HRP Conjugated (Elabscience, Catalogue number: E-AB-1003) were purchased from Biocom Africa (Centurion, South Africa). Anti-rabbit IgG, HRP-linked antibody (VDR) was purchased from Anatech (Randburg, South Africa).

A six-step process was followed in Western blot experiments to analyse protein extracts from HeLa cell cultures (Figure 2.12).

© University of Pretoria

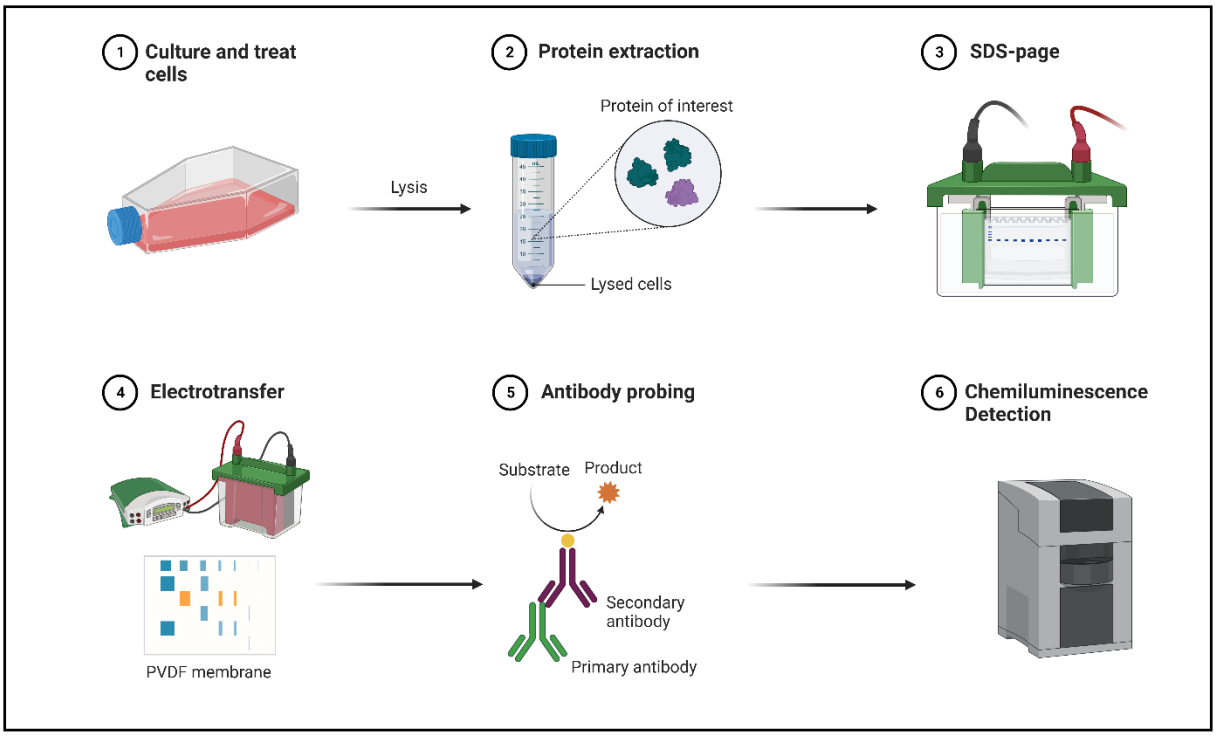

Figure 2.12 **Overview of workflow for Western blot experiments** (Source: personal collection adapted from Biorender.com)

2.14.3 Methodology

Western blot experiments were conducted according to the Abcam Western Blot protocol[85]. Cells were seeded at a concentration of 100000 cells/mL in a 6-well plate. After 72 hours of incubation with the treatment, experimental and control cultures were washed twice with ice-cold 1X PBS (pH 7.4). After washing, cells were incubated with 500 µL of M-PER™ Mammalian Protein Extraction Reagent (ThermoFisher) and 100x EDTA-free Halt™ Protease Inhibitor Cocktail (ThermoFisher) at a ratio of 100:1 on ice for 5 minutes. The cells were then scrapped off the plates with plastic cell scrapers and were transferred to pre-cooled 1.5 mL tubes. Cells were then centrifuged at 4°C for 20 minutes at 14000 x g. The lysate was removed, placed in clean 1.5 mL tubes, and kept on ice.

The total protein extracted in the lysate was quantified using the Pierce™ BCA protein assay kit (Thermo Fisher, Catalogue number: 23227) as described by the manufacturer[86]. A BCA working reagent (WR) solution was prepared and divided into 2 mL aliquots. 100 µL of the experimental and control lysates were added to the BCA WR. The samples were mixed and then incubated in a 60°C water bath for 30 minutes. Samples were then cooled to room temperature, and 200 µL of each sample was transferred to a 96-well plate. The optical density

© University of Pretoria

was measured at 562 nm using an ELx800 Absorbance Reader (BioTek Instruments Inc., Vermont, United States of America). Bovine serum albumin (BSA) reference standards, ranging from 5-250 µg/mL, were used to generate a standard curve for determining the protein concentration of each lysate. The remaining lysates were aliquoted and stored at -80°C.

The protein concentrations were standardised to 20 µg using M-PER Mammalian Protein Extraction Buffer. To each sample, 6.3 µL of 4X NuPAGE™ LDS Buffer (ThermoFisher) and 0.626 µL 2-Mercaptoethanol (Sigma-Aldrich) were added. The samples were then denatured on a 95°C hot plate for 7 minutes. The samples were allowed to cool to room temperature before loading 20 µL into the wells of a NuPAGE™ 4-12% Bis-Tris protein gel, starting at the second well. The first well was loaded with 5 µL of the Precision Plus Protein™ Dual Colour Standards (Bio-Rad). The gel was loaded into an Invitrogen™ XCell SureLock™ Mini-Cell and XCell II™ Blot Module, which was then filled with 1X XT MOPS running buffer (Bio-Rad). A current of 200 volts was applied to the system for 80 minutes.

After running the gel, the proteins were transferred to an Immun-Blot® PVDF Membrane (Bio-Rad) using the wet transfer sandwich method. Before transfer, the PVDF membrane was activated in methanol (Merck), whilst the sponges and filter paper were soaked in 1X Tris/Glycine buffer (Bio-Rad). The transfer sandwich was assembled (Appendix E) and placed in a Mini Trans-Blot® Electrophoretic Transfer Cell. The system was covered in ice and placed in a walk-in fridge. A current of 110 volts was applied to the system for 90 minutes.

Once the transfer was complete, the PVDF membrane was gently washed with deionised water and then blocked with 5 ml of 0.2% PBS Tween and 2.5% BSA for 1 hour at room temperature. The membrane was then washed three times with 0.2% PBS Tween. The membrane was incubated with primary antibody (anti-rabbit IgG VDR, anti-rabbit IgG CYP27B1 and anti-rabbit IgG CYP24A1) overnight at 4°C (Appendix F). The membrane was then washed three times with 0.2% PBS Tween before incubating with the secondary antibody, HRP Conjugated Goat anti-rabbit IgG (Appendix F), for 1 hour at room temperature. The membrane was washed thrice with 0.2% PBS Tween before viewing with the ChemiDoc™ MP System (Bio-Rad, Catalogue number 1708280).

To enhance viewing, an 800 µL 1:1 dilution of the Clarity™ Western ECL Substrate (Bio-Rad) was added to the membrane before viewing. The membrane blot was analysed semi-quantitively using the Image Lab™ v6.1 software (Windows, Bio-Rad, Hercules, CA, USA).

© University of Pretoria

The membrane was then washed with 0.2% PBS Tween and stained with the loading control, anti-β-actin (Appendix F), to check the specificity and effectiveness of the transfer.

The membrane was stripped and re-probed with a different antibody (VDR, CYP27B1 and CYP24A1). The membrane was incubated twice with 5 mL of stripping buffer (Appendix G), with agitation, at room temperature for 10 minutes. The membrane was then washed twice with 1X PBS (pH 7.4) for 10 minutes each, followed by two washes with 0.2% PBS Tween for 5 minutes each. The membrane was blocked, and the antibody staining process was repeated.

2.15 Statistics

Raw data was captured using Microsoft Excel (Microsoft), and statistical analysis was performed with GraphPad Prism v9.4.1 (GraphPad Software, San Diego, California, USA). At least three biological and three technical repeats were conducted for each experiment. All data are expressed as mean ± standard error of the mean (SEM). Statistical variations in means were tested using the one-way analysis of variance (ANOVA) test and the *post hoc* Bonferroni test. $p \leq 0.05$ was considered significant.

Qualitative data for microscopy were analysed using ImageJ (Java 1.8.0_172, Windows, National Institutes of Health, USA) and Western blots using Image Lab™ v6.1 software (Windows, Bio-Rad, Hercules, CA, USA).

© University of Pretoria

Chapter 3

Results

3.1 Determining growth inhibition concentration of 25(OH)D_3 in HeLa cells

The GI_{50} is defined as the concentration where cells are reduced by 50% from their initial value, and this can be determined through colorimetric assays[64]. A growth inhibition curve was constructed using the crystal violet assay in order to determine the treatment concentrations for assessing the anti-cancer actions of 25(OH)D_3 on HeLa cells.

The cells were subjected to incubation for 72 hours after treatment with 10-fold dilutions of 25(OH)D_3 in the range of $5.0x10^{-6}$ to $5.0x10^{-13}$ M The resulting cell numbers were used to calculate the percentage growth inhibition. A non-linear best fit line revealed that the highest treatment dose of $5.0x10^{-6}$ M (5000 nM) 25(OH)D_3 inhibited HeLa cell growth by 20% (Figure 3.1). The lowest treatment dose of $5.0x10^{-13}$ M inhibited the growth of HeLa cells by approximately 4%. The supraphysiological concentration of 5000 nM was selected for treatment and used in all subsequent assays. A second treatment dosage, 260 nM, in the physiological range of 25(OH)D_3, was also used for comparison in all subsequent assays. This physiological concentration resulted in approximately 12% growth inhibition.

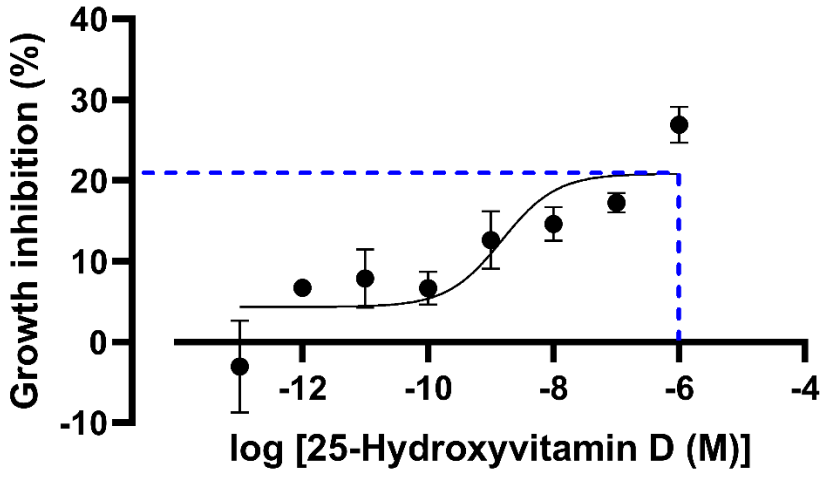

Figure 3.1 Growth inhibition of HeLa cells with various concentrations of 25(OH)D_3. HeLa cells were treated with a series of concentrations of 25(OH)D_3, and a growth inhibition curve was constructed from crystal violet assay results. Data are presented as mean±SEM. The blue dashed line indicates 20% growth inhibition.

© University of Pretoria

3.2 Cell count determination using the crystal violet assay

Cell count was assessed using the crystal violet assay. Crystal violet is an organic chloride salt that binds to the protein and DNA of cells[87]. During cell death, adherent cells detach from the surface of cell culture plates and are washed away, leaving live cells attached to the culture plates[65]. The live cells are stained with the crystal violet dye, and the absorbance values are read with a spectrophotometer. The absorbance is directly proportional to the cell number.

Significant decreases in cell number were observed with 5000 nM 25(OH)D_3 treatment (82.05%±1.758%) relative to the solvent control (101.0%±1.691%, $p<0.0001$) and to the medium control (100.7%±2.048%, $p<0.0001$). Significant reductions in cell number were also observed at the 260 nM treatment dose (90.64%±1.448%) compared to the medium ($p=0.0023$) and solvent ($p=0.0016$) controls and to the 5000 nM treatment ($p=0.0257$) (Figure 3.2).

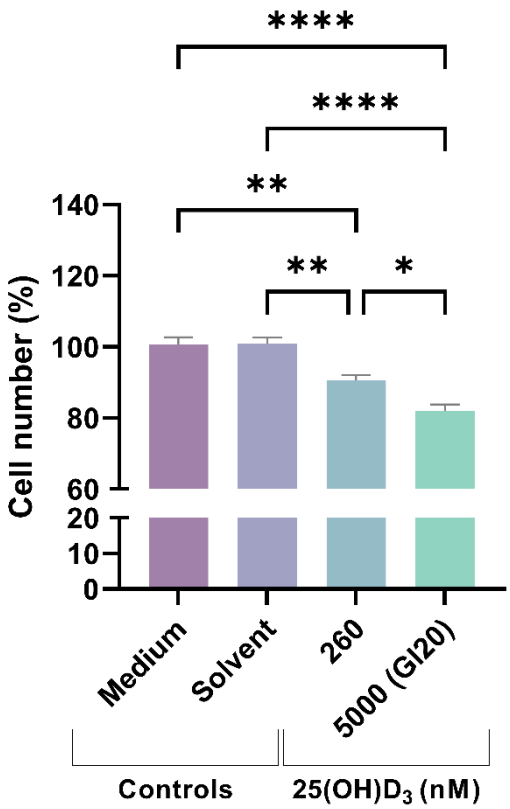

Figure 3.2 The effect of 25(OH)D_3 on cell count in HeLa cells. The crystal violet assay observed significant changes at the supraphysiological 25(OH)D_3 treatment dose. Data are expressed as mean±SEM (* $p<0.05$; ** $p<0.01$; **** $p<0.0001$**).**

© University of Pretoria

3.3 Assessment of cell viability with alamarBlue®

Cell viability was assessed with the AlamarBlue® assay. AlamarBlue® incorporates resazurin, a colorimetric oxidation-reduction (REDOX) indicator which detects the cellular metabolic activity of the mitochondria[66]. Metabolically active cells reduce Resazurin (blue) to resorufin (red). The colorimetric endpoint is measured by absorbance spectrophotometry. The absorbance is directly proportional to cell viability[66-67].

Significant decreases in cell viability were observed with the 5000 nM 25(OH)D_3 treatment dose (87.79%±1.834%) relative to the solvent control (99.27%±1.357%, p=0.0005) and the medium control (98.51%±1.525%, p=0.0012). Treatment at the physiological dose (91.43%±2.082%) significantly decreased cell viability relative to the solvent (p=0.0156) and medium controls (p=0.0360). There was no significant variation noted between the two 25(OH)D_3 treatments (Figure 3.3).

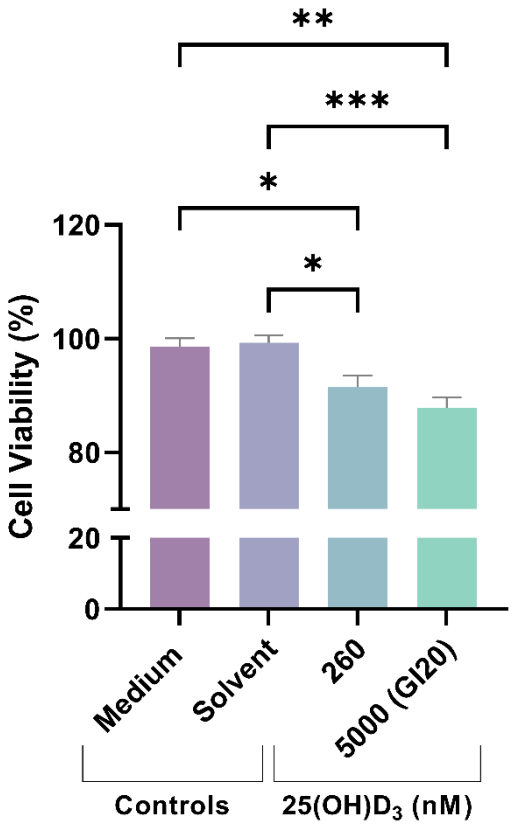

Figure 3.3 **The effect of 25(OH)D_3 on cell viability in HeLa cells**. Histogram plot of cell viability using the alamarBlue® assay. Data are expressed as mean±SEM (* p<0.05; ** p<0.01; *** p<0.001).

© University of Pretoria

3.4 Cell cycle analysis using flow cytometry

The cell cycle regulates cell growth and division. This flow cytometric assay discriminates cells in the distinct phases of the cell cycle using a formulation of propidium iodide (PI) and RNAse A[68]. PI stains nucleic acids and is used to identify RNA and DNA. RNAse A in the proprietary formation degrades RNA, and therefore cells containing DNA are identified.

Treatment with the 5000 nM dose of 25(OH)D_3 (8.30%±0.7506%) significantly increased the sub-G_1 cell population relative to the solvent control (5.57%±0.1202%, p=0.0305), medium control (5.63%±0.2404%, p=0.0348) and 260 nM treatment dose (5.37%±0.6227%, p=0206). (Figure 3.4)

The were no significant changes in the G_0/G_1 cell population observed with 5000 nM 25(OH)D_3 treatment (68.83%±2.341%) relative to the solvent control (65.95 %±3.384%) and medium control (66.48%±2.308%). Treatment at 260 nM 25(OH)D_3 (67.05%±2.775%) resulted in no significant changes relative to the controls and the supraphysiological treatment dose.

Treatment with the 5000 nM dose of 25(OH)D_3 (12.17%±0.8212%) showed no significant alteration in the number of cells in the S phase of the cell cycle relative to the solvent control (13.80%±0.4583%), medium control (14.13%±0.4333%) and 260 nM treatment (14.07%±0.1202%).

Treatment with the 5000 nM dose of 25(OH)D_3 (12.30%±1.457%) did not significantly increase the G_2/M cell population relative to the solvent control (16.57%±3.180%), medium control (15.70%±1.888%) and 260 nM treatment (15.47%±1.634%).

© University of Pretoria

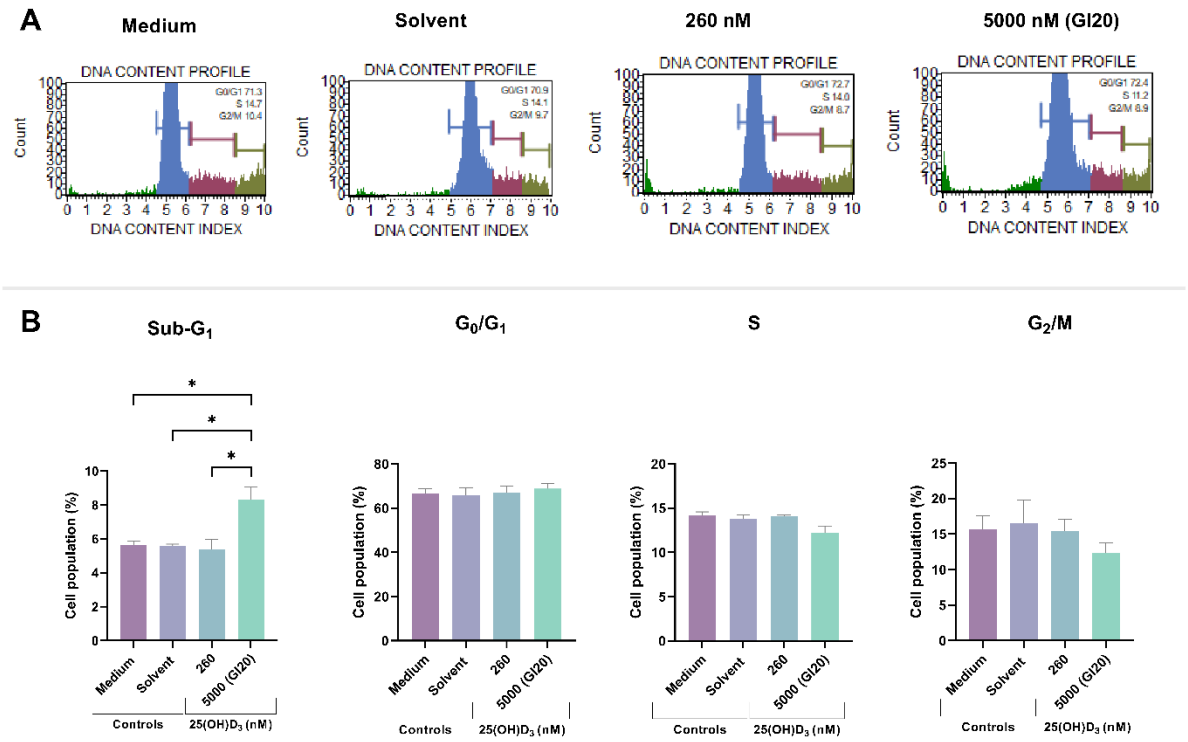

Figure 3.4 **Cell cycle analysis with flow cytometry.** (A) Histogram plots and (B) bar charts displaying the percentage of total cells in each phase of the cell cycle (sub-G_1, G_0/G_1, S and G_2/M) for experimental and control cultures. Data are expressed as mean±SEM (* $p<0.05$).

3.5 Assessing mitochondrial membrane depolarisation using flow cytometry

Changes to the mitochondrial membrane potential during apoptotic cell death were analysed using the Luminex Muse Mitopotential Assay. Changes in mitochondrial membrane potential can disrupt the function of the mitochondria and result in apoptotic cell death[40]. The flow cytometric assay used discriminated cells with damaged mitochondria and cells with normal mitochondrial, as well as live and dead cells[69].

Treatment with 5000 nM of 25(OH)D_3 significantly decreased the number of live (viable) cells (84.25%±1.156%) and relative to the solvent (97.28%±0.9052%, p=0.0006) and medium controls (96.22%±0.2689%, p=0.0012). A significant decrease in the cell population was observed in the 260 nM treatment (87.64%±1.9052%) relative to the solvent (p=0.0050) and medium (p=0.0105) controls. No significant differences in cell population size were observed between the two 25(OH)D_3 treatment doses. (Figure 3.6).

© University of Pretoria

For live cells with depolarised mitochondrial membranes, there was a significant decrease in the cell population with 5000 nM treatment (9.158%±1.490%) relative to the solvent (0.4167%±0.2619%, p=0.0028) and medium (0.7500% ± 0.1504%, p=0.0037) controls. No differences were observed in the cell population sizes between the 5000 nM and 260 nM (5.407%±1.190%) treatments. No statistical significance was observed in cell population with the 260 nM treatment dose compared to the solvent and medium controls.

The number of dead cells with depolarised mitochondrial membranes and dead cells did not differ significantly across the experimental and control treatments.

The total number of depolarised cells was significantly higher with 5000 nM treatment (13.86%±0.6120%) compared to the 260 nM treatment (9.537%±1.302%, p=0.0362), the solvent control (2.177%±0.4359%, p<0.0001) and the medium control (2.147%±0.05364%, p<0.0001). The total number of depolarised cells in 260 nM treatment culture were significantly higher than in the solvent (p=0.0012) and medium (p=0.0012) controls.

© University of Pretoria

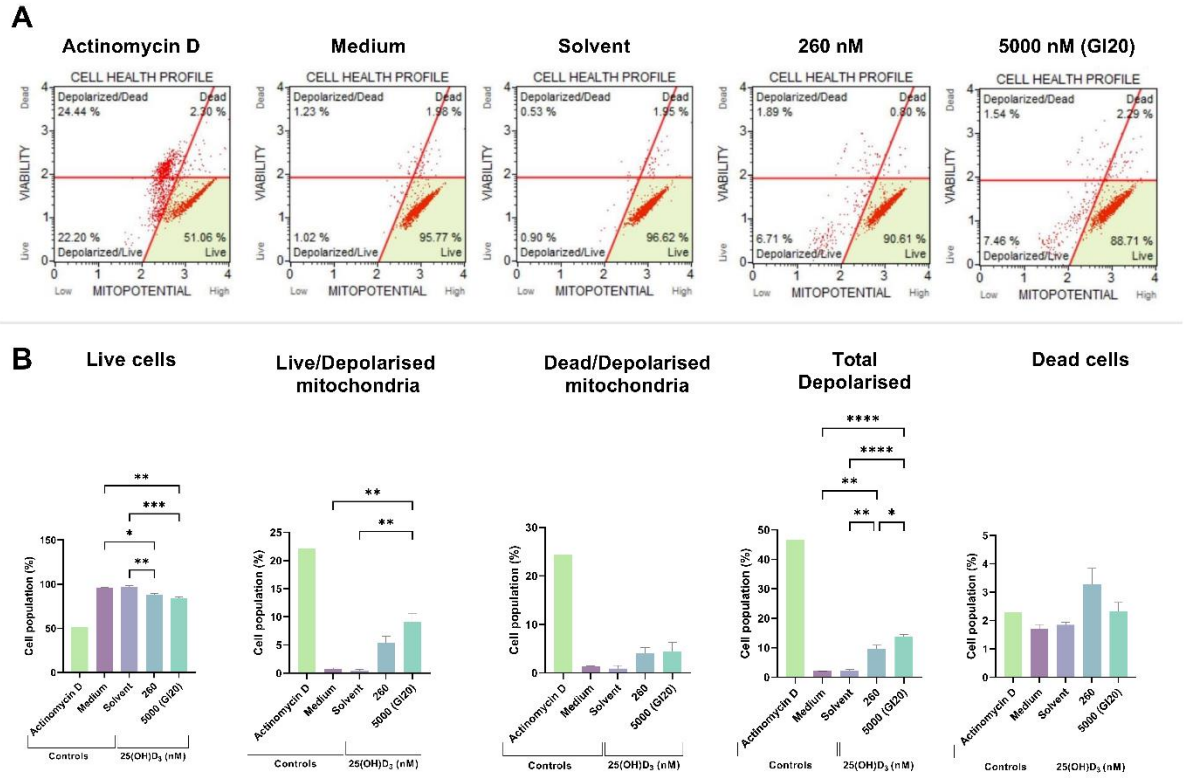

Figure 3.5 **Detection of mitochondrial membrane depolarisation with flow cytometry.** Two-dimensional dot-plot diagrams (A) and bar graphs (B) displaying live (viable), live cells with depolarised mitochondrial membranes, dead with depolarised mitochondrial membranes, total depolarised and dead cells for experimental and control cultures (* $p<0.05$; ** $p<0.01$; *** $p<0.001$; **** $p<0.0001$).

3.6 Assessment of phosphatidylserine externalisation using flow cytometry

Stimuli that induce apoptosis cause the translocation of phosphatidylserine residues in the inner leaflet of the cell membrane to the outer leaflet[37]. Flow cytometric analysis was conducted using Annexin V and 7-AAD. Annexin V binds to externalised phosphatidylserine residues, and 7-AAD binds to DNA[70].

Treatment at 5000 nM significantly decreased the number of healthy live (viable) cells (83.33%±1.274%) relative to the solvent control (96.10%±1.1815%, $p<0.0001$), the medium control (96.48%±0.2258%, $p<0.0001$) and the 260 nM treatment (91.18%±1.275%, $p=0.0024$). A significant decrease in the cell population was observed with the 260 nM treatment compared to the solvent ($p=0.0430$) and medium ($p=0.0283$) controls. (Figure 3.5).

© University of Pretoria

25(OH)D_3 treatment at 5000 nM (7.787%±1.477%) significantly increased the live, apoptotic cell population compared to the solvent (2.550%±0.1914%, p=0.0216) and medium (2.397%±0.3263%, p0.0182) controls. No statistical differences were observed with the 260 nM treatment dose (3.460%±0.6751%) and the controls.

For cells that were apoptotic and dead, there was a significant increase in the cell population with 5000 nM treatment (8.193%±0.5980%) relative to the solvent control (0.3733%±0.1910%, p<0.0001), medium control (0.1233%±0.09939%, p<0.0001) and the 260 nM treatment (4.683%±0.0.8239%, p=0.0141). Treatment at 260 nM significantly increased the cell population compared to the controls of the solvent (p=0.0038) and medium (p=0.0026).

Significant increases in the total apoptotic cell population were observed with 25(OH)D_3 treatments at 260 nM (8.147%±1.487%) and 5000 nM (15.98%±1.195%) relative to the medium control (2.917%±0.2490%, p=0.0495 and p=0.0001, respectively). Treatment at 5000 nM significantly increased the total apoptotic cell population compared to the solvent control (p=0.0001) and 260 nM treatment (p=0.0043).

There were no significant changes observed in the number of dead cells across the experimental treatments and controls.

© University of Pretoria

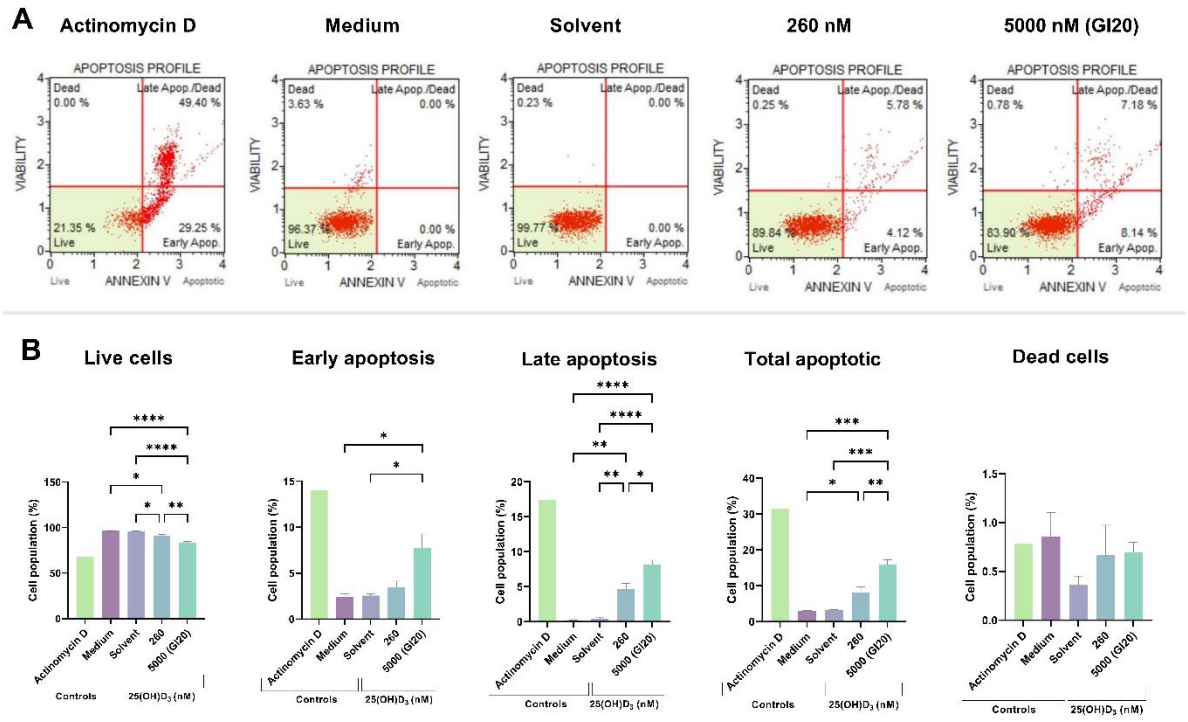

Figure 3.6 **Annexin V detection with flow cytometry.** Two-dimensional dot-plot diagrams (A) and bar graphs (B) displaying live, early apoptotic, late apoptotic, total apoptotic, and dead cell populations for experimental and control cultures (* $p < 0.05$; ** $p<0.01$; *** $p<0.001$; **** $p<0.0001$).

3.7 Activation of caspase-3 and -7 activity in 25(OH)D_3 treated HeLa cells

Caspase-3 and -7 activity was measured using the Luminex Muse Caspase-3/7 assay. Caspases are proteases that play a role in a cascade of reactions leading to apoptotic cell death[40]. This flow cytometric assay discriminated between apoptotic and normal cells and live and dead cells[72].

Treatment with 5000 nM of 25(OH)D_3 significantly decreased the number of healthy live (viable) cells (90.08%±1.919%) and relative to the solvent (98.08%±0.2589%, p=0.0095) and medium controls (97.26%±0.3044%, p=0.0184). No significant differences were observed in the 260 nM treatment (88.38%±1.055%) relative to the 5000 nM treatment. The 260 nM treatment significantly decreased the number of healthy live cells relative to the solvent (p=0.0027) and medium controls (p=0.0048). (Figure 3.7)

For live cells with activated caspases -3 and -7, there were no significant differences between the 5000 nM treatment (1.077%±0.5235%) relative to the solvent control (0.3800%±0.1943%),

© University of Pretoria

medium control (0.3333%±0.3038%) and 260 nM 25(OH)D_3 treatment (1.270 %±0.2150%) treatments. Both treatments of 25(OH)D_3 had a higher cell population of live cells with activated caspases than the controls.

Treatment at 5000 nM treatment (5.123%±0.8802%) significantly increased the number of dead cells with activated caspases -3 and -7 relative to the solvent (0.3933%±0.3122%, p=0.0.345) and medium (0.5500%±0.4136%, p=0.0416) controls. Treatment at 260 nM treatment (8.027%±1.273%) significantly increased the cell population relative to the solvent (p=0.0017) and medium (p=0.0019) controls.

Significant increases in the total apoptotic cell population were observed with 25(OH)D_3 treatments at 260 nM (9.297%±1.308%) and 5000 nM (6.207%±0.7477%) relative to the solvent control (0.7700%±0.4761%, p=0.0012 and p=0.0219, respectively) and medium control (0.8833%±0.7155%, p=0.0013 and p=0.0248, respectively).

Treatment with 25(OH)D_3 at both doses increased the percentage of dead cells, but no significant differences were observed relative to the controls.

© University of Pretoria

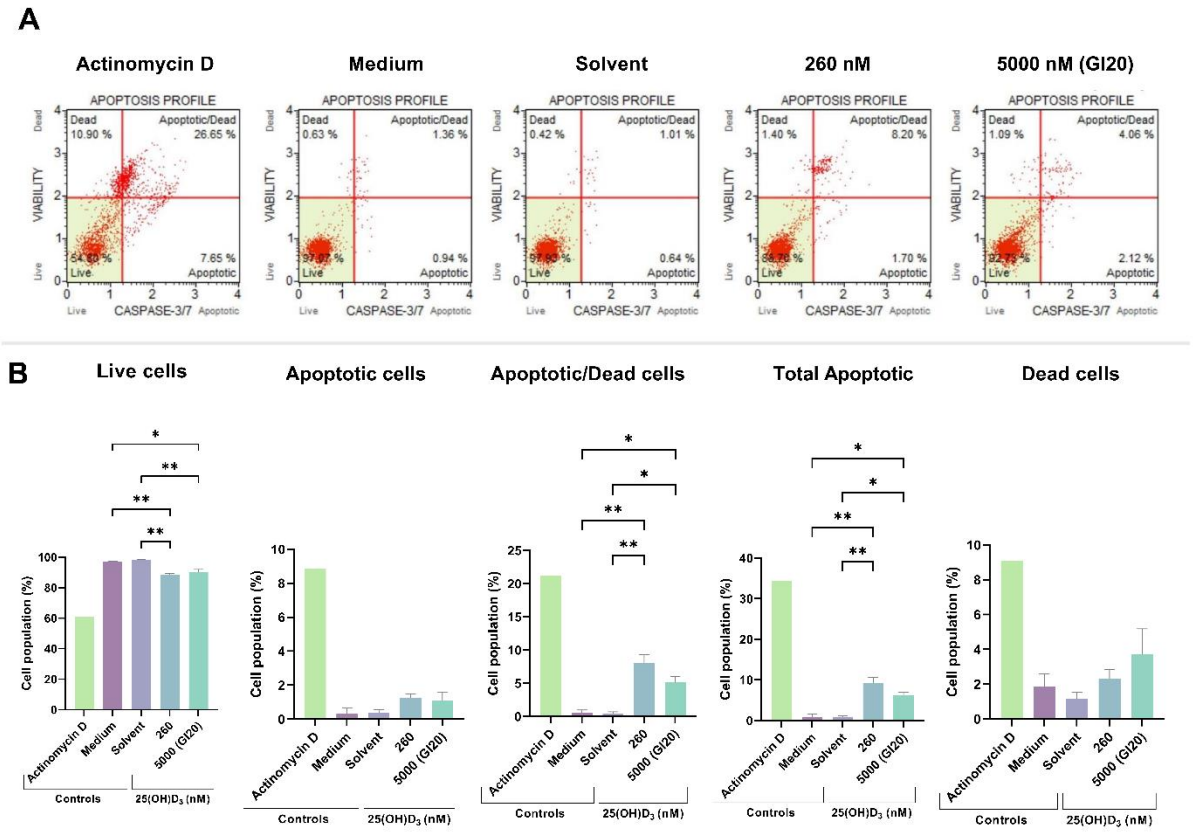

Figure 3.7 **Detection of caspases -3 and -7 activity with flow cytometry.** Two-dimensional dot-plot diagrams (A) and bar graphs (B) displaying live, apoptotic, apoptotic and dead, total apoptotic, and dead cell populations for experimental and control cultures (* $p < 0.05$; ** $p < 0.01$).

3.8 Induction of LC3-II in 25(OH)D_3 treated HeLa cells

The presence of autophagic cell death was assessed using the Luminex Muse Autophagy LC3-II assay. LC3 is a protein essential for the formation of autophagosomes. This assay discriminated between cells with cytosolic LC3-I and autophagosome-associated LC3-II[73,88].

Treatment with 25(OH)D_3 at 260 nM (4.600±0.4619) and 5000 nM (8.167±0.4667) did not significantly induce autophagic cell death when compared to the medium (5.733±0.4842) and solvent (5.300±0.2082) controls (Figure 3.8).

© University of Pretoria

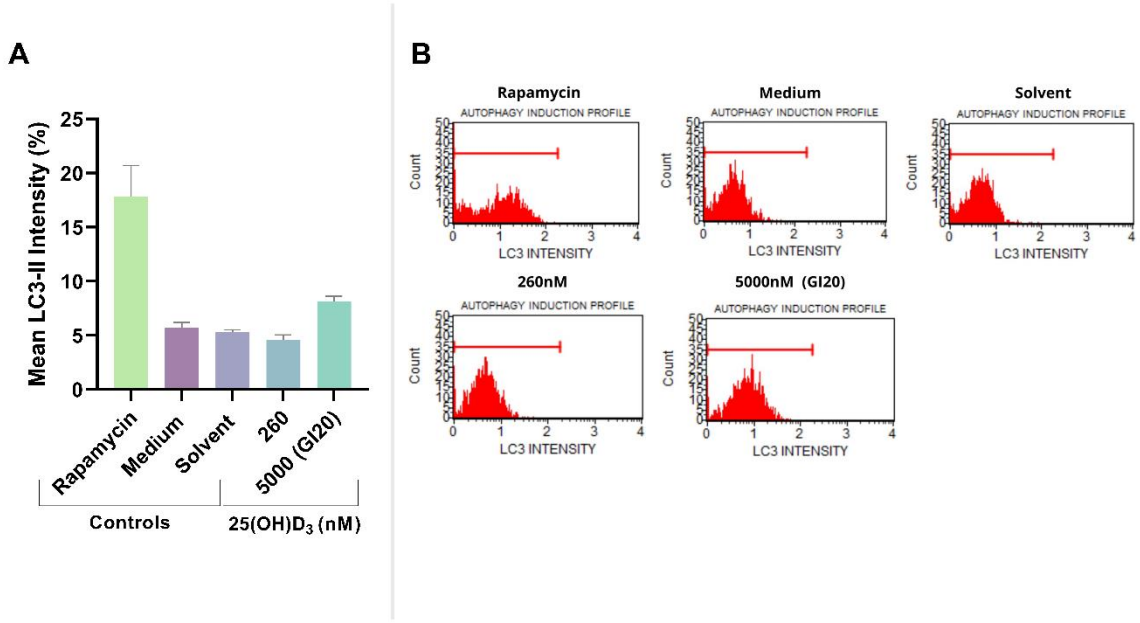

Figure 3.8 **Detection of LC3-II activity with flow cytometry.** (A) Bar graphs and (B) histogram plots of LC3-II intensity for experimental and control cultures detected through flow cytometry.

3.9 Lactate dehydrogenase release in 25(OH)D_3 treated HeLa cells

Necrotic cell death (cell cytotoxicity) was assessed using the lactate dehydrogenase (LDH) assay. The assay measures cytosolic LDH released from damaged cells.

Treatment with 5000 nM 25(OH)D_3 (6.173%±2.705%) increased the percentage of cell cytotoxicity; however, the increase was not significant relative to the solvent control (0.4325 ±2.156%) and medium control (1.514%±0.9826%) controls and the 260 nM treatment dose (0.3309%±1.755%). (Figure 3.9)

© University of Pretoria

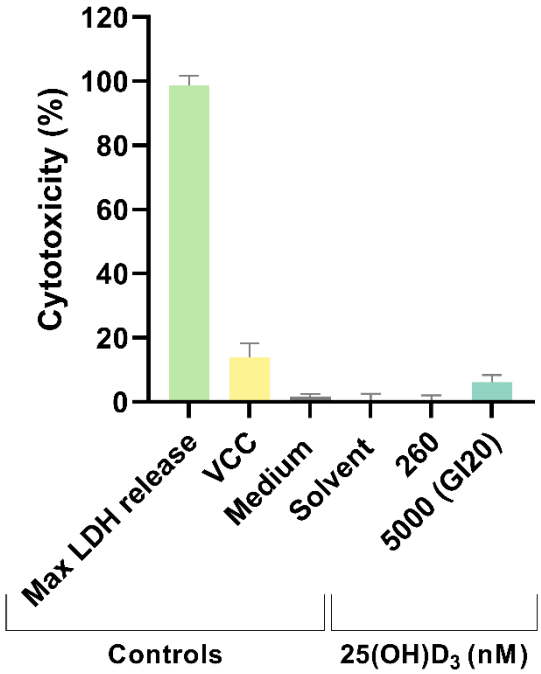

Figure 3.9 **Detection of lactate dehydrogenase.** Lactate dehydrogenase (LDH) release was measured in experimental and control cultures. A maximum LDH release and a volume correction control (VCC) were also included in the experiments (* $p < 0.05$; ** $p < 0.01$).

3.10 Assessment of gross morphological changes in 25(OH)D_3 treated HeLa cells

Gross morphological changes were analysed using light microscopy. Experimental and control samples were stained using haematoxylin and eosin, and samples were viewed with a brightfield microscope. Haematoxylin stains acidic structures blue and eosin stains basic structures pink[75].

Solvent and medium controls exhibited minimal cell death features, with most cells appearing healthy. Cells in experimental samples showed morphological features of cell death also present in the actinomycin treatment (positive control). Notable observed features include cell membrane blebbing, apoptotic bodies, hyper-condensed chromatin (pyknosis) and cytoplasmic shrinkage. Positive control and 25(OH)D_3 samples showed decreased cell density compared to medium and solvent controls (Figure 3.10A-I).

The samples were semi-quantitatively analysed. Approximately 1200 cells were counted for each sample, and the percentage of cells with features of apoptotic cell death was calculated.

© University of Pretoria

There was a significantly higher percentage of cells with morphological features of apoptosis in the 5000 nM 25(OH)D3 treatment (7.715%±1.443%, p=0.0159) relative to the medium control (3.064%±0.6881%). No significance was observed relative to the solvent control (4.228%±0.9296%) and 260 nM treatment (7.350%±1.215%) (Figure 3.10J).

© University of Pretoria

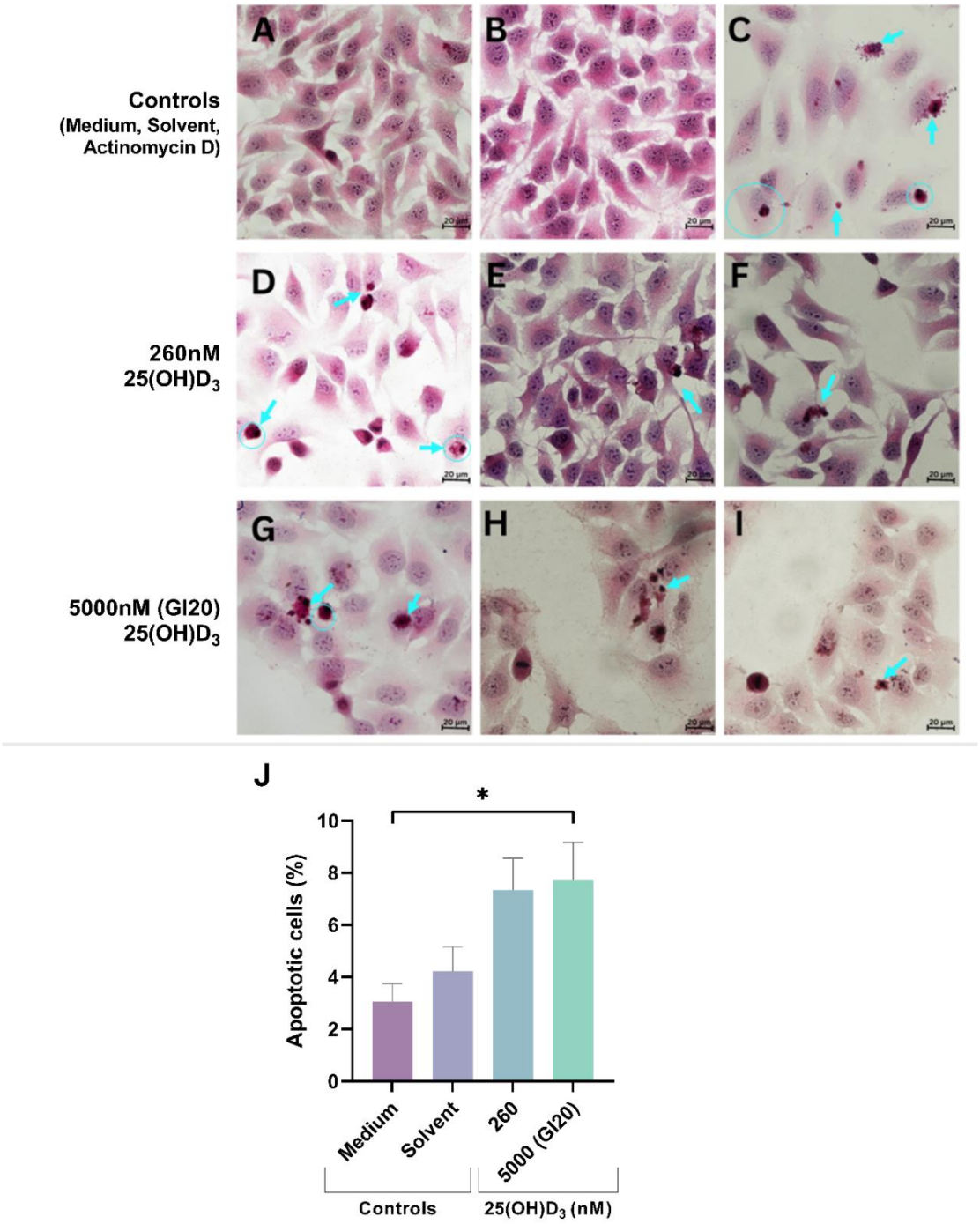

Figure 3.10 **Analysis of morphological changes using brightfield microscopy.** Growth medium (A) and solvent (B) treated cells showed a dense population with minimal signs of cell death. The positive control (actinomycin D) (C) and vitamin D treatments of 260 nM (D-E) and 5000 nM (G-I) revealed apoptotic bodies, blebbing, cytoplasmic shrinkage, hyper-condensed chromatin, and compromised cell density. Approximately 1200 cells were counted from each treatment and analysed for features of apoptosis and cell death. The percentage of apoptotic cells was calculated (J). The 5000 nM treatment significantly increased the percentage of apoptotic cells. Scale bar = 20µm.* $p < 0.05$.

© University of Pretoria

In addition to characteristics of cell death, mitotic cells were also visible in the different treatments. Cells were identified in the prophase, metaphase, anaphase, and telophase phases of mitosis (Figures 3.11A and 3.11B).

Approximately 1200 cells were counted in each experimental and control culture. The percentage of mitotic cells in each culture was calculated. The 5000 nM treatment has 5.56% of cells (Figure 3.11C) undergoing mitosis, which compared to the percentage of cells in the solvent control (4.63%), medium control (4.96%) and 260 nM 25(OH)D_3 treatment (3.95%).

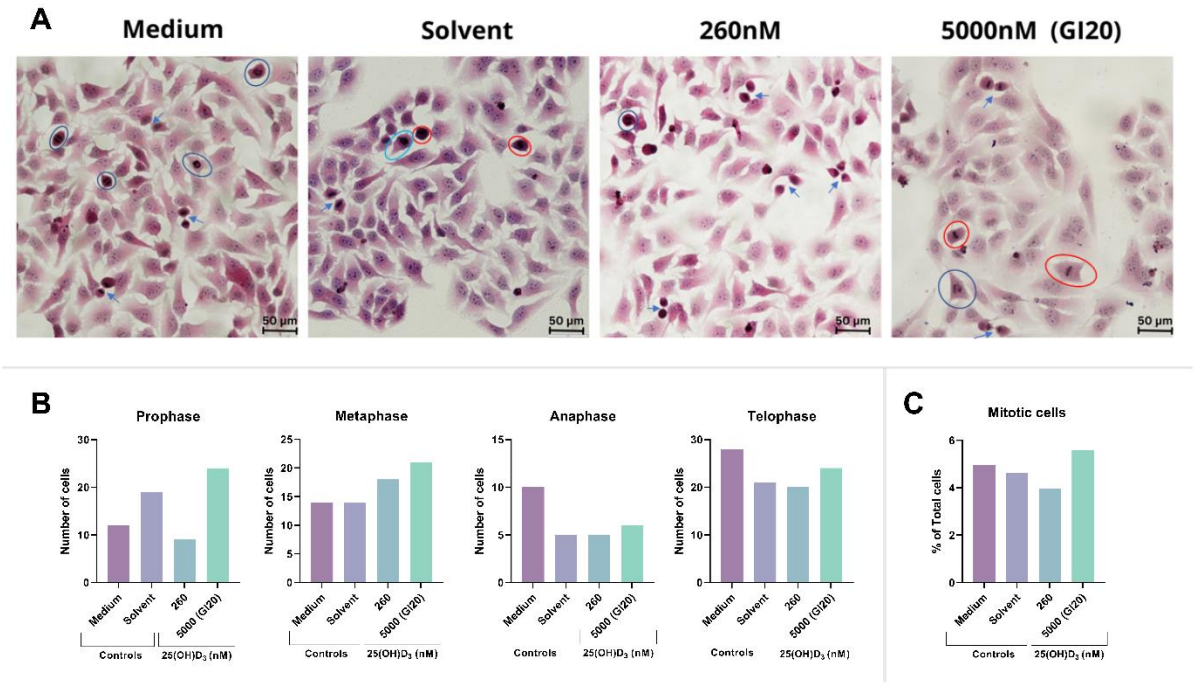

Figure 3.11 Brightfield microscopy images and semi-qualitative analysis of mitotic HeLa cells. Experimental and control cultures contained cells that were visibly undergoing mitosis. The cells were visualised using H&E staining (A). Cells in prophase (light blue circle), telophase (red circle), anaphase (dark blue circle) and telophase (blue arrow) were observed across treatments and controls. Cells in each phase of mitosis did not differ statistically across the cultures (B). The percentage of mitotic cells present did not differ across cultures (C).

Interestingly, multinucleated (polyploid) cells (MNCs) were observed in all cultures (Figure 3.12A). The percentage of MNCs cells varied across all cultures, with 2.884%±0.7720% of cells in the 5000 nM treatment, 1.775%±0.2171% in the solvent control, 1.552%±0.2702% in the medium control and 1.552%±0.2702% in the 260 nM treatment (Figure 3.12B). The size of the MNCs in the 5000 nM treatment averaged 2.413±0.2308 times larger relative to the size of normal cells in the same culture (Figure 3.12C). This was significantly larger than the MNCs

© University of Pretoria

in the solvent control and medium control cultures, which averaged 1.364±0.1056 (p=0.0374) and 1.555±0.09751 (p=0.0346), respectively. The MNCs in the 260 nM treatment culture were 1.675±0.4886 times larger than normal cells. In addition, the number of nuclei in each MNC was counted. MNCs in 5000 nM had an average of 3.200±0.4078 nuclei, the solvent control 2.000±0.000, the medium control 2.917±0.5833 and the 260 nM treatment 2.500±0.5000 (Figure 3.14D).

© University of Pretoria

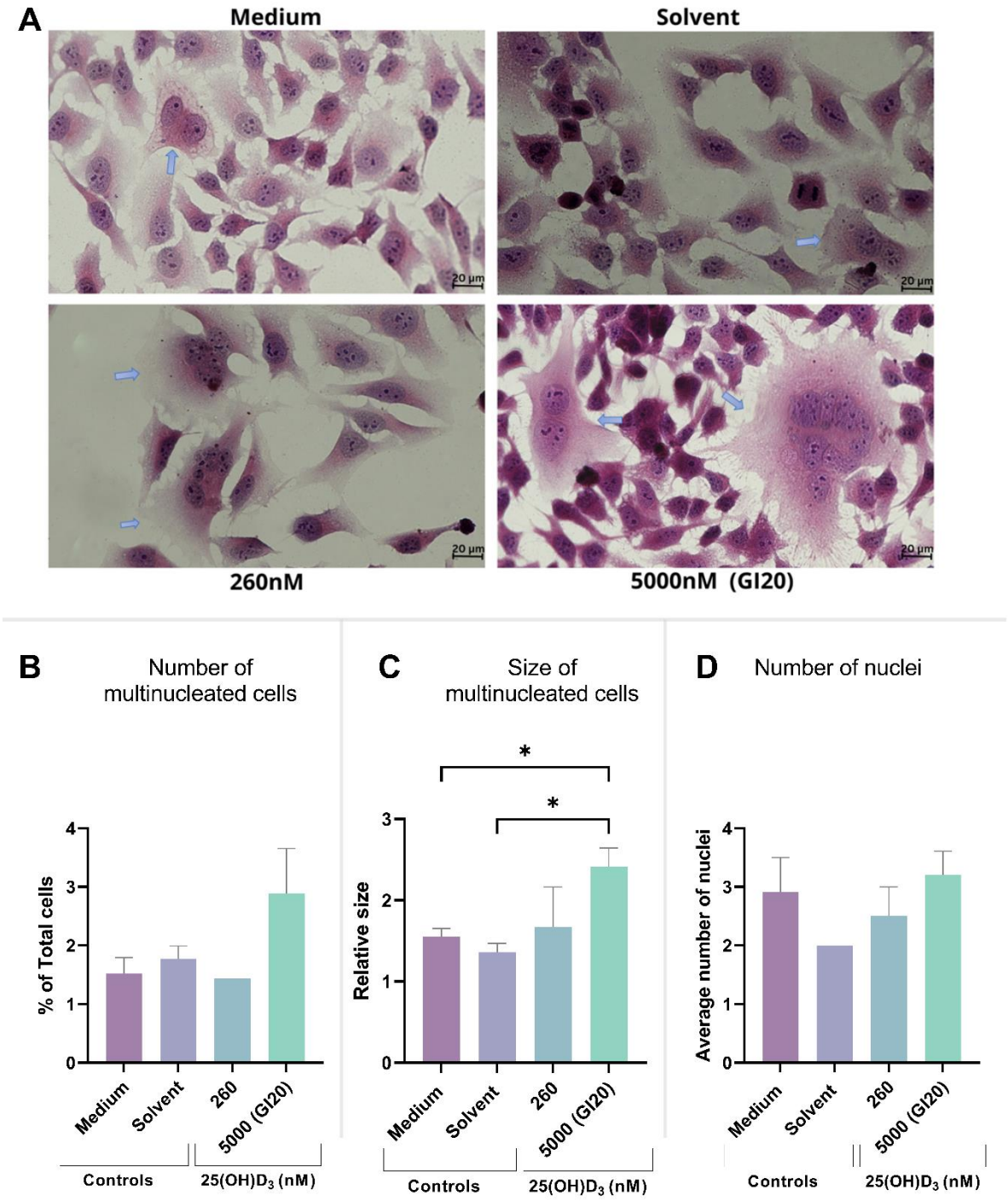

Figure 3.12 **Multinucleated HeLa cells visualised with H&E stain.** Experimental and control cultures were visualised with brightfield microscopy using H&E staining (A). Multinucleated cells (blue arrows) were present in all cultures. Bar graphs of the number of multinucleated cells (B), the size of multinucleated cells relative to the average size of normal cells (C) and the number of nuclei in multinucleated cells (D) show that 5000 nM treatment increased the number and size of multinucleated cells.

© University of Pretoria

3.11 Ultrastructural changes in 25(OH)D_3 treated HeLa cells

Ultrastructural changes were observed using transmission electron microscopy (TEM). In TEM, an image is mirrored by scattered electron waves from heavy metal-stained samples[78]. Cells were fixed, dehydrated, embedded, sectioned, and stained to allow for viewing of cellular organelles.

Cells in the solvent control appeared normal, indicating no signs of cellular damage or cell death. Cells treated with a supraphysiological dose (5000nM) displayed features of apoptosis such as nuclear membrane damage (Figure 3.13), apoptotic bodies (Figure 3.14) and membrane blebbing. The chromatin was not visible in images due to poor staining.

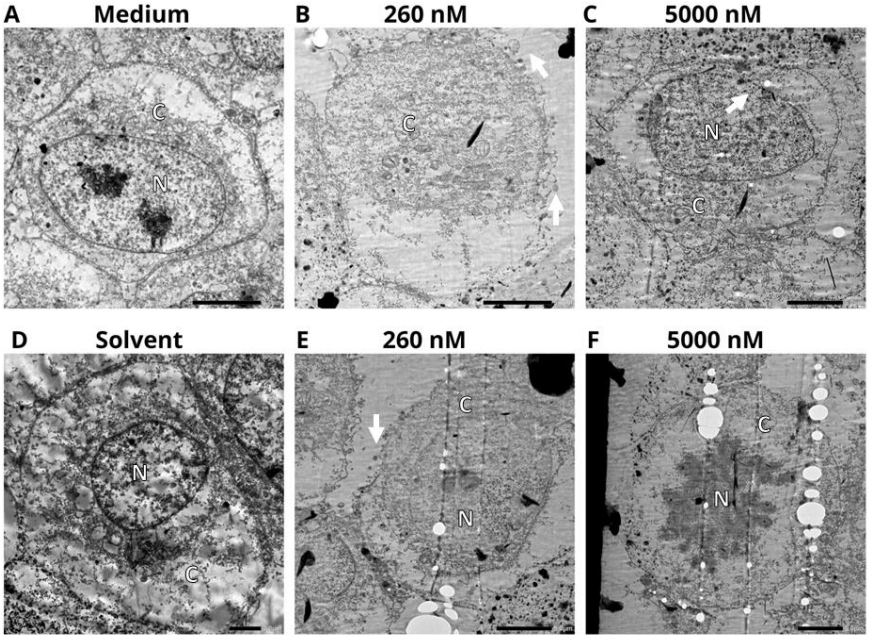

Figure 3.13 **Electron micrographs of experimental and control cultures**. Medium (A) and solvent (D) cultures show normal cell morphology with no signs of apoptosis. The 260nM (B and E) and 5000nM (C and F) treatments show features of apoptosis, including membrane blebbing, disrupted nuclear membrane, and nuclear damage. C, cytoplasm; N, nucleus.

At higher magnification, changes in mitochondria structure were visible for cells treated with 5000nM 25(OH)D_3. Some mitochondria appeared normal, whilst others were rounded with a swollen matrix (Figure 3.15). Nuclear membrane damage, apoptotic bodies, and membrane blebbing were also observed.

© University of Pretoria

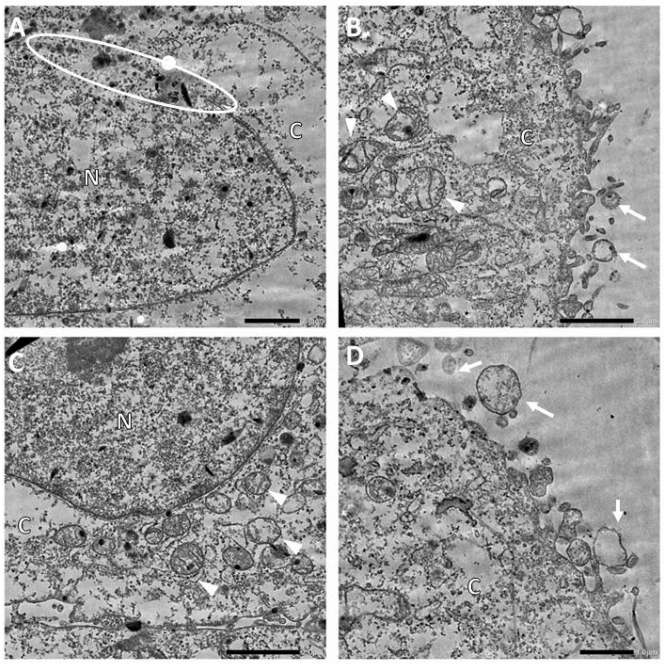

Figure 3.14 Transmission electron micrograph of HeLa treated with 5000nM 25(OH)D_3. Cells displaying features of apoptosis such as (A) nuclear membrane damage (oval), (B-C) round mitochondria with swollen matrix (arrowhead), (D) apoptotic bodies (arrow) and cytoplasmic blebbing. C, cytoplasm; N, nucleus.

3.12 Gene and enzyme expression of vitamin D metabolising system in 25(OH)D_3 treated HeLa cells

Total RNA extracts from cell cultures were synthesised into cDNA. The cDNA was amplified with real-time PCR. The mRNA expression for CYP27B1 was significantly upregulated at a 5000 nM treatment (1.335±0.01878) in comparison to the solvent control (1.000±0.06477, p=0.0151), medium control (0.8674±0.04684, p=0.0019) and 260 nM treatment (0.8532±0.07261, p=0.0015). There were no significant differences observed between the 260 nM 25(OH)D_3 treatment and the control cultures (Figure 3.15A).

Total protein was extracted from experimental and control cultures. Proteins were separated with gel electrophoresis and identified with immunoblotting. The CYP27B1 protein is approximately 47.5 kDa, and β-actin is approximately 42 kDa in size. There was a significant increase in CY27B1 protein expression observed in the 5000 nM treatment (2.409±0.6266) relative to the solvent control (1.000±0.000, p=0.0210) and medium control (0.9861±0.09133, p=0.0358). There were no significant differences observed between the 260 nM 25(OH)D_3 treatment (1.502±0.1152) and the control cultures (Figures 3.15B and 3.15C).

© University of Pretoria

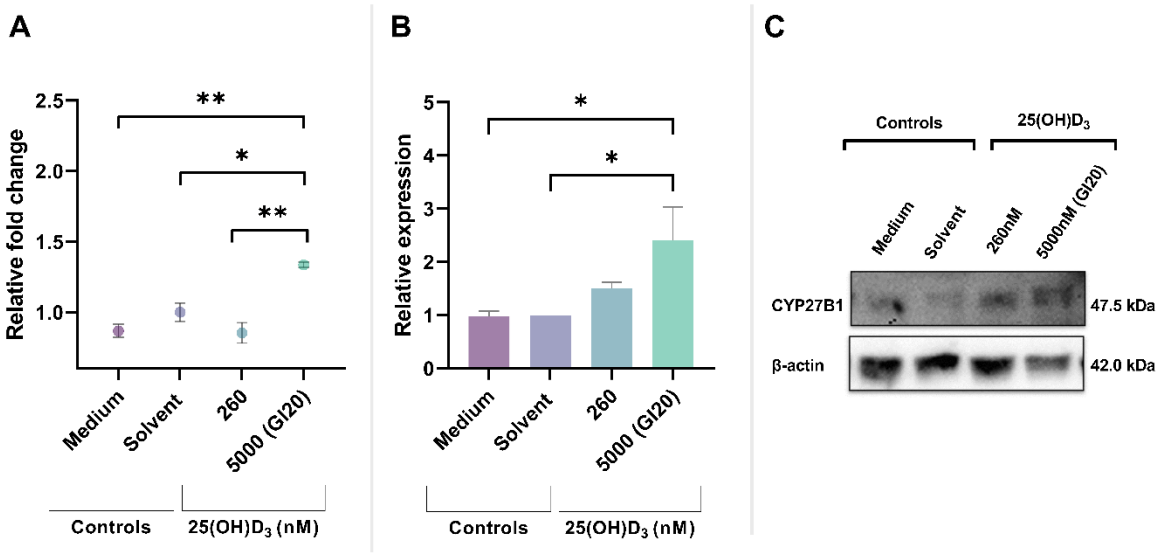

Figure 3.15 CYP27B1 gene and protein expression. Gene (A) and protein (B and C) were analysed with real-time qPCR and western blot analysis. Treatment with 5000nM of 25(OH)D_3 significantly increased CYP27B1 mRNA and protein expression. There was no statistically significant difference in protein expression (* $p < 0.05$; ** $p < 0.01$).

The mRNA expression for CYP24A1 was significantly upregulated at a 5000 nM treatment (1641±444.4) in comparison to the solvent control (1.000±0.05114, p=0.0107), medium control (4.257±0.2878, p=0.0108) and 260 nM treatment (13.07±4.195, p=0.0205). There were no significant differences observed between the 260 nM 25(OH)D_3 treatment and the control cultures (Figure 3.16A).

The CYP24A1 protein is approximately 56.0 kDa in relative molecular weight (M_r). 5000 nM treatment (1.871±0.3771) significantly increased protein expression relative to the solvent control (1.000±0.000, p=0.0482). No significant differences were observed between the 5000 nM 25(OH)D_3 treatment and the medium control (1.143±0.07208) and 260 nM treatment (1.240±0.05764). Additionally, no significant differences were observed between the 260 nM 25(OH)D_3 treatment and the control cultures (Figures 3.16B and 3.16C).

© University of Pretoria

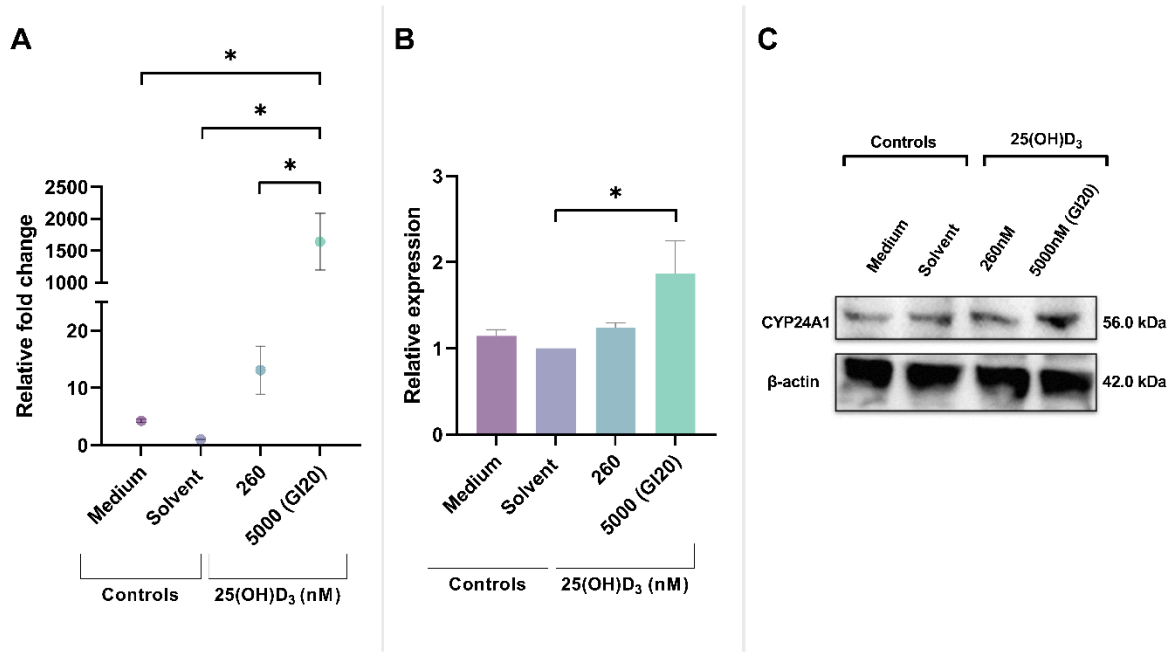

Figure 3.16 CYP24A1 gene and protein expression. Gene (A) and protein (B and C) were analysed with real-time qPCR and western blot analysis. Treatment with 5000nM of 25(OH)D_3 significantly upregulated CYP24A1 mRNA and protein expression (* $p < 0.05$).

3.13 Gene and protein expression of the vitamin D receptor in 25(OH)D_3 treated HeLa cells

The VDR mRNA was significantly upregulated with 5000 nM treatment (3.431±0.1673) in comparison to the solvent control (1.000±0.02935, p<0.0001), medium control (1.125±0.1212, p<0.0001) and 260 nM treatment (1.433±0.06940, p<0.0001). There was no significant difference between the 260 nM 25(OH)D_3 treatment and the control cultures (Figure 3.17A).

The VDR protein is approximately 46.7 kDa. Treatment with 5000 nM of 25(OH)D_3 (1.509±0.1823) significantly increased protein expression compared to the solvent control (1.000±0.000, p=0.0344). Treatment at 260 nM (1.678±0.06220) protein expression compared to the solvent (p=0.0091) and medium (1.020±0.01598, p=0.0173) control cultures (Figures 3.17B and 3.17C).

© University of Pretoria

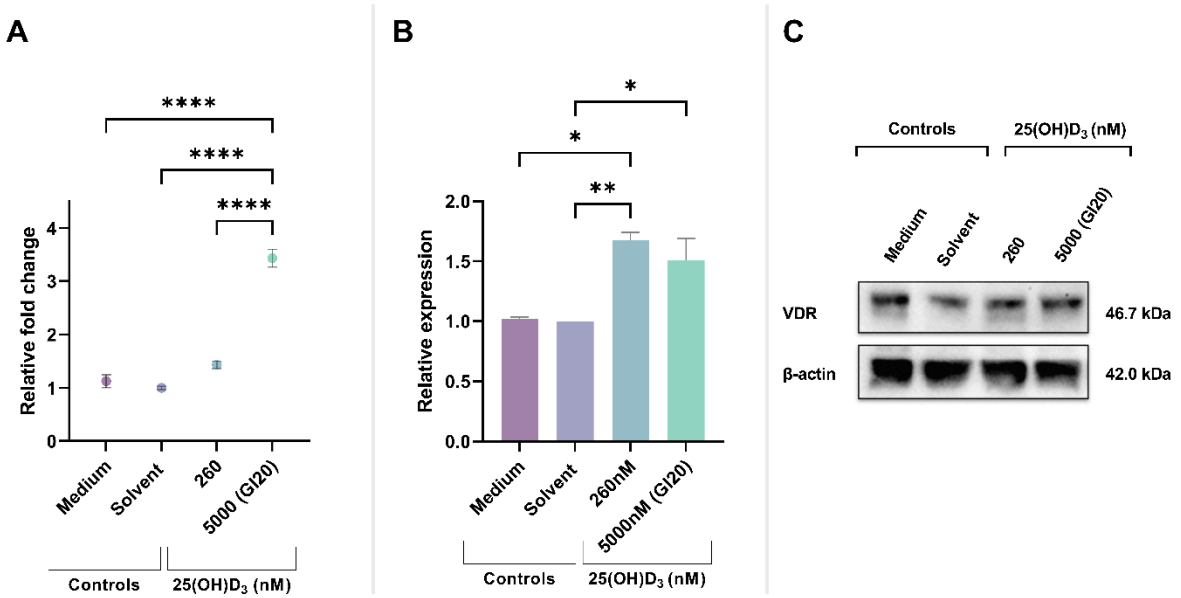

Figure 3.17 **VDR gene and protein expression.** Gene (A) and protein (B and C) were analysed with real-time qPCR and western blot analysis. Treatment with 5000 nM of 25(OH)D_3 significantly increased VDR mRNA expression. Both 260 nM and 5000 nM treatments statistically increased protein expression (* $p<0.05$; ** $p<0.01$; **** $p < 0.0001$).

© University of Pretoria

Chapter 4

Discussion

Vitamin D and its metabolites are secosteroid hormones widely recognized for their ability to facilitate the absorption of calcium and phosphorous[5,22]. In addition, *in vitro* and *in vivo* studies examining the anti-cancer effects of vitamin D metabolites in breast[89-90], colon[91-92], prostate[93], lung[94], and skin[95] cancers have established that vitamin D metabolites can effectively inhibit cancer cell growth and replication via a variety of pathways. However, the anti-tumour actions of vitamin D in cervical cancer remain insufficiently explored. The findings of this study demonstrate that 25(OH)D_3 reduced cell count and viability, prompted apoptotic cell death and upregulated gene and protein expression of CYP27B1, CYP24A1, and VDR.

25(OH)D_3 decreases cell number and cell viability in HeLa cells

The administration of 25(OH)D_3 caused a significant reduction in the cell number and viability of HeLa cells. Similar decreases in both parameters have been observed in other cervical cancer cell lines. CaSki cervical cancer cells, upon treatment with high concentrations of cholecalciferol (100 ng/mL and 1000 ng/mL), exhibited decreases in cell number to approximately 56.25% ± 7.08% ($p<0.05$) and 50.59% ± 5.14% ($p<0.001$), respectively[30]. The treatments also resulted in a decline in cell viability to 73.94% ± 3.16% ($p<0.01$) and 62.41% ± 1.64% ($p<0.0001$). In another study, Shruthi *et al*. demonstrated a 50% inhibition in the growth of HeLa cells with 1250 µM cholecalciferol treatment[96]. Together, these studies demonstrate that vitamin D metabolites negatively affect cell growth in cervical cancer cell lines.

25(OH)D_3 triggered accumulation in the sub-G1 phase without inducing cell cycle arrest

Accumulation of sub-G_1 population was observed with 5000 nM 25(OH)D_3 treatment in cell cycle analysis. The sub-G_1 population is associated with nuclear fragments, micronuclei, nuclei

© University of Pretoria

with different chromatin structures, clumps or chromosomes and apoptotic bodies[97]. This suggests that high-dose treatment of 25(OH)D_3 potentially induced DNA damage. Similar observations were seen in the CaSki cell line with high-dose cholecalciferol treatments of 100 ng/ml and 1000 ng/ml, which increased the sub-G_1 populations to 7.30%±1.04% and 9.75%±1.65%, respectively[30]. The sub-G_1 population is associated with cell death; however, supporting data is needed to confirm that cell death has I[25,98].

Vitamin D metabolites can induce cell cycle arrest in various cancer cell lines[98]. No significant changes in G_0/G_1, S, and G_2/M cell populations were observed in this study. In addition, brightfield microscopy revealed features of mitosis, with insignificant differences in the number of cells in all stages of mitosis, confirming the cell population numbers observed by flow cytometry. This differs from observations made in HeLa S3 cells treated with 200 nM and 500 nM calcitriol treatments, which increased the G_1 population[99]. The mechanism of G_1 phase arrest involves the upregulation of RB, p21 and p27, and the downregulation of c-Myc[98,100]. 25(OH)D_3, therefore, does not negatively promote alterations in intracellular tumorigenic pathways that promote cell cycle arrest in the HeLa cell line. This also suggests that a cell-specific response between HeLa and HeLa S3 may be operational. Furthermore, vitamin D metabolites calcitriol and 25(OH)D_3 may exert differential responses in adenocarcinoma cervical cell lines, like the HeLa and HeLa S3.

25(OH)D_3 induced apoptotic cell death in HeLa cells

In the present study, apoptosis was demonstrated by the increased depolarisation of mitochondrial membrane potential, increased phosphatidylserine externalisation and activation of terminal executioner caspases -3 and -7 with both 25(OH)D_3 treatments. Furthermore, morphological features of apoptosis described by the NCCD were discernible with brightfield microscopy images for both treatments of vitamin D, including hyper-condensed chromatin (pyknosis), apoptotic bodies, plasma membrane blebbing and cytoplasmic shrinkage[33,40]. Electron micrographs also showed signs of nuclear membrane damage, cytoplasmic blebbing, formation of apoptotic bodies and swollen, rounded mitochondria. The mitochondrial damage observed with flow cytometry and microscopy is supported by the cell viability assay results, which are associated with abnormal metabolic activity of the mitochondria. These results

© University of Pretoria

collectively suggest irregular mitochondrial function and caspase activation associated with intrinsic apoptosis[40,42].

Phosphatidylserine externalisation is a marker for both apoptosis and necrosis. However, the LDH cytotoxicity assay, 7-AAD dye staining in flow cytometry and morphological assessment showed insignificant necrotic cell death. Morphological analysis and LC3-II induction findings collectively did not suggest autophagic dependant cell death. Therefore, this suggests that 25(OH)D_3 did not induce necrosis and autophagic-dependent cell death in HeLa cells. Similar outcomes were observed in HeLa cells treated with calcitriol in a dose-dependent and time manner[101].

25(OH)D_3 enhances expression of CYP27B1, VDR and CYP24A1

Healthy and tumorigenic cervical tissue express VDMS[53]. This study indicates an autocrine response to 25(OH)D_3 in HeLa cells. Treatment with 5000 nM 25(OH)D_3 significantly increased CYP27B1, CYP24A1 and VDR gene and protein expression in HeLa cells. In contrast, treatment with 260 nM significantly increased VDR protein expression with no change at the mRNA transcript level. Physiological treatment also did not change CYP27B1 and CYP24A1 gene and protein expression, implying that treatment did not affect activation and catabolism of 25(OH)D_3.

The upregulation of the CYP27B1 gene and protein expression with 5000 nM treatment substantiates the autocrine conversion of 25(OH)D_3 to 1,25(OH)$_2D_3$. Similar findings were observed in SiHa cervical cells treated with 2500 nM 25(OH)D_3, which caused a 5-fold increase in CYP27B1 gene expression[102]. Treatment with a physiological dose did not statistically affect CYP27B1 mRNA expression in HeLa cells. Similar findings were demonstrated by Kloss *et al*. with 100 nM of 25(OH)D_3[62]. This suggests that supraphysiological doses induce the negative feedback regulation of 25(OH)D_3 levels by enhancing CYP27B1 expression. However, given the high concentration of 25(OH)D_3 at supraphysiological treatment, inactivated 25(OH)D_3 may directly inhibit cell growth and induce cell death without activation through 1αOHase, CYP27B1. This was demonstrated in LNCaP prostate adenocarcinoma cells when treated with 100 nM 25(OH)D_3 in combination with the CYP27B1 inhibitor genistein. The authors found that 25(OH)D_3 directly exerted an inhibitory effect on LNCaP cell growth and that the effect was enhanced by genistein[93]. Therefore, precursors of calcitriol may operate

© University of Pretoria

as a therapeutic agent in cervical cancer either directly or by means of autocrine activation of CYP27B1.

24-Hydroxylase is crucial in the catabolism of $25(OH)D_3$ and $1,25(OH)_2D_3$. Several studies show that its expression is markedly induced by $1,25(OH)_2D_3$.[8] Interestingly, inhibiting or knocking down CYP24A1 has been shown to impede tumour growth significantly. Conversely, overexpressing CYP24A1 has been found to promote tumour progression and metastasis[103-105]. In this study, treatment at 5000 nM resulted in the overexpression of the CYP24A1 gene and significantly increased protein expression. Although cell growth was inhibited, the maximum inhibition was about 20%. Approximately 15% growth inhibition has been achieved with only 100 nM $25(OH)D_3$ in LNCaP cells[93] and 50% inhibition with 800-900 nM $25(OH)D_3$ in BxPC-3 and AsPC-1 pancreatic cell lines[106]. These concentrations are about 10-fold less than the concentration used in this study, suggesting that CYP24A1 may have exerted oncogenic effects on the HeLa cells with high doses of $25(OH)D_3$.

The VDR protein is primarily known for regulating the expression of the target genes of vitamin D hormones. While precursor $25(OH)D_3$ and active hormone $1,25(OH)_2D_3$ can bind to VDR, they exhibit different potencies[15]. Notably, VDR protein expression increased with physiological and supraphysiological doses of $25(OH)D_3$ treatment, indicating that VDR mediates cell growth inhibition and cell death mechanisms. VDR protein expression was increased with both physiological and supraphysiological dose treatments of $25(OH)D_3$, suggesting that HeLa cell growth inhibition and cell death mechanisms were mediated by VDR. Interestingly, treatment at a physiological dose (250 nM) did not significantly change VDR expression in SiHa cervical cells and supraphysiological treatment dose significantly down-regulated VDR gene and protein expression ($p=0.0380$)[102]. This suggests that intracellular signalling by VDR is cell line and dose-dependent.

As previously mentioned, $25(OH)D_3$ may exert direct effects in the supraphysiological treatment of HeLa cells. Whether this is through VDR or other mechanisms needs to be further investigated.

In summary, $25(OH)D_3$ inhibits cell growth and directly induces cell death via CYP27B1 activation to calcitriol and VDR binding in a dose-dependent manner. Higher doses induce the overexpression of CYP24A1, which limits the anti-cancer actions of the $25(OH)D_3$ through catabolic activity.

© University of Pretoria

Reports have shown that splice variants may limit the enzymatic activity of CYP24A1[107] and CYP27B1[108]. There raises the possibility that polymorphisms of VDMS enzymes may exist in the HeLa cell line, and they may also be affecting the growth inhibitory actions of vitamin D. Genetic sequencing and mRNA analysis may clarify understanding of the effects of 25(OH)D_3 on the VDMS and mechanisms by which anti-cancer actions are exerted in cervical cancer. In addition, 25(OH)D_3 is highly concentrated in blood serum and further studies are needed to assess the effects of high doses of 25(OH)D_3 in patients with cervical cancer.

The HeLa cell line contains multinucleated cells potentially resistant to 25(OH)D_3 treatment

The identification of isolated multinucleated cells (MNCs) in the experimental and control cultures was an unexpected observation. MNCs, also known as polyploid giant cancer cells (PGCCs), are believed to arise from chemotherapy-induced stress[109-112]. They can survive *in vitro* and produce daughter cells through budding, splitting and bursting[113]. Their function is not fully understood, but they have been identified in tumours of different cancers and have distinct morphological features such as enlarged cell size and multiple nuclei[114].

Semi-quantitative analysis of microscopy images revealed that 25(OH)D_3 treatment significantly increased the size of MNCs in the HeLa cell line. The number of MNCs and number of nuclei in the 5000 nM dose treatment were higher than in the other cultures; however, there were no statistical differences observed. This suggests that the MNCs in the HeLa cultures may resist high doses of 25(OH)D_3 treatment. An increase in the size of MNCs supports the hypothesis that MNCs are senescent cells undergoing G_1 cell cycle arrest[109,114], however, cell cycle analysis on isolated MNCs is required to inform a conclusion.

Studies show that MNCs are common in tumours triggered by oncoviruses[115]. This supports claims that MNCs are resistant to the anti-cancer actions of chemotherapeutic drugs. Oncoviruses such as HPV can affect tumour heterogeneity, thereby hindering the anti-cancer actions of chemotherapeutic drugs. A noteworthy correlation has been identified between high-risk HPV oncogenic subtypes infection, the occurrence of high-grade squamous intraepithelial lesions, and the identification of polyploidy[115]. Studies have also shown that both E6 and E7 oncoproteins deregulate kinases essential for mitosis and cytokinesis, resulting in polyploid cells[116], and E6 and E7 are implicated in HPV-mediated cervical tumorigenesis.

© University of Pretoria

It is not clear if and how 25(OH)D_3 affected MNCs in the HeLa culture. Investigations with isolated cells are required to assess how the MNCs arise and how they are affected by vitamin D treatment. Also, investigations on the presence of MNCs *in vivo* with vitamin D treatment could give insight into the use of vitamin D as a therapeutic agent for cervical cancer treatment.

© University of Pretoria

Chapter 5

Conclusions

Currently, most cervical cancer cases are treated with surgery and chemo-radiotherapy. Vitamin D treatment may prove to be a less invasive treatment option. It is well documented that $1,25(OH)_2D_3$ is the most active and potent vitamin D metabolite; however, its administration is associated with dose-dependent hypercalcaemia. Therefore, there is immense potential in using $25(OH)D_3$ as an alternative therapeutic due to its low calcaemic effects. This study revealed that $25(OH)D_3$ inhibits cell growth and induces apoptotic cell death in the HeLa cell line via VDMS in an autocrine manner. Therefore, the cells can regulate their survival and growth with $25(OH)D_3$ treatment through activation by CYP27B1 and VDR. A possibility exists that $25(OH)D_3$ may exert its effects directly without activation by CYP27B1; however, further investigations are needed to conclude the mechanism of action. In addition, the catabolic CYP24A1 action that degrades early and activated vitamin D hormone may mitigate the anti-tumour action of $25(OH)D_3$, especially at very high-dose of $25(OH)D_3$ treatment via a negative autocrine feedback system.

Further studies are needed to determine how $25(OH)D_3$ treatment affects serum $25(OH)D_3$ levels and whether the anti-cancer actions of $25(OH)D_3$ are similar *in vivo*. In addition, it is well known that there is a correlation between HIV infection and the development of cervical cancer. Investigations on the therapeutic effects of vitamin D in HIV-positive cervical cancer patients may broaden the understanding of the mechanisms of action of vitamin D in cervical cancer.

The collective results of this study suggest that the autocrine VDMS mediates the effects of $25(OH)D_3$ on the growth and death of HeLa cells in a dose-dependent manner. These findings highlight the therapeutic potential of $25(OH)D_3$ for treating cervical cancer and indicate the need for further clinical investigations to explore this potential.

© University of Pretoria

References

1. Herbst MC. CANSA Fact Sheet on Cervical Cancer. Cancer Association of South Africa (CANSA); 2022.

2. Norman AW. The History of the Discovery of Vitamin D and Its Daughter Steroid Hormone. Annals of Nutrition and Metabolism. 2012; 61(3):199-206. doi:10.1159/000343104

3. Feldman D, Pike JW, Bouillon R Vitamin D. Volume 1, Biochemistry, physiology and diagnostics. [Internet] London ;: Academic Press is an imprint of Elsevier; 2018 [cited Access 2018 Access Date]. Available from: https://www.clinicalkey.com/dura/browse/bookChapter/3-s2.0-C20150059214.

4. Dixon KM, Mason RS. Vitamin D. The International Journal of Biochemistry & Cell Biology. 2009; 41(5):982-5. doi:https://doi.org/10.1016/j.biocel.2008.06.016

5. Holick MF. Vitamin D Deficiency. New England Journal of Medicine. 2007; 357(3):266-81. doi:10.1056/NEJMra070553

6. Holick MF. Vitamin D: importance in the prevention of cancers, type 1 diabetes, heart disease, and osteoporosis. Am J Clin Nutr. 2004; 79(3):362-71. doi:10.1093/ajcn/79.3.362

7. Feldman D, Krishnan AV, Swami S, Giovannucci E, Feldman BJ. The role of vitamin D in reducing cancer risk and progression. Nat Rev Cancer. 2014; 14(5):342-57. doi:10.1038/nrc3691

8. Bikle DD. Vitamin D metabolism, mechanism of action, and clinical applications. Chemistry & biology. 2014; 21(3):319-29. doi:10.1016/j.chembiol.2013.12.016

9. Berridge MJ. Vitamin D cell signalling in health and disease. Biochem Biophys Res Commun. 2015; 460(1):53-71. doi:10.1016/j.bbrc.2015.01.008

10. Deuster E, Jeschke U, Ye Y, Mahner S, Czogalla B. Vitamin D and VDR in Gynecological Cancers-A Systematic Review. International journal of molecular sciences. 2017; 18(11):2328. doi:10.3390/ijms18112328

11. Moukayed M, Grant WB. Molecular link between vitamin D and cancer prevention. Nutrients. 2013; 5(10):3993-4021. doi:10.3390/nu5103993

12. Rosen CJ, Adams JS, Bikle DD, Black DM, Demay MB, Manson JE, et al. The nonskeletal effects of vitamin D: an Endocrine Society scientific statement. Endocrine reviews. 2012; 33(3):456-92. doi:10.1210/er.2012-1000

13. Holick MF. Biological Effects of Sunlight, Ultraviolet Radiation, Visible Light, Infrared Radiation and Vitamin D for Health. Anticancer Res. 2016; 36(3):1345-56.

14. Welsh J. Cellular and molecular effects of vitamin D on carcinogenesis. Archives of biochemistry and biophysics. 2012; 523(1):107-14. doi:10.1016/j.abb.2011.10.019

15. Dusso AS, Brown AJ, Slatopolsky E. Vitamin D. American Journal of Physiology-Renal Physiology. 2005; 289(1):F8-F28. doi:10.1152/ajprenal.00336.2004

16. Ferlay J, Colombet M, Soerjomataram I, Parkin DM, Piñeros M, Znaor A, et al. Cancer statistics for the year 2020: An overview. International Journal of Cancer. 2021; 149(4):778-89. doi:10.1002/ijc.33588

17. Fouad YA, Aanei C. Revisiting the hallmarks of cancer. American journal of cancer research. 2017; 7(5):1016-36.

18. Hanahan D. Hallmarks of Cancer: New Dimensions. Cancer Discovery. 2022; 12(1):31-46. doi:10.1158/2159-8290.Cd-21-1059

© University of Pretoria

19. Ruijtenberg S, van den Heuvel S. Coordinating cell proliferation and differentiation: Antagonism between cell cycle regulators and cell type-specific gene expression. Cell Cycle. 2016; 15(2):196-212. doi:10.1080/15384101.2015.1120925

20. Samuel S, Sitrin MD. Vitamin D's role in cell proliferation and differentiation. Nutr Rev. 2008; 66(10 Suppl 2):S116-24. doi:10.1111/j.1753-4887.2008.00094.x

21. Jeon S-M, Shin E-A. Exploring vitamin D metabolism and function in cancer. Experimental & molecular medicine. 2018; 50(4):20-. doi:10.1038/s12276-018-0038-9

22. Fleet JC, Desmet M, Johnson R, Li Y. Vitamin D and cancer: a review of molecular mechanisms. Biochemical Journal. 2012; 441(1):61-76. doi:10.1042/bj20110744

23. Park MT, Lee SJ. Cell cycle and cancer. J Biochem Mol Biol. 2003; 36(1):60-5. doi:10.5483/bmbrep.2003.36.1.060

24. Bower JJ, Vance LD, Psioda M, Smith-Roe SL, Simpson DA, Ibrahim JG, et al. Patterns of cell cycle checkpoint deregulation associated with intrinsic molecular subtypes of human breast cancer cells. npj Breast Cancer. 2017; 3(1):9. doi:10.1038/s41523-017-0009-7

25. Williams GH, Stoeber K. The cell cycle and cancer. The Journal of Pathology. 2012; 226(2):352-64. doi:10.1002/path.3022

26. Voet DV, Judith G.; Pratt, Charlottle W. Principles of Biochemistry. Principles of Biochemistry. 4th ed. Asia: John Wiley & Sons, Inc; 2013. p. 581-622.

27. Pierce BA. Cancer Genetics. Genetics: A Conceptual Approach. 5th ed. United States of America: W. H. Freeman and Company; 2014. p. 661-82.

28. Ding L, Cao J, Lin W, Chen H, Xiong X, Ao H, et al. The Roles of Cyclin-Dependent Kinases in Cell-Cycle Progression and Therapeutic Strategies in Human Breast Cancer. International Journal of Molecular Sciences. 2020; 21(6):1960. doi:10.3390/ijms21061960

29. Umar M, Sastry KS, Chouchane AI. Role of Vitamin D Beyond the Skeletal Function: A Review of the Molecular and Clinical Studies. International journal of molecular sciences. 2018; 19(6):1618. doi:10.3390/ijms19061618

30. Bhoora S, Pather Y, Marais S, Punchoo R. Cholecalciferol Inhibits Cell Growth and Induces Apoptosis in the CaSki Cell Line. Medical Sciences. 2020; 8(1):12.

31. Ouyang L, Shi Z, Zhao S, Wang FT, Zhou TT, Liu B, et al. Programmed cell death pathways in cancer: a review of apoptosis, autophagy and programmed necrosis. Cell Prolif. 2012; 45(6):487-98. doi:10.1111/j.1365-2184.2012.00845.x

32. Galluzzi LM, M.C.; Vitale, I.; Zischka, H.; Castedo, M.; Zitvogel, L.; Kroemer, G. . Cell death modalities: classification and pathophysiological implications. Cell Death & Differentiation. 2007; 14:1237-43. doi:10.1038/sj.cdd.4402148

33. Galluzzi L, Cubillos-Ruiz JR, Kepp O, Kroemer G, Vitale I, Campanella M, et al. Molecular mechanisms of cell death: Recommendations of the Nomenclature Committee on Cell Death 2018. Cell Death and Differentiation. 2018; 25(3):486-541. doi:10.1038/s41418-017-0012-4

34. Kroemer G, El-Deiry WS, Golstein P, Peter ME, Vaux D, Vandenabeele P, et al. Classification of cell death: recommendations of the Nomenclature Committee on Cell Death. Cell Death and Differentiation. 2005; 12(S2):1463-7. doi:http://dx.doi.org/10.1038/sj.cdd.4401724

35. Edinger AL, Thompson CB. Death by design: apoptosis, necrosis and autophagy. Current Opinion in Cell Biology. 2004; 16(6):663-9. doi:10.1016/j.ceb.2004.09.011

© University of Pretoria

36. Saelens X, Festjens N, Lieselotte Vande W, Maria van G, Geert van L, Vandenabeele P. Toxic proteins released from mitochondria in cell death. Oncogene. 2004; 23(16):2861-74. doi:http://dx.doi.org/10.1038/sj.onc.1207523

37. Vermes I, Haanen C, Steffens-Nakken H, Reutelingsperger C. A novel assay for apoptosis. Flow cytometric detection of phosphatidylserine expression on early apoptotic cells using fluorescein labelled Annexin V. Journal of Immunological Methods. 1995; 184(1):39-51. doi:10.1016/0022-1759(95)00072-i

38. McIlwain DR, Berger T, Mak TW. Caspase functions in cell death and disease. Cold Spring Harbor Perspectives in Biology. 2013; 5(4):a008656. doi:10.1101/cshperspect.a008656

39. Wigdal SS, Kirkland RA, Franklin JL, Haak-Frendscho M. Cytochrome c release precedes mitochondrial membrane potential loss in cerebellar granule neuron apoptosis: lack of mitochondrial swelling. Journal of Neurochemistry. 2002; 82(5):1029-38. doi:https://doi.org/10.1046/j.1471-4159.2002.01049.x

40. Elmore S. Apoptosis: A Review of Programmed Cell Death. Toxicologic Pathology. 2007; 35(4):495-516.

41. Mishra AP, Salehi B, Sharifi-Rad M, Pezzani R, Kobarfard F, Sharifi-Rad J, et al. Programmed Cell Death, from a Cancer Perspective: An Overview. Molecular Diagnosis & Therapy. 2018; 22(3):281-95. doi:10.1007/s40291-018-0329-9

42. D'Arcy MS. Cell death: a review of the major forms of apoptosis, necrosis and autophagy. Cell Biology International. 2019; 43(6):582-92. doi:https://doi.org/10.1002/cbin.11137

43. Zong WX, Ditsworth D, Bauer DE, Wang ZQ, Thompson CB. Alkylating DNA damage stimulates a regulated form of necrotic cell death. Genes & development. 2004; 18(11):1272-82.

44. He C, Klionsky DJ. Regulation Mechanisms and Signaling Pathways of Autophagy. Annual Review of Genetics. 2009; 43(1):67-93. doi:10.1146/annurev-genet-102808-114910

45. Liu B, Cheng Y, Liu Q, Bao J-k, Yang J-M. Autophagic pathways as new targets for cancer drug development. Acta Pharmacologica Sinica [Internet]. 2010; 31:1154-64. [cited Access Year Access Date|]|. Available rom: URL

46. Singletary K, Milner J. Diet, autophagy, and cancer: a review. Cancer Epidemiol Biomarkers Prev. 2008; 17(7):1596-610. doi:10.1158/1055-9965.Epi-07-2917

47. Amaravadi RK, Thompson CB. The roles of therapy-induced autophagy and necrosis in cancer treatment. Clin Cancer Res. 2007; 13(24):7271-9. doi:10.1158/1078-0432.Ccr-07-1595

48. Wang J, Lian H, Zhao Y, Kauss MA, Spindel S. Vitamin D3 Induces Autophagy of Human Myeloid Leukemia Cells*. Journal of Biological Chemistry. 2008; 283(37):25596-605. doi:https://doi.org/10.1074/jbc.M801716200

49. Maes M, Vanhaecke T, Cogliati B, Yanguas SC, Willebrords J, Rogiers V, et al. Measurement of Apoptotic and Necrotic Cell Death in Primary Hepatocyte Cultures. Methods in molecular biology (Clifton, N.J.). 2015; 1250:349-61. doi:10.1007/978-1-4939-2074-7_27

50. Feldman D, Pike JW, Bouillon R, Giovannucci E, Goltzman D, Hewison M Vitamin D : Volume 2: Health, Disease and Therapeutics. [Internet] Saint Louis: Elsevier Science; 2017 [cited Access 2017 Access Date]. Available from: https://www.clinicalkey.com/dura/browse/bookChapter/3-s2.0-C20150059226.

51. Hsu JY, Feldman D, McNeal JE, Peehl DM. Reduced 1alpha-hydroxylase activity in human prostate cancer cells correlates with decreased susceptibility to 25-hydroxyvitamin D3-induced growth inhibition. Cancer Res. 2001; 61(7):2852-6.

© University of Pretoria

52. Hu N, Zhang H. CYP24A1 depletion facilitates the antitumor effect of vitamin D3 on thyroid cancer cells. Exp Ther Med. 2018; 16(4):2821-30. doi:10.3892/etm.2018.6536

53. Friedrich M, Rafi L, Mitschele T, Tilgen W, Schmidt W, Reichrath J. Analysis of the vitamin D system in cervical carcinomas, breast cancer and ovarian cancer. Recent Results Cancer Res. 2003; 164:239-46. doi:10.1007/978-3-642-55580-0_17

54. Anderson MG, Nakane M, Ruan X, Kroeger PE, Wu-Wong JR. Expression of VDR and CYP24A1 mRNA in human tumors. Cancer Chemotherapy and Pharmacology. 2006; 57(2):234-40. doi:10.1007/s00280-005-0059-7

55. Burmeister CAK, Saif F.; Schafer, Georgia; Mbatani, Nomonde; Adams, Tracy; Moodley, Jennifer; Prince, Sharon Cervical cancer therapies: Current challenges and future perspectives. Tumor Virus Research 2022; 13 doi:https://doi.org/10.1016/j.trv.2022.200238

56. Cohen PA, Jhingran A, Oaknin A, Denny L. Cervical cancer. The Lancet. 2019; 393(10167):169-82. doi:https://doi.org/10.1016/S0140-6736(18)32470-X

57. WHO. Assessing national capacity for the prevention and control of noncommunicable diseases: report of the 2019 global survey. 2020.

58. CANSA [Internet]. Cervical Cancer. Cancer Assosciation of South Africa (CANSA); 2022 [cited 2023 9 January]. Available from: https://cansa.org.za/cervical-cancer/.

59. Waggoner SE. Cervical cancer. The Lancet. 2003; 361(9376):2217-25. doi:https://doi.org/10.1016/S0140-6736(03)13778-6

60. ICO/IARC. South Africa Human Papillomavirus and Related Cancers, Fact Sheet 2021. ICO/IARC HPV Information Centre: Institut Catalia d'Oncologia, 2021 22 October 2021. Report No.

61. Krishnan AV, Feldman D. Mechanisms of the Anti-Cancer and Anti-Inflammatory Actions of Vitamin D. Annual Review of Pharmacology and Toxicology. 2011; 51(1):311-36. doi:10.1146/annurev-pharmtox-010510-100611

62. Kloss M, Fischer D, Thill M, Friedrich M, Cordes T, Salehin D, et al. Vitamin D, calcidiol and calcitriol regulate vitamin D metabolizing enzymes in cervical and ovarian cancer cells. Anticancer research. 2010; 30(11):4429-34.

63. Bhoora S, Pillay TS, Punchoo R. Cholecalciferol Mediates Apoptosis in Siha Cervical Cancer Line via Autocrine Mechanisms. Journal of the Endocrine Society. 2021; 5(Supplement_1):A1013-A. doi:10.1210/jendso/bvab048.2072

64. Brooks EA, Galarza S, Gencoglu MF, Cornelison RC, Munson JM, R. PS. Applicability of Drug Response Metrics for Cancer Studies using Biomaterials. Philosophical Transactions B. 2019; 374 doi:10.1098/rstb.2018.0226

65. Feoktistova M, Geserick P, Leverkus M. Crystal Violet Assay for Determining Viability of Cultured Cells. Cold Spring Harb Protoc. 2016; 2016(4):pdb.prot087379. doi:10.1101/pdb.prot087379

66. Aslantürk ÖS. In Vitro Cytotoxicity and Cell Viability Assays: Principles, Advantages, and Disadvantages. InTech; 2018.

67. alamarBlue® Cell Viability Reagent. Invitrogen; 2008.

68. Luminex Corporation [Internet]. Muse® Cell Cycle Kit. Texas, USA: Luminex Corporation; 2019 [cited 2021]. Available from: https://www.luminexcorp.com/muse-cell-cycle-kit/#overview.

69. Luminex Corporation [Internet]. Muse™ MitoPotential Kit User's Guide. Germany: Luminex Corporation; 2013 [cited 2021]. Available from: https://www.luminexcorp.com/muse-mitopotential-kit/.

© University of Pretoria

70. Luminex Corporation [Internet]. Muse® Annexin V & Dead Cell Kit. Texas, USA: Luminex Corporation; 2019 [cited 2021]. Available from: https://www.luminexcorp.com/muse-annexin-v-dead-cell-kit/.

71. Darzynkiewicz Z, Traganos F. Measurement of apoptosis. In: Al-Rubeai M, editor. Apoptosis. Berlin, Heidelberg: Springer Berlin Heidelberg; 1998. p. 33-73.

72. Luminex Corporation [Internet]. Muse® Caspase-3/7 Kit. Texas, USA: Luminex Corporation; 2019 [cited 2021]. Available from: https://www.luminexcorp.com/muse-caspase-3-7-kit/#overview.

73. Luminex Corporation [Internet]. Muse® Autophagy LC3-antibody Based Kit User's Guide. Texas, USA: Luminex Corporation; 2019 [cited 2021]. Available from: https://www.luminexcorp.com/muse-autophagy-lc3-antibody-based-kit/#overview.

74. Chan FK-M, Moriwaki K, De Rosa MJ. Detection of necrosis by release of lactate dehydrogenase activity. Methods in molecular biology (Clifton, N.J.). 2013; 979:65-70. doi:10.1007/978-1-62703-290-2_7

75. Histopathology. 1 ed: Humana New York; 2014.

76. Current protocols in molecular biology. New York: Greene Publishing Associates and John Wiley & Sons, Ltd; 1989.

77. Conn HJ, Lillie RD, Stotz EH, Emmel VM. H.J. Conn's Biological stains : a handbook on the nature and uses of the dyes employed in the biological laboratory. 9th ed / ed. Baltimore: Williams & Wilkins; 1977.

78. Madsen J, Susi T. The abTEM code: transmission electron microscopy from first principles [version 2; peer review: 2 approved]. Open Research Europe. 2021; 1(24) doi:10.12688/openreseurope.13015.2

79. Weakley BS. A beginner's handbook in biological transmission electron microscopy. 2d ed. ed. Edinburgh, New York: Churchill Livingstone; 1981.

80. Nolan T, Hands RE, Bustin SA. Quantification of mRNA using real-time RT-PCR. Nature Protocols. 2006; 1(3):1559-82. doi:10.1038/nprot.2006.236

81. Chomczynski P, Sacchi N. The single-step method of RNA isolation by acid guanidinium thiocyanate–phenol–chloroform extraction: twenty-something years on. Nature Protocols. 2006; 1(2):581-5. doi:10.1038/nprot.2006.83

82. Bio-Rad Laboratories I. iScript cDNA Synthesis Kit [package insert]. 2021. p. 2.

83. Bio-Rad Laboratories I. iTaq Universal SYBR Green Supermix [package insert]. 2021:2.

84. Mahmood T, Yang PC. Western blot: technique, theory, and trouble shooting. N Am J Med Sci. 2012; 4(9):429-34. doi:10.4103/1947-2714.100998

85. Abcam [Internet]. Western Blot Protocol. Abcam plc; 2021 [updated December 14 2020; cited 2021 January 10]. Available from: https://www.abcam.com/protocols/general-western-blot-protocol.

86. ThermoFisher S [Internet]. Pierce™ BCA Protein Assay Kit. ThermoFisher Scientific; 2021 [cited 2021 January]. Available from: https://www.thermofisher.com/document-connect/document-connect.html?url=https%3A%2F%2Fassets.thermofisher.com%2FTFS-Assets%2FLSG%2Fmanuals%2FMAN0011430_Pierce_BCA_Protein_Asy_UG.pdf&title=VXNlciBHdWlkZTogUGllcmNlIEJDQSBQcm90ZWluIEFzc2F5IEtpdA==.

87. NCBI [Internet]. PubChem Compound Summary for CID 11057, Gentian violet. Nation Center for Biotechnology; 2022 [cited 2022 27 December]. Available from: https://pubchem.ncbi.nlm.nih.gov/compound/Gentian-violet.

© University of Pretoria

88. Tanida I, Ueno T, Kominami E. LC3 conjugation system in mammalian autophagy. The International Journal of Biochemistry & Cell Biology. 2004; 36(12):2503-18. doi:https://doi.org/10.1016/j.biocel.2004.05.009

89. Mathiasen IS, Lademann U, Jäättelä M. Apoptosis induced by vitamin D compounds in breast cancer cells is inhibited by Bcl-2 but does not involve known caspases or p53. Cancer Res. 1999; 59(19):4848-56.

90. Swami S, Raghavachari N, Muller UR, Bao YP, Feldman D. Vitamin D growth inhibition of breast cancer cells: gene expression patterns assessed by cDNA microarray. Breast Cancer Res Treat. 2003; 80(1):49-62. doi:10.1023/a:1024487118457

91. Grant WB. 25-Hydroxyvitamin D and Breast Cancer, Colorectal Cancer, and Colorectal Adenomas: Case–Control versus Nested Case–Control Studies. Anticancer Research. 2015; 35(2):1153.

92. González-Sancho JM, Larriba MJ, Ordóñez-Morán P, Pálmer HG, Muñoz A. Effects of 1alpha,25-dihydroxyvitamin D3 in human colon cancer cells. Anticancer Res. 2006; 26(4a):2669-81.

93. Karlsson S, Diaz Cruz MA, Faresjö M, Khamou AP, Larsson D. Inhibition of CYP27B1 and CYP24 Increases the Anti-proliferative Effects of 25-Hydroxyvitamin D(3) in LNCaP Cells. Anticancer Res. 2021; 41(10):4733-40. doi:10.21873/anticanres.15288

94. Jones G, Ramshaw H, Zhang A, Cook R, Byford V, White J, et al. Expression and Activity of Vitamin D-Metabolizing Cytochrome P450s (CYP1α and CYP24) in Human Nonsmall Cell Lung Carcinomas*. Endocrinology. 1999; 140(7):3303-10. doi:10.1210/endo.140.7.6799

95. Reichrath J, Rech M, Moeini M, Meese E, Tilgen W, Seifert M. In vitro comparison of the vitamin D endocrine system in 1,25(OH)2D3-responsive and -resistant melanoma cells. Cancer Biol Ther. 2007; 6(1):48-55. doi:10.4161/cbt.6.1.3493

96. Shruthi N, Prashanthkumar M, Venugopalreddy B, Suma M, Subba Rao V. Analysis of the Cytotoxic Effects of Vitamin D3 on Colorectal, Breast and Cervical Carcinoma Cell Lines. Biochemistry & Analytical Biochemistry. 2017; 06(02) doi:10.4172/2161-1009.1000318

97. Riccardi C, Nicoletti I. Analysis of apoptosis by propidium iodide staining and flow cytometry. Nature Protocols. 2006; 1(3):1458-61. doi:http://dx.doi.org/10.1038/nprot.2006.238

98. Bhoora S, Punchoo R. Policing Cancer: Vitamin D Arrests the Cell Cycle. International Journal of Molecular Sciences [Internet]. 2020; 21(9296). [cited Access Year Access Date|]|. Available rom: URL

99. Wang G, Lei L, Zhao X, Zhang J, Zhou M, Nan K. Calcitriol Inhibits Cervical Cancer Cell Proliferation Through Downregulation of HCCR1 Expression. Oncology Research Featuring Preclinical and Clinical Cancer Therapeutics. 2015; 22(5-6):301-9. doi:10.3727/096504015X14424348425991

100. Thompson L, Wang S, Tawfik O, Templeton K, Tancabelic J, Pinson D, et al. Effect of 25-hydroxyvitamin D3 and 1α,25-dihydroxyvitamin D3 on differentiation and apoptosis of human osteosarcoma cell lines. J Orthop Res. 2012; 30(5):831-44. doi:10.1002/jor.21585

101. Setiawan I, Lesmana R, Goenawan H, Suardi D, Gatera V, Abdulah R, et al. Calcitriol potentially alters HeLa cell viability via inhibition of autophagy. Journal of Cancer Research and Therapeutics. 2022; 18(4):1144-51. doi:10.4103/jcrt.JCRT_82_20

102. Punchoo R, Dreyer G, Pillay TS. 25-Hydroxycholecalciferol Inhibits Cell Growth and Induces Apoptosis in SiHa Cervical Cells via Autocrine Vitamin D Metabolism. Biomedicines. 2023; 11(3):871. doi:10.3390/biomedicines11030871

103. Zeng R, Li H, Jia L, Lee SH, Jiang R, Zhang Y, et al. Association of CYP24A1 with survival and drug resistance in clinical cancer patients: a meta-analysis. BMC Cancer. 2022; 22(1) doi:10.1186/s12885-022-10369-x

© University of Pretoria

104. Shiratsuchi H, Wang Z, Chen G, Ray P, Lin J, Zhang Z, et al. Oncogenic Potential of CYP24A1 in Lung Adenocarcinoma. J Thorac Oncol. 2017; 12(2):269-80. doi:10.1016/j.jtho.2016.10.010

105. Horváth HC, Lakatos P, Kósa JP, Bácsi K, Borka K, Bises G, et al. The candidate oncogene CYP24A1: A potential biomarker for colorectal tumorigenesis. J Histochem Cytochem. 2010; 58(3):277-85. doi:10.1369/jhc.2009.954339

106. Schwartz GG, Eads D, Rao A, Cramer SD, Willingham MC, Chen TC, et al. Pancreatic cancer cells express 25-hydroxyvitamin D-1α-hydroxylase and their proliferation is inhibited by the prohormone 25-hydroxyvitamin D 3. Carcinogenesis. 2004; 25(6):1015-26. doi:10.1093/carcin/bgh086

107. Horváth HC, Khabir Z, Nittke T, Gruber S, Speer G, Manhardt T, et al. CYP24A1 splice variants—Implications for the antitumorigenic actions of 1,25-(OH)2D3 in colorectal cancer. The Journal of Steroid Biochemistry and Molecular Biology. 2010; 121(1-2):76-9. doi:10.1016/j.jsbmb.2010.03.080

108. Cordes T, Diesing D, Becker S, Fischer D, Diedrich K, Friedrich M. Expression of splice variants of 1α-hydroxylase in mcf-7 breast cancer cells. The Journal of Steroid Biochemistry and Molecular Biology. 2007; 103(3):326-9. doi:https://doi.org/10.1016/j.jsbmb.2006.12.034

109. Weihua Z, Lin Q, Ramoth AJ, Fan D, Fidler IJ. Formation of solid tumors by a single multinucleated cancer cell. Cancer. 2011; 117(17):4092-9. doi:10.1002/cncr.26021

110. Mirzayans R, Andrais B, Murray D. Roles of Polyploid/Multinucleated Giant Cancer Cells in Metastasis and Disease Relapse Following Anticancer Treatment. Cancers. 2018; 10(4):118. doi:10.3390/cancers10040118

111. Saini G, Joshi S, Garlapati C, Li H, Kong J, Krishnamurthy J, et al. Polyploid giant cancer cell characterization: New frontiers in predicting response to chemotherapy in breast cancer. Seminars in Cancer Biology. 2022; 81:220-31. doi:https://doi.org/10.1016/j.semcancer.2021.03.017

112. Liu J, Niu N, Li X, Zhang X, Sood AK. The life cycle of polyploid giant cancer cells and dormancy in cancer: Opportunities for novel therapeutic interventions. Semin Cancer Biol. 2022; 81:132-44. doi:10.1016/j.semcancer.2021.10.005

113. Zhang S, Mercado-Uribe I, Xing Z, Sun B, Kuang J, Liu J. Generation of cancer stem-like cells through the formation of polyploid giant cancer cells. Oncogene. 2014; 33(1):116-28. doi:10.1038/onc.2013.96

114. Zhou X, Zhou M, Zheng M, Tian S, Yang X, Ning Y, et al. Polyploid giant cancer cells and cancer progression. Frontiers in Cell and Developmental Biology. 2022; 10 doi:10.3389/fcell.2022.1017588

115. Herbein G, Nehme Z. Polyploid Giant Cancer Cells, a Hallmark of Oncoviruses and a New Therapeutic Challenge. Front Oncol. 2020; 10:567116. doi:10.3389/fonc.2020.567116

116. Patel D, Incassati A, Wang N, McCance DJ. Human papillomavirus type 16 E6 and E7 cause polyploidy in human keratinocytes and up-regulation of G2-M-phase proteins. Cancer Res. 2004; 64(4):1299-306. doi:10.1158/0008-5472.can-03-2917

117. Gounden S, Phulukdaree A, Moodley D, Chuturgoon A. Increased SIRT3 Expression and Antioxidant Defense under Hyperglycemic Conditions in HepG2 Cells. Metabolic Syndrome and Related Disorders. 2015; 13(6):255-63. doi:10.1089/met.2014.0140

118. Blomberg Jensen M, Andersen CB, Nielsen JE, Bagi P, Jørgensen A, Juul A, et al. Expression of the vitamin D receptor, 25-hydroxylases, 1alpha-hydroxylase and 24-hydroxylase in the human kidney and renal clear cell cancer. J Steroid Biochem Mol Biol. 2010; 121(1-2):376-82. doi:10.1016/j.jsbmb.2010.03.069

© University of Pretoria

Appendices

Appendix A

Table 6.1: Preparation of 10X PBS Buffer stock solution (pH 7.4).

Sodium Chloride	80g
Potassium Chloride	2g
Sodium dihydrogen phosphate	10.5g
Potassium dihydrogen phosphate	2g
Distilled water	800ml

Once pH has been adjusted using hydrochloric acid (HCl) and sodium hydroxide (NaOH), the solution will be made up to 1 L with distilled water.

© University of Pretoria

Appendix B

Table 6.2 Preparation LDH assay buffer.

Buffer	Concentration and pH	Components	Notes
Tris Buffer	200mM, pH 8.0	24.4 g Tris base 1 L milli-Q water	Sterilize by autoclave
2X LDH assay Buffer		223 mg INT 57 mg PMS 575 mg NAD 3.2 g lactic acid 480 ml Tris	Protect aliquots from light Store in small aliquots at -20°C
10X Lysis solution	9% Triton X-100	9 ml Triton X-100 91 ml milli-Q water	

© University of Pretoria

Appendix C

Table 6.3: Palade's fixative preparation.

Palade's solution A	Barbital sodium	14.7 g
	Sodium acetate	9.7 g
	Distilled water	500 ml
Palade's solution B	(2%) Osmium tetroxide	1 g (capsule)
	Distilled water	50 ml
Palade's solution C	(0:1N HCC) HCL	1.96 ml
	Distilled water	200 ml
Palade's fixative	Solution A	5 ml
	Solution C	5 ml
	Distilled water	2.5 ml
	Solution B	27.5 ml

Table 6.4: Resin solution preparation for 5g mixture.

	5g
Quetol	1.94
MNA	2.23
DDSA	0.83
RD2	0.10

Table 6.5: Embedding solution preparation for 5g mixture.

	5g
EmBed812	2.617
MNA	1.767
DDSA	0.683
S1	0.05

© University of Pretoria

Appendix D

Table 6.6: RT-qPCR primer sequences. Primer pairs[117-118] for genes to be investigated in this study.

Amplicon	Forward (5' → 3')	Reverse (5' → 3')	Primer Concentration	Denaturation	Annealing	Extension
VDR	GGA GAA AAC ACT TGT AAG TTG CT	TGG TCA GGT TGG TCT CGA ACT	700 nM	95°C 15s	56°C 15s	72°C 10s
CYP27B1	CCT GGC AGA GCT TGA ATT GCA	GGG GAA GAT GTA TAC CTT GGT	700 nM	95°C 15s	58.5°C 15s	72°C 10s
CYP24A1	CGG ACT CTT GAC AAG GCA ACA	TGA GGC GTA TTA TCG CTG GCA	600 nM	95°C 15s	64.5°C 15s	72°C 10s
18s rRNA	ACA CGG ACA GGA TTG ACA GA	CAA ATC GCT CCA ACT AA	500 nM	-	-	-

Melt curve conditions:

- 65-95 °C
- 0.5°C each step
- 90 sec hold at start
- 5 sec after each step

© University of Pretoria

Appendix E

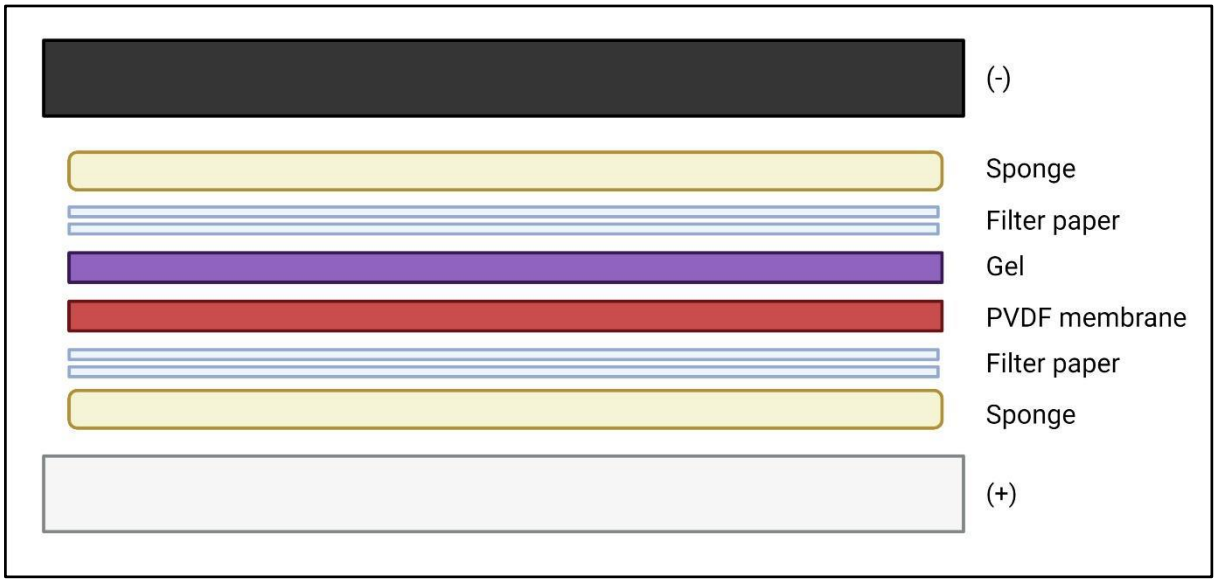

Figure 6.1: **Western blot transfer sandwich orientation.** Proteins contain a negative charge, so the gel will be placed near the cathode (negatively charged, in black). The polyvinylidene fluoride (PVDF) membrane will be placed on the side nearer to the anode (positively charged, in grey). The sandwich will be supported by filter paper (in dark blue) and sponges (in yellow).

© University of Pretoria

Appendix F

Table 6.7: Western blot antibody concentrations and conditions.

Protein name	Antibody (catalogue number)	Calculated molecular weight (kDa)	Concentration	Incubation time and temperature	Blocking solution	Secondary antibody
CYP27B1	Anti-rabbit IgG, monoclonal CYP27B1 antibody (#ab206655)	56	1:500	4°C Overnight	0.125g BSA in 0.2% PBS-Tween	Goat Anit-Rabbit HRP-conjugated
CYP24A1	Polyclonal CYP241 antibody (#ab203308)	59	1:1000			
VDR	Rabbit IgG, monoclonal VDR antibody (#12550)	48	1:500			
β-Actin	Monoclonal anti-β-Actin peroxidase antibody (#A3854)	42	1:5000	1 hour at room temperature		-
2° Antibody	Goat Anit-Rabbit HRP-conjugated antibody (#E-AB-1003)	-	1:5000		-	-

© University of Pretoria

Appendix G

Table 6.8: **Stripping buffer recipe** (pH 2.2)

Glycine	**15 g**
Sodium dodecyl sulphate (SDS)	1 g
Tween-20	10 mL
Distilled water	800 mL

Once pH has been adjusted using hydrochloric acid (HCl) and sodium hydroxide (NaOH), the solution will be made up to 1 L with distilled water.

© University of Pretoria

Appendix H

Abstract published in the Microscopy Society of Southern Africa 2022 Proceedings (ISSN 0250-0418 and ISBN 978-0-6398435-0-6).

25-HYDROXYVITAMIN D_3 INDUCES BIOCHEMICAL AND MORPHOLOGICAL APOPTOSIS IN THE HELA CELL LINE

E.V.M. Zhou[1], S. Bhoora[1], T.S. Pillay[1,2] and R. Punchoo[1,2]

[1]Department of Chemical Pathology, University of Pretoria, Pretoria, [2]National Health Laboratory Services Tshwane Division, Pretoria

Vitamin D and its metabolites have exhibited numerous anti-cancer actions, such as apoptotic cell death, in various pre-clinical cancer studies. Apoptosis is most commonly known as programmed cell death (PCD) type I and is essential during development, after injury and in disease prevention. Biochemical features include cell membrane asymmetry, caspase activation, changes in mitochondrial membrane potential ($\Delta\Psi m$), and DNA damage. Morphological features of apoptosis include reduction of cellular volume, chromatin condensation (pyknosis), nuclear fragmentation (karyorrhexis), nuclear breakdown (karyolysis), cytoplasmic blebbing and apoptotic bodies.[1,2]

Cervical cancer is one of the leading causes of cancer related deaths among South African women, affecting approximately 1 in 40 women. Few studies have explored the anti-cancer effects of vitamin D metabolites in cervical cancer.[3] In this study, cervical adenocarcinoma cell line, HeLa was treated with 25-hydroxyvitamin D_3 ($25(OH)D_3$), and biochemical and morphological features of apoptosis were assessed.

HeLa cells were seeded at a concentration of 30 000 cells/ml an incubated for 16 hours. Cells were then treated with $25(OH)D_3$ at a physiological concentration (260 nM) and a supraphysiological concentration (5000 nM). Medium and solvent (0.5 % ethanol v/v controls were also used. After a 72 hours incubation, cells were trypsinised and resuspended in fresh culture media. The cells were then stained with either annexin V, tetramethyl rhodamine ethyl ester (TMRE) or DEVD peptide-linked DNA dye. All samples were then stained with 7-aminoactinomycin D (7-AAD). Samples were then acquired using the Luminex® Guava® Muse® Cell Analyzer. Biological and technical repeats were triplicated (expressed as mean ± SEM) and analysed by one-way ANOVA with post-hoc Bonferroni testing at significance $p< 0.05$.

To assess morphological features of apoptosis, HeLa cells were seeded on glass coverslips at a concentration of 50 000 cells/ml and treated as previously described. After 72 hours incubation with treatment, cells were fixed and stained with Mayer's Hemalum and eosin. Cells were viewed with brightfield microscopy.

Annexin V staining and DEVD peptide-linked dye showed that $25(OH)D_3$ treatment at 5000 nM significantly increased the percentage of apoptotic cells when compared to the solvent control ($p=0.0323$ and $p=0.0219$, respectively). In addition, 5000 nM treatment significantly induced mitochondrial membrane depolarisation when compared to the solvent control ($p= 0.0061$).

Brightfield microscopy showed that treatment with $25(OH)D_3$ at both the physiological and supraphysiological concentrations induced apoptosis. Vitamin D treated cells exhibited apoptotic bodies, cytoplasmic blebbing, hyper-condensed chromatin, shrunken nuclei and a reduction in cell volume (Fig. 1).

In the intrinsic pathway of apoptosis, the exposure of cells to external stimuli initiates a cascade of molecular events.[1,2] Our results showed that annexin V staining was increased with $25(OH)D_3$ treatment, indicating an increased externalisation of phosphatidylserine on the plasma membrane. Similar results were seen in osteosarcoma cell lines (SAOS-2 and 143B)[4] treated with $25(OH)D_3$ at 1000 nM. Depolarisation of the mitochondrial membrane releases proteins that activate caspases.[1] Our results show that $25(OH)D_3$ treatment resulted in the depolarisation of the mitochondria and induction of caspase-3 and -7 activity[2], implying that $25(OH)D_3$ induces the intrinsic pathway of apoptosis. Active caspase-3 and -7 are involved in the fragmentation of DNA during apoptosis. Brightfield microscopy revealed cells with hyper-condensed chromatin, indicating potential DNA damage. The presence of apoptotic bodies in $25(OH)D_3$ further confirms the induction of apoptosis. In conclusion, $25(OH)D_3$ induces apoptosis at a supraphysiological concentration, potentially via the intrinsic pathway. Further investigation of the cell cycle and DNA content need to be conducted to corroborate findings.

References

1 Elmore, S. (2007) Toxicol Pathol. 35(4), 495-516.
2 Galluzzi, L. et al. (2018) Cell Death Differ. 25, 486–541.
3 Herbst, M.C. (2022) Fact Sheet on Cervical Cancer. Johannesburg, Cancer Association of South Africa.
4 Thompson, L. et al. (2012) Journal of Orthopaedic Research, 30, 831–844.

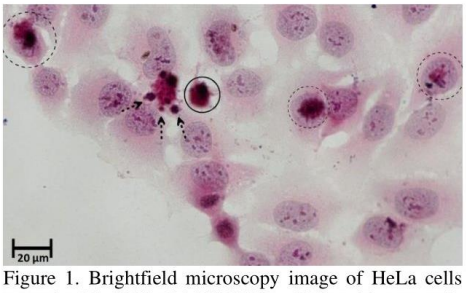

Figure 1. Brightfield microscopy image of HeLa cells treated with 5000 nM $25(OH)D_3$. Cells with apoptotic bodies (arrow), shrunken cells (circle) and hyper-condensed chromatin (dashed circle) were visible.

Corresponding author: *rivak.punchoo@up.ac.za*

© University of Pretoria